Red supergiant counterparts of ULXs

Paving the way to dynamical mass measurements

Proefschrift

ter verkrijging van de graad van doctor
aan de Radboud Universiteit Nijmegen
op gezag van de rector magnificus,
volgens besluit van het college van decanen
in het openbaar te verdedigen op woensdag 9 december 2015
om 10:30 uur precies

door

Marianne Heida

geboren op 2 januari 1989
te Voorburg, Nederland

PROMOTOR:	Prof. dr. G. A. Nelemans	(KU Leuven, België)
COPROMOTOREN:	dr. P. G. Jonker	
	dr. M. A. P. Torres	(SRON)
MANUSCRIPTCOMMISSIE:	Prof. dr. J. Oomens	
	Prof. dr. P. J. Groot	
	Prof. dr. M. C. Miller	(University of Maryland, Verenigde Staten)
	Dr. E. M. Rossi	(Universiteit Leiden)
	Prof. dr. E. Tolstoy	(Rijksuniversiteit Groningen)

Red supergiant counterparts of ULXs
Thesis, Radboud University Nijmegen, The Netherlands
Illustrated; with bibliographic information and Dutch summary

ISBN: 978-94-6259-891-1
Cover design by Jan de Leeuw. Cover: VST composite image of NGC 253, with part of the X-shooter spectrum of RX J004722.4-252051
Credits: ESO/INAF-VST, A. Grado/L. Limatola/INAF-Capodimonte Observatory
Printed by Ipskamp Drukkers, Enschede

This work was supported by SRON Netherlands Institute for Space Research and the Netherlands Research School for Astronomy (NOVA).

Don’t panic
- Douglas Adams, ‘The hitchhiker’s guide to the Galaxy’

CONTENTS

CHAPTER 1

INTRODUCTION

1.1 The discovery of ultraluminous X-ray sources

Unlike visible light and radio waves, X-ray radiation from space does not permeate the Earth's atmosphere. Although this is probably a good thing for life on Earth, it means that we cannot study the Universe at X-ray wavelengths with ground-based facilities. The detection of X-ray radiation from space therefore had to wait until the advent of the Space Era. In 1962, Giacconi et al. (1962) used the ASE/MIT Aerobee 150 sounding rocket to discover an X-ray source a million times brighter than the Sun, in the constellation Scorpius. Subsequent rocket flights, balloon-borne experiments and eventually the first dedicated X-ray satellites (*Uhuru* and *Ariel 5*) allowed for the discovery of many more X-ray sources, both point-like and extended, in the Milky Way and in other galaxies.

We now know that the majority of the point-like X-ray sources are powered by accretion of matter on to a compact object, when gravitational energy is converted into radiation. Accretion on to a black hole or neutron star typically releases $\sim 10\%$ of the rest-mass energy of the infalling matter as radiation. This is the most efficient way to convert mass into energy — for comparison, nuclear fusion of hydrogen into helium yields only $\sim 0.8\%$ of the rest-mass energy of the proton. The matter falling towards the compact object forms an accretion disc, which is heated by friction. X-ray photons are then produced either directly as blackbody radiation from the hot and ionized plasma, or through compton-upscattering of thermal optical seed photons. X-ray sources in our own Galaxy are mostly neutron stars or stellar mass black holes (BHs) that are fed by a companion star. The donor star can lose mass either through a stellar wind, or if the gravitational attraction of the compact object on the outer layers of the star is stronger than that of the star itself (Roche-lobe overflow). These systems are known as X-ray binaries (XRBs; see Figure 1.1). Supermassive black holes (SMBHs) can be found in the centre of most galaxies. When these accrete material from their surroundings, they become visible as very bright extragalactic sources called active galactic nuclei (AGN; Elvis et al. 1978; Tananbaum et al. 1978).

Before the launch of the *Einstein* Observatory in 1978 (Giacconi et al. 1979), the only galaxies where XRBs could be detected were the Milky Way and its neighbours, M31 and the Magellanic Clouds. With *Einstein*, which was 100 times more sensitive than previous

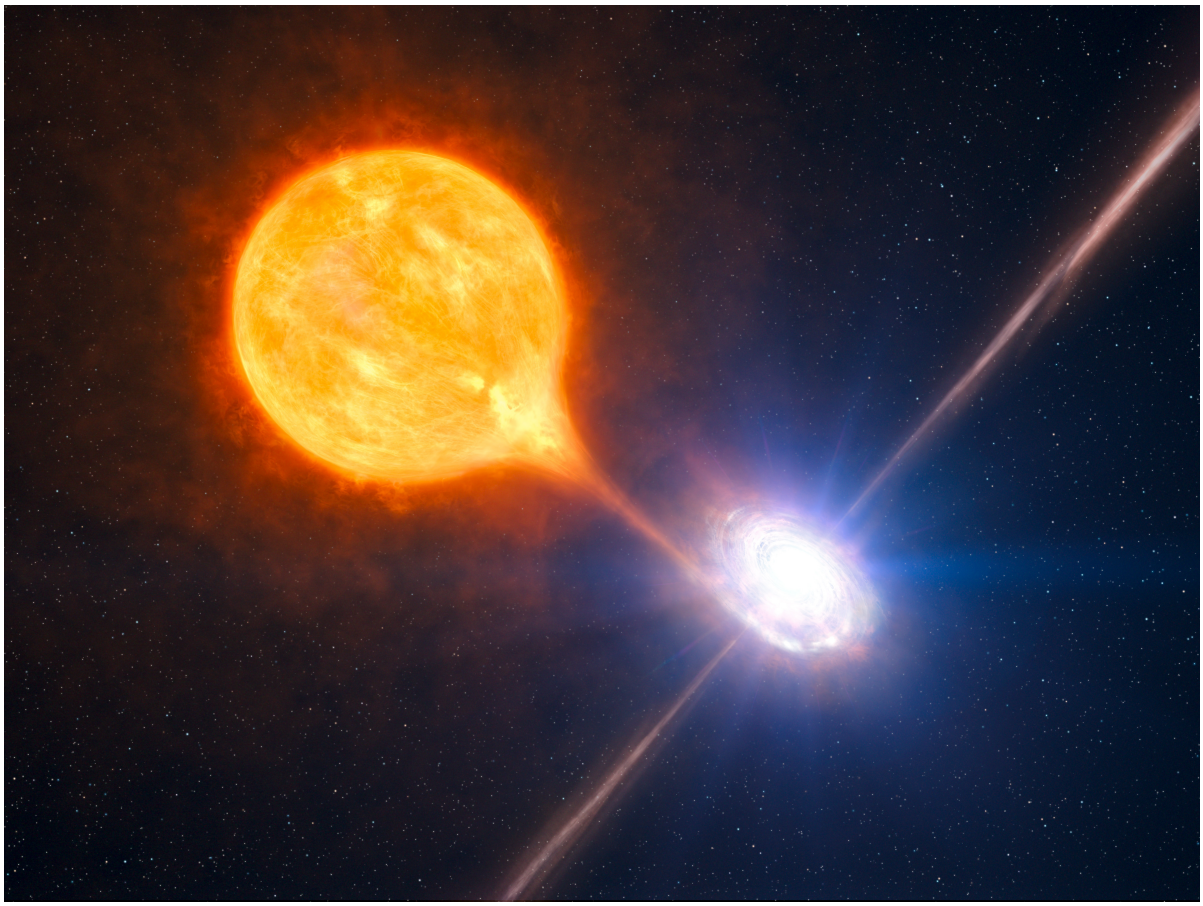

Figure 1.1: An artist impression of an XRB containing a stellar mass BH, fed through Roche-lobe overflow of its stellar companion. The material flows from the donor star and forms an accretion disc around the BH. Also visible are the jets launched from the vicinity of the BH. Image credit: ESO/L. Calçada/M. Kornmesser

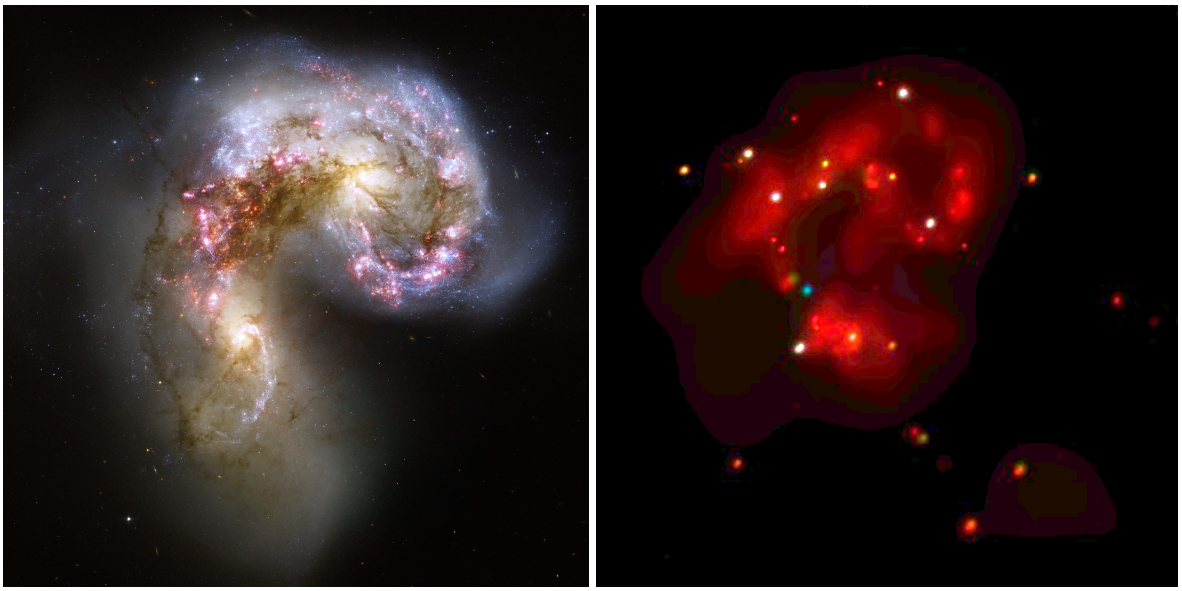

Figure 1.2: The Antennae galaxies are a pair of merging galaxies with a high star formation rate and many ULXs. *Left:* A *Hubble Space Telescope* image of the Antennae in optical light (image credit: Hubble/European Space Agency). *Right:* The same region as seen in X-rays by the *Chandra* satellite. The bright dots are all ULXs (image credit: NASA/SAO/CXC/Fabbiano et al. 2001).

X-ray missions, many more galaxies could be studied in X-rays. This led to the discovery of point-like X-ray sources that were much more luminous than the Galactic XRBs, yet not situated at the centre of these galaxies (and therefore not AGN; Fabbiano 1989). These objects were eventually dubbed 'ultraluminous X-ray sources' (ULXs): off-nuclear, point-like X-ray sources with a luminosity in the 0.3–10.0 keV range $> 10^{39}$ erg s^{-1} (e.g. Feng & Soria 2011).

Many more ULXs were later discovered with ROSAT and the XMM-*Newton* and *Chandra* X-ray observatories (e.g. Liu & Bregman 2005; Liu & Mirabel 2005; Winter et al. 2006; Walton et al. 2011a; Swartz et al. 2011, see Figure 1.2). These catalogues of ULXs are contaminated by other bright X-ray sources that are not accreting compact objects, such as X-ray bright supernovae (particularly of type IIn; Immler & Lewin 2003) and supernova remnants. Background AGN that are coincident with a galaxy but are actually located much further away, causing their luminosity to be underestimated, are another important source of contamination. A useful way to select the bona fide ULXs is looking at the variability of the X-ray emission. If a source is variable this excludes the possibility that it is a supernova remnant or that the high luminosity is caused by a number of XRBs located close together instead of by a single source. X-ray bright supernovae slowly fade after they reach their peak luminosity and can, therefore, also be distinguished by their X-ray light curve. Distance measurements can be used to weed out the background AGN, for example by measuring their redshift from an optical spectrum (see also Chapter 3).

The main question that the discovery of ULXs raised is how they reach their observed X-ray luminosities. There exists a theoretical upper limit to the luminosity that an accreting object can emit without blowing away its mass supply, called the Eddington limit (see Section 1.2). ULXs are above the Eddington limit of a typical stellar mass BH. This leaves two op-

tions: either ULXs contain stellar mass BHs or neutron stars that are somehow exceeding their Eddington limit, or they contain BHs that are (much) more massive than the stellar mass BHs we know of so far (see Section 1.3).

1.2 The Eddington limit

A self-graviting object with an energy source at its center, like a star, has a maximum luminosity for which the (inwardly directed) gravitational force on its outer layers exactly balances the (outwardly directed) radiation pressure. At a higher luminosity, the material would be ejected and the object would no longer be stable. This maximum luminosity is called the Eddington luminosity ($L_{\rm Edd}$) or Eddington limit. It was originally derived by Eddington (1916) for giant stars, but is also applicable to accreting systems (where the outer layers correspond to the infalling material). Because in such systems the luminosity depends on the rate at which material is accreted, there is a corresponding maximum accretion rate called the Eddington rate ($\dot{M}_{\rm Edd}$). If the accreting material is purely fully ionized hydrogen, and assuming spherical symmetry, the Eddington luminosity is

$$L_{\rm edd} = \frac{4\pi G M m_{\rm p} c}{\sigma_{\rm T}} \cong 1.3 \times 10^{38} \left(\frac{M}{M_\odot}\right) \text{erg s}^{-1} \tag{1.1}$$

(see Frank et al. 2002), where $m_{\rm p}$ is the proton mass, $\sigma_{\rm T}$ the Thomson cross-section, M the mass of the accreting object, and $M_\odot$the solar mass. If an accreting source exceeds its Eddington luminosity, the outward radiation pressure on the infalling material would exceed the gravitational attraction and accretion would be halted. However, in the case of accretion through a disc, the assumptions made in the derivation of the 'classical' Eddington limit may not hold: especially the assumption of spherical symmetry clearly breaks down. Analytical work on slim disc models (e.g. Abramowicz et al. 1988; Watarai et al. 2001; Ebisawa et al. 2003; Heinzeller & Duschl 2007), backed up by magnetohydrodynamic (MHD) simulations (e.g. Ohsuga et al. 2009; Ohsuga & Mineshige 2011), have shown that the Eddington limit can be breached. A moderately super-Eddington mass supply of $\dot{M} \approx 5\ \dot{M}_{\rm Edd}$ is enough to produce a total luminosity of $\sim 1.7\ L_{\rm Edd}$, and an apparent luminosity of $\sim 22\ L_{\rm Edd}$ for a face-on observer (due to geometrical beaming; Mineshige & Ohsuga 2011).

On the other hand, the Eddington limit as a maximum luminosity for accreting BHs seems to work well for Galactic XRBs and AGN (Steinhardt & Elvis 2010; Raimundo et al. 2010). In the words of Feng & Soria (2011): "Perhaps like the bumblebee, the Eddington limit should not fly, but does."

If ULXs are stellar mass BHs that are exceeding their Eddington limit, this may be visible in their X-ray spectra. 'Normal' (i.e. sub-Eddington) XRBs have X-ray spectra that are either dominated by black body radiation from the disc (when they are in outburst, the 'high/soft state') or by a simple power law (the 'low/hard state'; see e.g. Zdziarski & Gierliński 2004; Done et al. 2007; Gilfanov & Merloni 2014). For a super-Eddington source the X-ray spectrum is predicted to be different. When the mass supply onto a BH exceeds the Eddington rate, models predict that a wind will be launched from the disc, obscuring the radiation from the

disc itself and creating a funnel where the radiation can escape (Shakura & Sunyaev 1973; King et al. 2001; King 2004; Poutanen et al. 2007; King 2009). The shape of the X-ray spectrum then depends on the viewing angle of the observer and will be different from what is observed in sub-Eddington XRBs.

1.3 Intermediate mass black holes

Astrophysical black holes (BHs) cover a wide range of masses. At the low end of the spectrum are the stellar mass BHs, that are formed when the core of a massive ($M \gtrsim 20 - 25\ M_{\odot}$) star implodes at the end of its lifetime. Stellar mass BHs with masses of 5 – 15 $M_{\odot}$ are known in our Galaxy (see for example McClintock & Remillard 2006; Casares & Jonker 2014). The most massive stellar mass BH known to date is located in the nearby star-forming galaxy IC-10 and has a mass between 20 – 40 $M_{\odot}$ (Prestwich et al. 2007; Silverman & Filippenko 2008), although recently Laycock et al. (2015) argued that the compact object in this system could be a much less massive BH or even a neutron star, showing how difficult it is to reliably determine the mass of the compact object in extragalactic objects. From theory it is expected that the most massive BHs that can be formed through core-collapse of a star have masses $\sim 100\ M_{\odot}$ (Belczynski et al. 2010). BHs in the mass range 20 – 100 $M_{\odot}$ are sometimes referred to as *massive stellar BHs* (Feng & Soria 2011) to distinguish them from the more common stellar mass BHs.

At the other end of the mass spectrum are the supermassive black holes (SMBHs) that are found in the centre of almost every galaxy. In our own Milky Way, there is strong evidence for the presence of a $4 \times 10^6\ M_{\odot}$ BH (Ghez et al. 2008; Gillessen et al. 2009). This BH is not currently active; its mass has been determined by studying the orbits of stars in the innermost part of the nuclear star cluster in the Galactic centre. In other galaxies there is also evidence for the presence of SMBHs, either active (as AGN) or quiescent. Their masses range from a few 100.000 to billions of solar masses (Greene & Ho 2007; Ghisellini et al. 2010).

BHs with masses in between those of the stellar mass and supermassive BHs are called intermediate mass black holes (IMBHs). We use the mass range $10^2 - 10^5\ M_{\odot}$ for IMBHs throughout this thesis. The existence of IMBHs has not yet been conclusively proven. BHs of a few times $10^5\ M_{\odot}$ have been discovered in dwarf galaxies (Peterson et al. 2005; Greene & Ho 2007; Reines et al. 2013). The masses of most of these BHs are determined assuming that certain scaling relations, that were derived for SMBHs, are still valid for lower mass galaxies. By extrapolating these relations even further, we expect IMBHs with masses of a few thousand $M_{\odot}$ to be present in the centres of globular clusters. However, dedicated searches for massive BHs in globular clusters have so far yielded negative or inconsistent results. Deep X-ray and radio observations looking for signals from accreting IMBHs have only put upper limits on the masses of putative BHs (Strader et al. 2012; Haggard et al. 2013). Future radio facilities such as the Square Kilometer Array (SKA) will allow us to improve on these limits further. An IMBH can also be discovered because of the effect it has on the velocities of the stars in its gravitational sphere of influence. Detailed investigation of the velocities of stars close to the centres of globular clusters, using adaptive optics-assisted near-infrared integral field

spectroscopy, seems a promising technique to discover quiescent IMBHs. However, at the moment it is limited by systematic uncertainties, and different groups investigating the same sources reach inconsistent conclusions (Lützgendorf et al. 2011; Lanzoni et al. 2013).

The interest in finding IMBHs is mainly driven by their possible role as seeds for SMBH formation in the early universe. Observations of quasars show that already at redshifts 6 – 7, SMBHs exist with masses more than $10^9\ M_\odot$. The current record holder for 'most distant quasar', ULAS J1120+0641, has a redshift $z = 7.085$ and is powered by a BH of $2 \times 10^9\ M_\odot$ (Mortlock et al. 2011). At that redshift the Universe was only 0.77 billion years old. Another quasar, at $z = 6.3$ but with a BH mass of $\sim 1.2 \times 10^{10}\ M_\odot$, was recently discovered by Wu et al. (2015). Forming such a massive BH in less than a billion years is very difficult if the seed BH is only of order 10 $M_\odot$. However, it is possible if the seed BH is an IMBH (Haiman & Loeb 2001; Ebisuzaki et al. 2001; Volonteri & Rees 2006; Volonteri 2012). Finding these IMBHs may provide valuable information about the formation and evolution of SMBHs.

1.4 ULXs: a diverse group of sources

When ULXs were first discovered, the idea that they contained IMBHs seemed a natural explanation for their high X-ray luminosity (Fabbiano 1989). However, information gained from new observations has necessitated adjustments of this simple picture. It now seems that ULXs are in fact a mixed bag of sources, containing both stellar mass BHs and neutron stars accreting at or above their Eddington limit and probably also more massive BHs in the sub-Eddington regime. The faintest ULXs, with $L_{\rm X} < 3 \times 10^{39}$ erg s^{-1}, can be readily explained as stellar mass BHs accreting at or close to their Eddington limit. The most extreme ULXs, a small group of sources with $L_{\rm X} > 10^{41}$ erg s^{-1}, are referred to as hyperluminous X-ray sources (HLXs). Unless very high beaming factors (> 100) are invoked, it is difficult to explain these sources as stellar mass BHs and they are generally considered to be strong candidates to contain IMBHs. The category in between, with 3×10^{39} erg s^{-1}$< L_{\rm X} < 10^{41}$ erg s^{-1}, contains sources that are most likely stellar mass or massive stellar BHs in the super-Eddington regime, but may also contain IMBHs.

1.4.1 ULXs as super-Eddington sources

High-quality XMM-*Newton* observations of nearby ULXs have revealed that their spectra differ from those of sub-Eddington XRBs. Gladstone et al. (2009) and Sutton et al. (2013) distinguish three different states based on spectral shape and variability properties: the 'broadened disc', predominantly seen in ULXs with $L_{\rm X} < 3 \times 10^{39}$ erg s^{-1}, a 'hard ultraluminous state', and a 'soft ultraluminous state'. Observations with *NuSTAR* (Harrison et al. 2013) at higher energies than can be probed with XMM-*Newton* have confirmed the peculiar shape of these spectra (Bachetti et al. 2013; Walton et al. 2013, 2014, 2015b,a). Middleton et al. (2015) suggest that the 'broadened disc' spectra occur in sources accreting at their Eddington limit, whereas the hard and soft ultraluminous states are a sign of truly super-Eddington accretion. The difference between these last two states could then be due to different viewing angles, as

the spectral shape depends on whether the source is viewed through the disc wind or down the funnel.

M82 X-2, the second brightest ULX in the nearby starburst galaxy M82 (see Figure 1.3), sometimes exhibits X-ray pulsations that were discovered with *NuSTAR* (Bachetti et al. 2014), proving that the accretor is a neutron star and not a BH. Thus, it is the first ULX with a confirmed neutron star accretor, with a luminosity of $\gtrsim 100\ L_{\rm Edd}$. Exactly how it reaches such a high luminosity is not yet clear, but several theories have been put forward (Dall'Osso et al. 2015; Ekşi et al. 2015; Kluźniak & Lasota 2015; Tong 2015). The discovery of one ULX with a neutron star of course raises the question what fraction of ULXs contains a neutron star instead of a BH. No others have as yet been found (Doroshenko et al. 2015), but based on binary population synthesis combined with binary evolution calculations Shao & Li (2015) claim that super-Eddington neutron stars may be responsible for a sizeable fraction of the ULX population.

In the past, strong beaming (beaming factor $\gg 1$) has been proposed as an explanation for the apparent high luminosity of ULXs (e.g. Körding et al. 2002). In that scenario, no super-Eddington accretion would be needed even if the accretor is a stellar mass BH or neutron star, because the real luminosity would be much lower than what is calculated assuming isotropic emission. It also predicts that for every ULX with $L_{\rm X}> 10^{40}$ erg s^{-1}, there should be ≈ 30 sources with $L_{\rm X}\approx 10^{39}$ erg s^{-1} (as for every source that is seen face-on, there should be a large number of sources seen at higher inclination). However, there is no evidence for this population (Davis & Mushotzky 2004; Walton et al. 2011a). Several ULXs are surrounded by nebulae of ionized gas (Pakull & Mirioni 2002; Kaaret et al. 2004; Miller et al. 2005; Lang et al. 2007; Kaaret & Corbel 2009). The luminosity of these ULXs, assuming that the emission is isotropic, is comparable to the energy input necessary to ionize the gas of the extended, diffuse nebulae. This provides another argument against strong beaming, at least in these sources.

1.4.2 ULXs as IMBH candidates

Although there are indications that several ULXs contain stellar mass BHs or, in one case, even a neutron star, not all ULXs can be explained as super-Eddington sources. This is especially true for the HLXs: it is very difficult to explain their high luminosities with super-Eddington accretion onto stellar mass BHs. This makes them some of the best candidates to host IMBHs (see Chapter 2). There are not many confirmed HLXs, as several candidates have turned out to be AGN at much larger distances than their putative host galaxy (Sutton et al. 2015, see also Chapter 3, Figure 1.4).

HLX-1 in ESO 243-49 is the most extreme HLX known to date (Farrell et al. 2009). Its association with its host galaxy, at a distance of 95 Mpc, has been confirmed by the detection of an Hα emission line in the spectrum of the optical counterpart (Wiersema et al. 2010). The X-ray spectrum of the source varies in a way that is similar to Galactic XRBs, but at a much higher luminosity. In quiescence, it shows a hard X-ray spectrum at $\approx 10^{40}$ erg s^{-1}; when it goes into outburst the spectrum softens, reaching a peak luminosity $> 10^{42}$ erg s^{-1} (Godet et al. 2009; Servillat et al. 2011). These outbursts at first seemed to have a recurrence time of approximately one year, suggestive of an orbital period, but the last three outbursts were

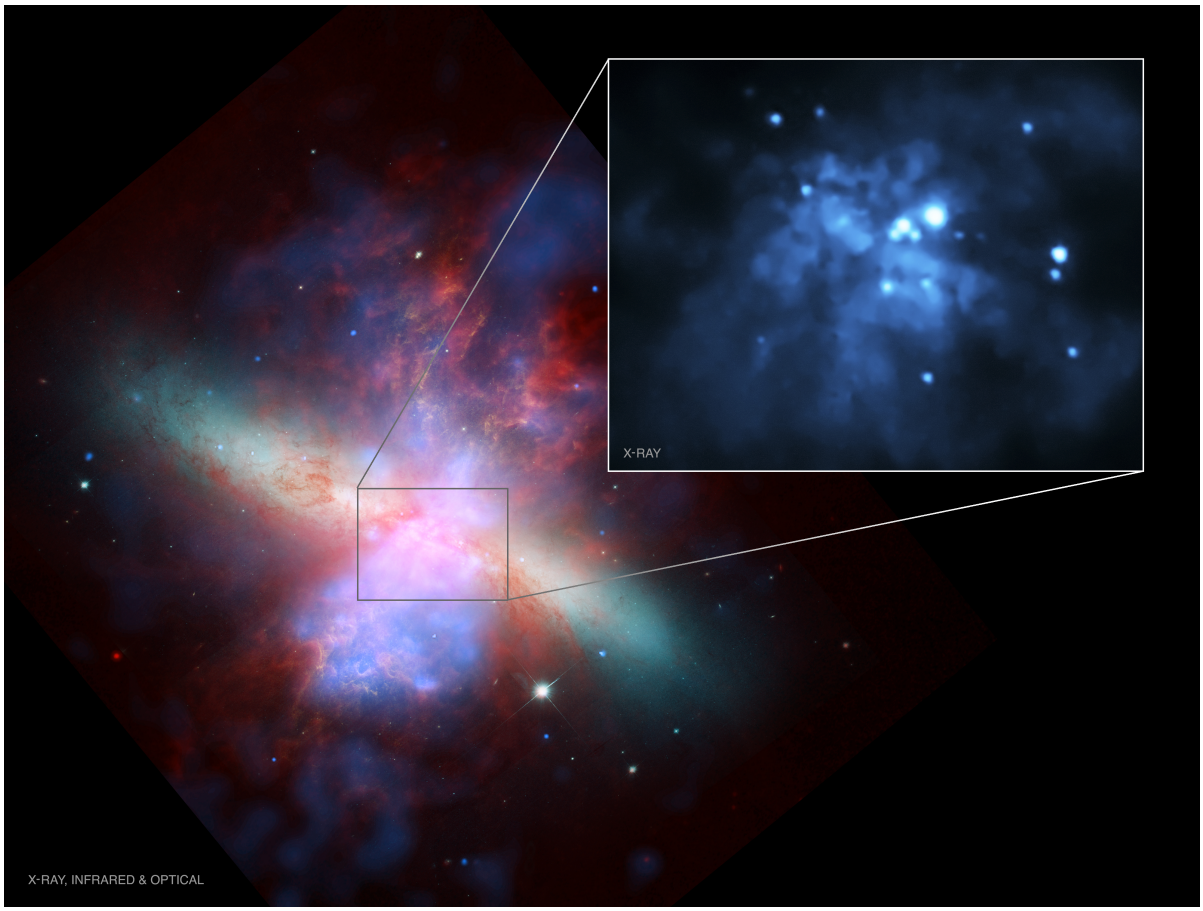

Figure 1.3: A combined X-ray (*Chandra*, in blue), infrared (*Spitzer*, in red) and optical (*Hubble*, in green/yellow) image of M82, a nearby starburst galaxy that hosts several ULXs. The inset shows a zoom-in of the central region of the galaxy in X-rays. The brightest source is M82 X-1, an HLX and candidate IMBH. The second brightest source just to the lower left of it is M82 X-2, a ULX with a neutron star accretor. Image credits: Inset: NASA/CXC/Tsinghua Univ./H. Feng et al.; Full-field: X-ray: NASA/CXC/JHU/D.Strickland; Optical: NASA/ESA/STScI/AURA/The Hubble Heritage Team; IR: NASA/JPL-Caltech/Univ. of AZ/C. Engelbracht.

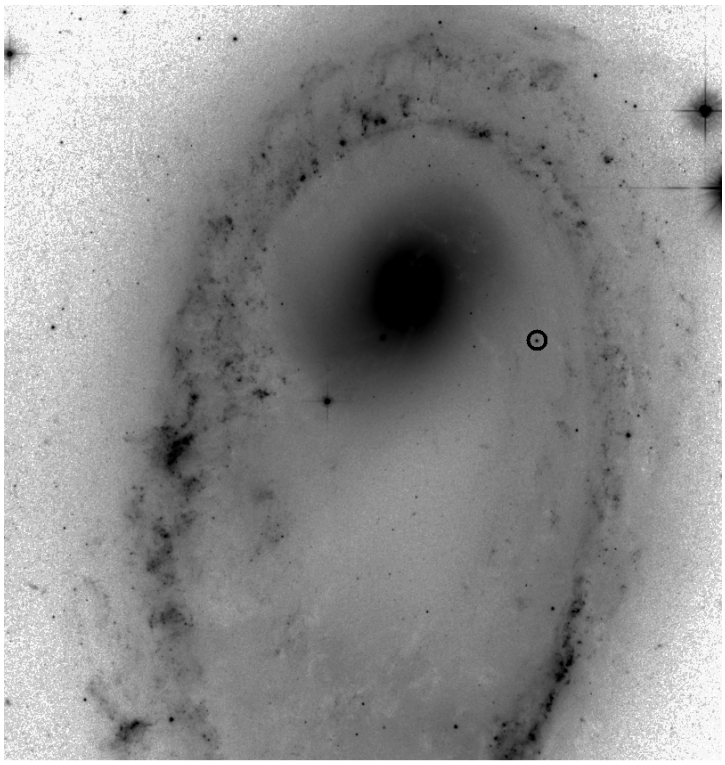

Figure 1.4: A Hubble image of the galaxy AM 0644-741. The ring around the central part of the galaxy contains many star forming regions and is a sign of a recent merger. The point-source that is located in between the nucleus and the ring (indicated by the black circle) is the counterpart to a bright X-ray source that was a candidate ULX, but optical spectroscopy showed that it is in fact an AGN located behind AM 0644-741 (see Chapter 3).

delayed by a few weeks to months (Godet et al. 2014; Kong et al. 2015). Radio flares have been detected during outbursts (Webb et al. 2012), and recently Cseh et al. (2015) reported the detection of persistent radio emission in the low hard state. The most plausible scenario is that HLX-1 contains an IMBH of $10^4 - 10^5\ M_\odot$, but it is not yet clear what the mechanism behind the outbursts is. One suggestion is that the BH is fed by a donor star on an elliptical orbit that transfers mass every time it passes periapse (Lasota et al. 2011; Godet et al. 2014), but the delay of the last outbursts poses difficulties for this scenario (King & Lasota 2014). Other scenarios also have their specific problems (see for instance Yan et al. 2015). HLX-1 is associated with a star cluster. It is possible that this is the remnant of a dwarf galaxy that merged with ESO 243-49, and the BH is the central BH of that dwarf (Farrell et al. 2012; Mapelli et al. 2013).

A second HLX candidate that shows outbursts is CXO J122518.6+144545 (CXO J1225; Jonker et al. 2010, Chapter 2). This system is much less studied than HLX-1, due in part to the fact that it is located twice as far away and has a peak luminosity that is a factor 10 lower, making it difficult to monitor in X-rays. However, the discovery of a second HLX-1-like object is promising for IMBH studies.

M82 X-1 is another HLX, located in the nearby galaxy M82 (see Figure 1.3). It reaches a peak X-ray luminosity of $\sim 10^{41}$ erg s^{-1}, but does not show regular outbursts like HLX-1. Using data from the Rossi X-ray Timing Explorer (RXTE, Bradt et al. 1993), Strohmayer & Mushotzky (2003) and Pasham et al. (2014) detected quasi-periodic oscillations (QPOs) in the power density spectrum of this source. In some Galactic X-ray binaries, similar QPOs have been discovered and their frequency seems to scale inversely proportional to the mass of the BH (McClintock & Remillard 2006). Assuming that this relation holds for ULXs, Pasham et al. (2014) infer a BH mass of $\sim 400\ M_\odot$ for the BH in M82 X-1. This makes the source an interesting IMBH candidate. However, since the physical nature of QPOs is not well understood an independent confirmation of the BH mass in this system is necessary.

A ULX that does not qualify as an HLX, but is still a good candidate to host an IMBH, is NGC 2276-3c (Mezcua et al. 2015). Its peak luminosity is 'only' 6×10^{40} erg s^{-1}, but unlike those of most ULXs, its X-ray spectrum is consistent with a low/hard state. In addition, a compact radio jet has been discovered at the location of the X-ray source. Based on quasi-simultaneous radio and X-ray observations, Mezcua et al. (2015) report a mass of $\sim 5 \times 10^4$ $M_\odot$ for the BH.

1.5 Black hole mass determination

To find out whether ULXs are super-Eddington sources containing stellar mass BHs, or IMBHs in the sub-Eddington regime, we need to determine their accretor mass in a robust way. The X-ray spectra of ULXs vary from source to source (and sometimes within the same source, Pintore et al. 2014) and are not well understood. Below I will discuss methods to measure BH masses that do not depend on modelling of broad-band X-ray spectra.

1.5.1 Dynamical methods

The most reliable method to determine the masses of stars in a binary system is to measure the orbital parameters of the system and apply Kepler's laws. The radial velocity of a star can be measured through optical or near-infrared spectroscopy, by cross-correlating its spectrum with that of a star (or stellar model) of the same spectral type and known radial velocity for a range of velocity shifts. Measuring the radial velocity of the star at several points in its orbit then yields the orbital period and the orbital velocity of the star in the radial direction. In a double-lined spectroscopic binary, where this can be done for both components of the system, it is possible to calculate the masses of both binary components. In a binary containing a black hole or neutron star only the orbital motion of the donor star can be measured. Combining Kepler's third law with the measured radial velocity amplitude yields the mass function (see Casares & Jonker 2014):

$$f(m) = \frac{P_{\rm orb} K_C^3}{2\pi G} = \frac{M_{\rm BH} \sin^3 i}{(1+q)^2} \tag{1.2}$$

Here $P_{\rm orb}$ is the orbital period of the binary, K_C is the semi-amplitude of the radial velocity of the donor star, i the inclination of the system to our line of sight, and q the mass ratio $\frac{M_{\rm donor}}{M_{\rm BH}}$ (see also Figure 1.5). In this expression it is assumed that the orbit is circular, which is reasonable for X-ray binaries given the short circularization timescales expected in these systems (e.g. Witte & Savonije 1999, 2001). If the mass of the donor star is known, measuring the orbital period and radial velocity amplitude of the donor and assuming $q = 0$ and $i = 90^\circ$ gives a lower limit to the mass of the accretor. If the inclination of the system and q can be measured also, Equation 1.2 can be used to calculate the accretor mass. In the case of an XRB containing a neutron star or stellar mass BH with an intermediate-mass donor, where $q \approx 1$, the donor star mass has to be accurately known if one wants to put useful limits on the mass of the accretor (see Equation 1.2). If the accretor is a massive stellar or intermediate mass BH, the donor star mass is of less importance for deriving an accurate BH mass, because $q \ll 1$ and the denominator in Equation 1.2 is close to 1 anyway.

This method has been applied to several Galactic X-ray binaries (e.g. McClintock & Remillard 1986; Marsh et al. 1994; Filippenko & Chornock 2001; Corral-Santana et al. 2011; Steeghs et al. 2013, Figure 1.6). These systems are discovered when they go into outburst and brighten dramatically in X-rays and optical. When they fade into quiescence it becomes possible to detect the donor star in optical light, and phase-resolved optical spectroscopy can then be used to measure $P_{\rm orb}$ and K_C. Often, the orbital period can be independently measured from light curves, from brightness variations as a function of the orbital period brought about by the changing aspect of the tidally deformed mass donor star. In some systems, modelling of ellipsoidal variations in the light curve allows for a measurement of the inclination (and sometimes the mass ratio q) as well. In this way, BH masses have been determined for 21 systems (see Casares & Jonker 2014 for a recent review and more elaborate description of the techniques).

In the case of SMBHs it is usually not possible to resolve single stars in their gravitational sphere of influence. Only for Sgr A*, the SMBH in the centre of the Milky Way, are we able to follow the orbits of individual stars using time-resolved high spatial resolution observations that are obtained using the technique called adaptive optics. Combined with spectroscopic

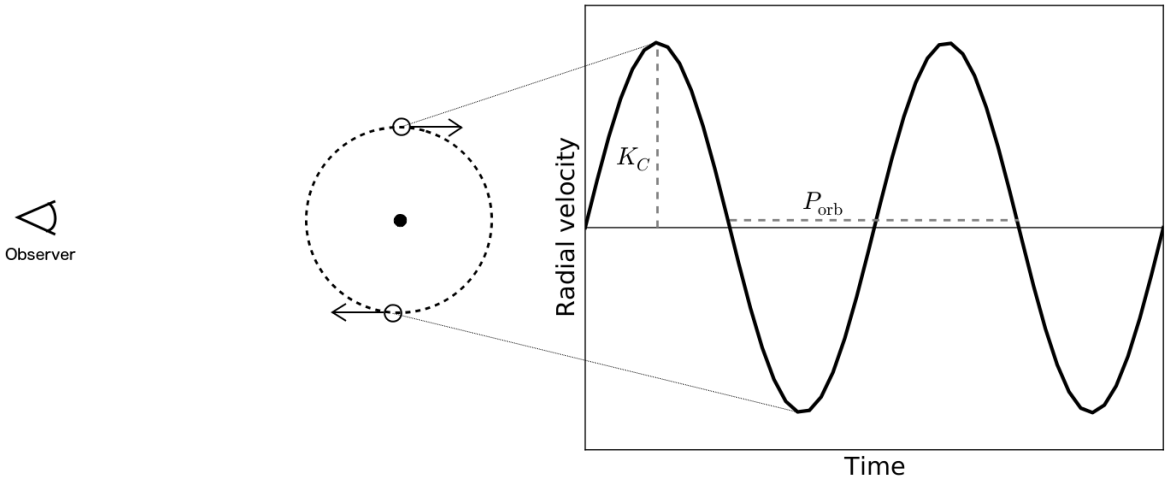

Figure 1.5: A theoretical radial velocity curve of a star orbiting around a BH. The orbital period ($P_{\rm orb}$) and the semi-amplitude (K_C) can be measured from the radial velocity curve.

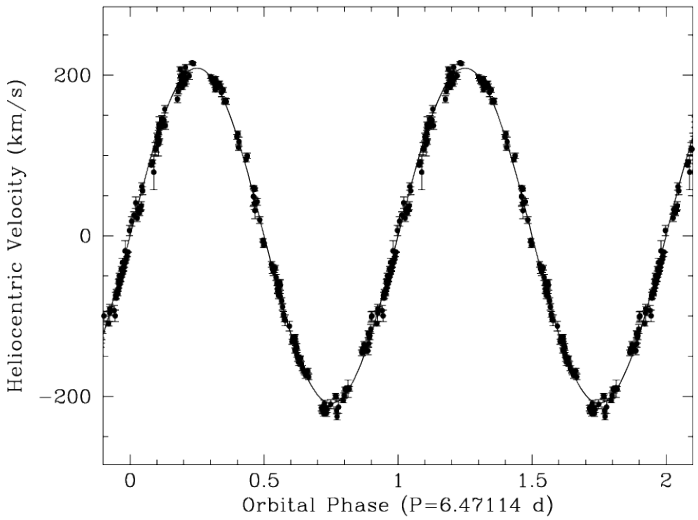

Figure 1.6: The radial velocity curve of the donor star of V404 Cyg (Casares & Jonker 2014).

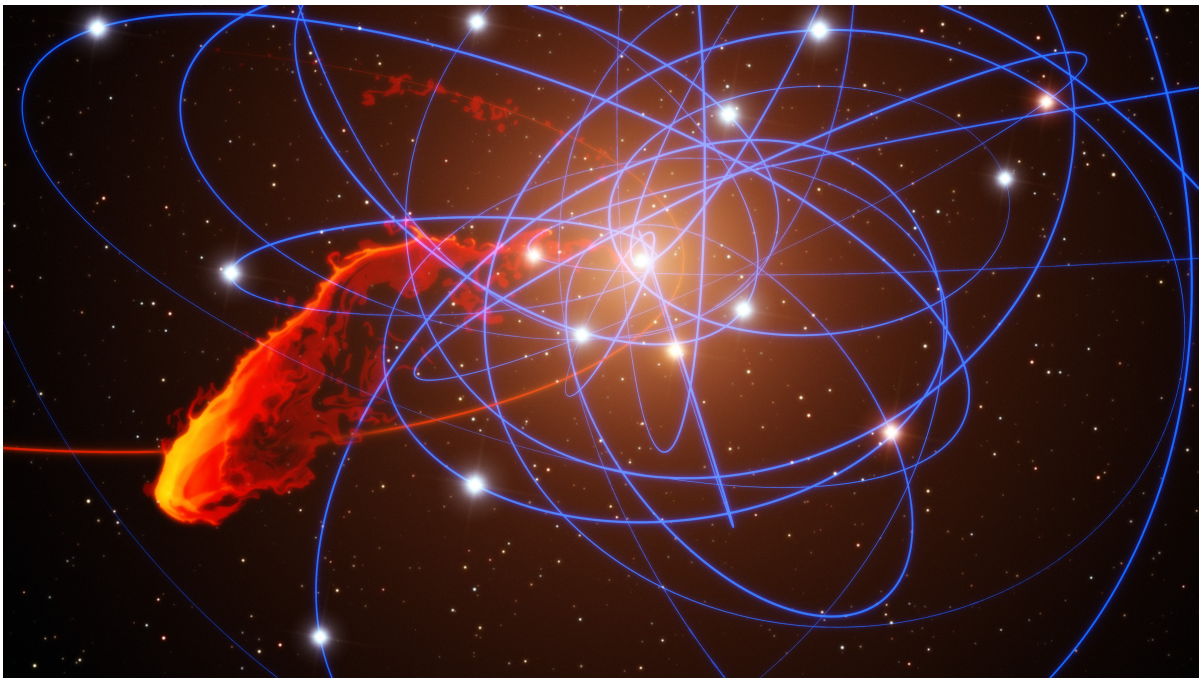

Figure 1.7: Simulation of the orbits of stars around the central SMBH in the Milky Way (blue lines). This artist impression also shows the trajectory of a gas cloud (red line) that was recently discovered close to the SMBH. Image credits: ESO/MPE/Marc Schartmann.

radial velocity measurements this yields the full 3-D information of the stellar orbits, and a mass for the SMBH of $\approx 4 \times 10^6\ M_\odot$ (Ghez et al. 2008; Gillessen et al. 2009, Figure 1.7).

For SMBHs in nearby ($D \lesssim 20$ Mpc) galaxies, it is possible to measure global properties of the stars within the sphere of influence of the BH, such as the surface brightness profile and radial velocity distribution. The BH mass can then be inferred from modelling of stellar dynamics to best match these observables (see e.g. Ferrarese & Ford 2005 for a review).

1.5.2 Other methods

There are several other methods to measure SMBH masses, such as reverberation mapping and the use of scaling relations such as the $M_{\rm BH} - \sigma$ and the $M_{\rm BH} - L_{\rm bulge}$ relations (Blandford & McKee 1982, see Peterson 2014 for an overview and more references). However, these are of little relevance for mass measurements of BHs in ULXs.

There is one relation that is potentially valid for sources across the entire range of BH masses: the so-called fundamental plane of black hole activity (Merloni et al. 2003; Falcke et al. 2004). The fundamental plane is a relation between the radio luminosity, X-ray luminosity and mass of a BH:

$$\log M_{BH} = (1.638 \pm 0.070) \log L_R - (1.136 \pm 0.077) \log L_X - (6.86 \pm 0.79) \qquad (1.3)$$

(Miller-Jones et al. 2012), and can be used to infer the mass of the BH if the radio and X-ray luminosities are measured (quasi-)simultaneously. The relation is only valid for BHs in the

low/hard state that have a compact radio jet. BHs transitioning from the low/hard to the intermediate or high/soft state also show (transient) radio jets, but do not follow the fundamental plane. This makes it impossible to use the relation to derive BH masses for ULXs that harbour stellar mass BHs, as they are accreting at or above their Eddington limit and are not in the low/hard state. However, ULXs that contain IMBHs can be in the low/hard state and for such sources, the fundamental plane can be a useful tool to estimate BH masses. Compact radio jets combined with a low/hard X-ray spectral state have only recently been detected in two ULXs: HLX-1 (Cseh et al. 2015) and NGC 2276-3c (Mezcua et al. 2015). Transient jet emission has been detected in more ULXs (e.g. Mezcua et al. 2013; Middleton et al. 2013; Cseh et al. 2014), but cannot be used to calculate BH masses.

1.6 Black hole masses in ULXs

Currently, the masses of the accretors in ULXs are still very uncertain. The best constrained mass is that of M82 X-2, of which we know that the accretor is a neutron star and hence has a mass $\leq 3\ M_{\odot}$ (Lattimer 2012). It may seem straightforward to apply the dynamical mass measurement method to ULXs, but in practice this has turned out to be fraught with complications.

In the first place, we know of no ULXs in the Milky Way, which means that we have to deal with large distances and hence faint sources. ULX candidates with very bright optical counterparts, that can be studied with 4 m class telescopes, were the obvious first candidates for spectroscopic studies. Most of them turned out to be background AGN (Gutiérrez & López-Corredoira 2005; Gutiérrez 2006; Gutiérrez & López-Corredoira 2007; Wong et al. 2008; Gutiérrez 2013; Sutton et al. 2015, see also Chapter 3). With the currently available telescopes, only the nearest ULXs (within ~ 5 Mpc or so) are suitable targets for optical spectroscopy.

Second, in order to get reliable results from dynamical mass measurements, we need to observe absorption lines from the atmosphere of the donor star. There are several bona fide ULXs with confirmed optical counterparts, but their spectra are often dominated by emission from the accretion disc (Grisé et al. 2012; Tao et al. 2012a; Sutton et al. 2014). The first attempts to measure the mass function in ULXs therefore used emission lines from the accretion disc. In principle this should be possible if the velocities of these emission lines reflect the velocity of the BH. However, due to variability in the disc, these lines do not always originate in the same place in the disc and this causes their radial velocity to vary erratically (Roberts et al. 2011; Liu et al. 2012), an effect well known from a long history of observations of Galactic XRBs (e.g. Orosz et al. 1994). Also, unless $M_{\rm donor} > M_{\rm BH}$, the orbital velocity of the BH will be small and hard to detect.

To date there are only two ULXs whose optical spectra show features from the donor star. The first one is M101 ULX1 (Liu et al. 2013). Its mass donor is most likely a Wolf-Rayet (WR) star, bright enough ($V = 23.5$) to observe spectroscopically with an 8 m telescope. Liu et al. (2013) obtained 10 spectra of this star with the Gemini-North telescope and the GMOS spectrograph and from the radial velocity curve that they measured, concluded that the orbital

period of the system is 8.2 days and that $M_{\rm BH} \geq 4.6 \pm 0.3\ M_{\odot}$, with a most likely mass of 20 – 30 $M_{\odot}$. Their radial velocity curve was not very well sampled, however, so that the orbital period determination hinges on only a few data points. A potentially bigger problem is that the WR features they used to measure radial velocities are emission lines. It is not yet clear where in the star these lines are formed. WR stars have strong outflows, and if the lines are formed in this wind, their radial velocities may vary due to variations in the wind speed and density.

The second ULX whose donor star was detected in optical spectra is P13 in NGC 7793 (Motch et al. 2014). In this ULX, the donor star is a blue supergiant, and Motch et al. (2014) detected absorption lines in its spectrum (taken with the Very Large Telescope [VLT] and FORS2 spectrograph). These absorption lines are formed in the atmosphere of the star and do not suffer from the same uncertainties as the emission lines in WR stars. However, X-ray heating of the donor star makes it impossible to use the absorption lines to measure a radial velocity curve. By modelling the effects of this X-ray heating that are visible in data from an extensive X-ray-UV-optical spectrophotometric monitoring campaign, Motch et al. 2014 constrain the mass of the BH to be less than 15 $M_{\odot}$, but they could not determine the mass function from the radial velocity curve.

1.7 Near-infrared observations

It has proven to be very difficult to measure BH masses in ULXs through optical spectroscopy, because of the reasons outlined above. One possible way around this is to use near-infrared (NIR) observations. The accretion discs that dominate most ULX spectra in the optical regime are hot and blue: their spectra are similar to those of O, B or A stars (Kaaret & Corbel 2009; Tao et al. 2011). A cool donor star, with a spectral energy distribution that peaks at NIR wavelengths, may outshine the disc in that part of the spectrum (Copperwheat et al. 2005, 2007).

Many ULXs are found near star-forming regions, and there is a clear connection between the star formation rate in a galaxy and the number of ULXs it contains (Swartz et al. 2009; Poutanen et al. 2013). This, combined with the fact that the mass transfer rate in ULXs needs to be high to sustain their high luminosities, has led to the idea that most ULX donor stars should be massive (super)giant stars. Because of the blue colours of many ULX counterparts it was originally believed that they were mostly blue supergiants. However, these colours are also consistent with emission from a hot accretion disc, and an (unknown) fraction of ULXs may very well contain red supergiant (RSG) donor stars.

If a ULX is formed from a binary system with two massive stars, one of which undergoes core-collapse to form a (stellar mass or massive stellar) BH, the donor star will start to transfer mass when it overflows its Roche lobe. If the orbital separation is small, this will happen while the donor is still a blue supergiant. In this case the donor star never reaches the RSG stage. If the orbital separation is large enough, the system will only become visible as a ULX once the donor star expands and starts overflowing its Roche lobe as a red supergiant.

Prior to this thesis, there had been several photometric studies of ULX counterparts at optical wavelengths (see for instance Ptak et al. 2006; Patruno & Zampieri 2008; Tao et al.

2011; Gladstone et al. 2013). However, only a handful of sources had been looked at in the NIR regime (e.g. M82 X-1: Ebisuzaki et al. 2001). Our survey of ULX counterparts at NIR wavelengths shows that $\sim 10\%$ of ULXs may have a RSG counterpart (see Chapter 4).

1.7.1 Excellent targets for dynamical mass measurements

Although ULXs with RSG donor stars may only constitute a small fraction of the ULX population, they are excellent targets for dynamical mass measurements. K- and M-type supergiants reach absolute magnitudes in the *H*- and *K*-band up to -10. The limiting magnitude for spectroscopy with 8 – 10 meter telescopes is around 20th magnitude in the *H*-band, which means we can observe these stars out to a distance of 10 Mpc.

RSGs are so luminous because they have very large radii, $R_\star \approx 100 - 1500\ R_\odot$; this in turn means they have to orbit at a large distance from the BH to fit inside their Roche radius, which means that heating of the star through X-ray radiation is not as important as for blue supergiants, that are much smaller and orbit closer to the BH (Copperwheat et al. 2005). It also means that the orbital periods expected for these systems are very long: for an RSG of 10 $M_\odot$ the orbital period varies from ~ 0.3 year (for $R_\star$ = 100 $R_\odot$) to ~ 18 years (for $R_\star$ = 1500 $R_\odot$), assuming the star fills its Roche lobe. If the BH is fed from the stellar wind rather than through Roche lobe overflow, as some have speculated, the orbital periods can be even longer. If the RSG is more massive than 10 $M_\odot$ the orbital periods are somewhat shorter, but still on the order of years. From an observational perspective this has both advantages and disadvantages. On the plus side, X-ray heating of the donor star is not important and we do not have to worry about smearing of absorption lines due to radial velocity variations within one observation, even if that observation lasts for hours. On the downside, of course, it takes a long time to measure the full radial velocity curve. In the *H*-band and *K*-band, RSG are easily recognizable because their spectra contain many absorption lines from neutral metals and deep CO-bandheads (see Figure 1.8). These can also be used to measure their radial velocities, as is shown in Chapters 5 and 6.

1.8 This Thesis

In this thesis we explore several aspects of the diverse group of sources that are ULXs, using X-ray, optical and near-infrared observations, with the objective of gaining insight in the masses of the accretors in these objects.

The small subgroup of HLXs are of great interest as these sources are good candidates to contain IMBHs. As only a handful of HLXs have been discovered, and only two have reliable distance measurements confirming that they are not background AGN or foreground objects, finding more of these sources is of great importance. In Chapter 2: *Discovery of a second outbursting hyperluminous X-ray source* we report the confirmation of CXO J1225 (Jonker et al. 2010) as a probable HLX with recurrent outbursts, that shows similarities with HLX-1.

Chapter 3: *VLT/FORS2 observations of four high-luminosity ULX candidates* describes the results of optical spectroscopic observations of four ULX candidates. We selected these

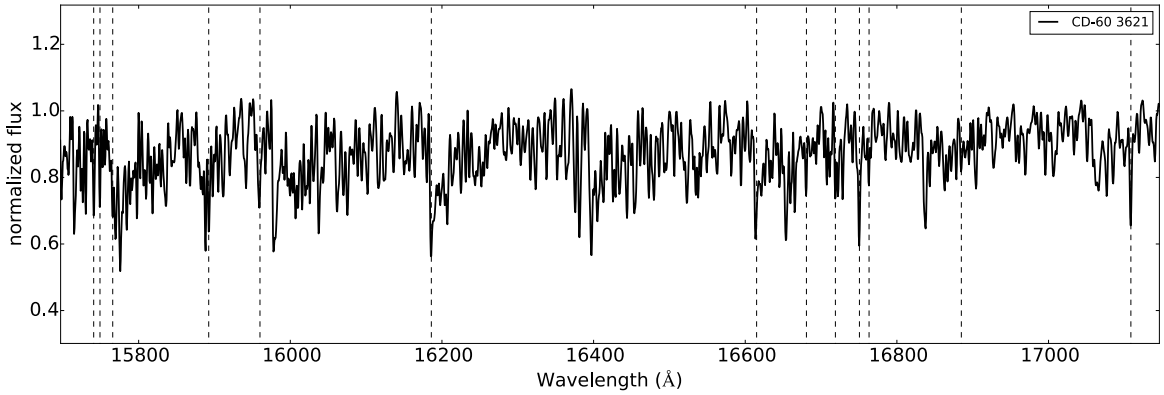

Figure 1.8: Part of the normalized *H*-band spectrum of CD-60 3621, a Galactic RSG, observed with VLT/X-shooter as part of the X-shooter Spectral Library (Chen et al. 2014). Many absorption lines are visible, mainly due to neutral metals and CO. Dashed lines indicate the positions of some lines that are generally used for diagnostic purposes — from left to right: Mg I triplet (1.574, 1.575, 1.577 μm), Si I (1.589 μm), Si I (1.596 μm), CO bandhead (1.62 μm), CO bandhead (1.66 μm), Si I (1.67 μm), Al I triplet (1.672, 1.675, 1.676 μm), OH (1.69 μm), Mg I (1.71 μm). The noise in this spectrum is at the level of 1%, so that all the visible features are real absorption lines.

for their high luminosities ($L_{\rm X} \geq 10^{40}$ erg s^{-1}) and the fact that their optical counterparts are bright and relatively isolated, so that optical spectroscopy from the ground, without the aid of adaptive optics, was feasible. Previous studies from several authors have found that ULX candidates with bright optical counterparts are predominantly background AGN. Even so, studying ULX candidates with bright counterparts is important, because an accreting IMBH in an extragalactic globular cluster would have the same appearance.

Since optical observations of ULX donor stars are hampered by emission from the accretion disc and X-ray irradiation of the donors, NIR observations may prove a valuable alternative. In Chapter 4: *Near-infrared counterparts of ultraluminous X-ray sources*, we report the results of the first survey of nearby ($D < 10$ Mpc) ULXs in the NIR. Using three ground-based telescopes (VLT in the Southern hemisphere, WHT and MMT in the North) we obtained *H*- and/or *Ks*-band images of 62 ULXs. 11 of those have counterparts with NIR properties consistent with those of RSGs. If confirmed spectroscopically, these could be excellent targets for dynamical mass measurements.

Chapters 5: *Discovery of a red supergiant counterpart to RX J004722.4-252051, a ULX in NGC 253* and 6: *Keck/MOSFIRE spectroscopy of five ULX counterparts* describe the NIR spectroscopic follow-up observations of six counterparts discovered in our survey. In Chapter 5 we describe our VLT/X-shooter and Magellan/MMIRS observations of RX J004722.4-252051 (J0047), a ULX in NGC 253. In Chapter 6 we report on our Keck/MOSFIRE *H*-band spectroscopic observations of five ULX counterparts: J022721+333500 and J022727+333443 in NGC 925, J120922+295551 and J120922+295559 in NGC 4136, and Ho II X-1.

CHAPTER 2

DISCOVERY OF A SECOND OUTBURSTING HYPERLUMINOUS X-RAY SOURCE

M. Heida, P. G. Jonker and M. A. P. Torres

Published in MNRAS: Letters, 454, 2015, p.L26-L30

Abstract

We report on six *Chandra* and one *HST*/WFC3 observation of CXO J122518.6+144545, discovered by Jonker et al. (2010) as a candidate hyperluminous X-ray source (HLX), X-ray bright supernova or recoiling supermassive black hole at $L_{\rm X} = 2.2 \times 10^{41}$ erg s^{-1} (if associated with the galaxy at 182 Mpc). We detect a new outburst of the source in a *Chandra* image obtained on Nov 20, 2014 and show that the X-ray count rate varies by a factor > 60. New *HST*/WFC3 observations obtained in 2014 show that the optical counterpart is still visible at g' = 27.1 ± 0.1, 1 ± 0.1 magnitude fainter than in the discovery *HST*/ACS observation from 2003. This optical variability strongly suggests that the optical and X-ray source are related. Furthermore, these properties strongly favour an HLX nature of the source over the alternative scenarios. We therefore conclude that CXO J122518.6+144545 is most likely an outbursting HLX. It is only the second such object to be discovered, after HLX-1 in ESO 243-49. Its high X-ray luminosity makes it a strong candidate to host an intermediate mass black hole.

2.1 Introduction

Intermediate mass black holes (IMBHs) are defined as objects with masses in between those of stellar mass and supermassive black holes (BHs; we use the mass range $10^2 - 10^5$ $M_{\odot}$for IMBHs; for a review see van der Marel 2004). In the λ cold dark matter cosmology with hierarchical structure formation IMBHs are important as possible seeds for supermassive BHs (SMBHs; Ebisuzaki et al. 2001). Scenarios to form IMBHs include direct collapse of gas in

atomic cooling haloes in the early Universe (e.g. Begelman et al. 2006; Ferrara et al. 2014), the collapse of extremely massive Pop III stars (e.g. Madau & Rees 2001) and merging of stars in the nuclei of dense star clusters (e.g. Portegies Zwart & McMillan 2002).

However, observational evidence for the existence of IMBHs is scarce. Dynamical studies searching for IMBHs in the centers of globular clusters have yielded inconsistent results (Lützgendorf et al. 2011; Lanzoni et al. 2013). Radio and X-ray observations have yielded no evidence for accreting IMBHs in globular clusters (Strader et al. 2012; Haggard et al. 2013). There is evidence for the presence of IMBHs with masses around 10^5 $M_\odot$ in the nuclei of dwarf galaxies (e.g. Greene & Ho 2007; Reines et al. 2013), although these mass determinations depend on extrapolating scaling relations established for SMBHs to lower BH masses.

Ultraluminous X-ray sources (ULXs) are off-nuclear X-ray sources with an X-ray luminosity $> 10^{39}$ erg s^{-1} (see Feng & Soria 2011 for a review). Assuming isospherical emission and if these sources are Eddington-limited they should contain BHs that are more massive than ordinary stellar mass BHs. Detailed X-ray spectra have revealed that many ULXs are in a so-called ultraluminous state (Gladstone et al. 2009; Sutton et al. 2013) that may be a sign of super-Eddington accretion. These ULXs probably contain stellar mass BHs. For a handful of ULXs there is dynamical evidence for a stellar mass BH (Liu et al. 2013; Motch et al. 2014) and the detection of X-ray pulsations from M82 X-2 proves that that system contains a neutron star (Bachetti et al. 2014).

However, the most luminous ULXs, often referred to as hyperluminous X-ray sources (HLXs), are still strong candidates to host IMBHs. The best example is HLX-1 in ESO 243-49 (Farrell et al. 2009; Webb et al. 2010). This is the brightest HLX known to date; it shows outbursts reminiscent of those in Galactic X-ray binaries, but with a peak luminosity of 10^{42} erg s^{-1} (Godet et al. 2009; Servillat et al. 2011). This luminosity is hard to explain if the accretor is a stellar mass BH (but see King & Lasota 2014; Lasota et al. 2015). The outbursts are possibly related to a donor star in a very eccentric orbit that transfers mass when it passes pericentre (Lasota et al. 2011; Godet et al. 2014). Other HLXs containing candidate IMBHs include M82-X1 (peak X-ray luminosity $\sim$ 10^{41} erg s^{-1}, Strohmayer & Mushotzky 2003; Kaaret et al. 2009; Pasham et al. 2014) and NGC2276-3c (peak X-ray luminosity $\sim 6 \times 10^{40}$ erg s^{-1}, Mezcua et al. 2015).

Jonker et al. (2010) reported the discovery of a luminous off-nuclear X-ray source (CXO J122518.6+144545; hereafter CXO J1225) in the galaxy SDSS J122518.86+144547.7 (hereafter SDSS J1225). The X-ray source was discovered in an archival 5 ks *Chandra* observation taken in 2008. A blue optical counterpart was detected in an *HST*/ACS image of the field, with $g' = 26.4 \pm 0.1$ and $z' > 25.7$. Assuming CXO J1225 is at the same distance as the galaxy ($z = 0.0445 \pm 0.0001$, 182 Mpc, Adelman-McCarthy et al. 2007), its 0.3 – 8 keV luminosity in this observation was 2.2×10^{41} erg s^{-1}, making it one of the most luminous ULXs known to date. Alternative explanations proposed by Jonker et al. (2010) were a recoiling SMBH as a result of the merger of two SMBHs or a Type IIn supernova.

To determine which of these scenarios is correct, we obtained new *Chandra* and *HST* observations of CXO J1225 in 2012 and 2014. We describe these observations, the analysis and results in Section 2. In Sections 3 and 4, we discuss the different scenarios and present our conclusions. All errors quoted in this Letter are 1–σ errors unless otherwise specified. We

Table 2.1: Journal of the *Chandra*/ACIS-S observations of CXO J1225 used in this Letter. The last column represents the unabsorbed flux. The count rate and flux columns list the 95% confidence interval calculated following Gehrels (1986).

Obs. ID	Date (UT)	MJD	Exp. time (ks)	Counts	Count rate (10^{-4} cts s^{-1})	Flux (0.5 – 10 keV) (10^{-15} erg cm^{-2} s^{-1})
8055	2008 Feb 19	54515.69	5.09	22	30 – 60	33 – 70
13295	2012 Nov 26	56257.80	9.78	0	0 – 3	0 – 4
16476	2014 Apr 28	56775.84	18.87	3	0.4 – 4	0.5 – 5
16477	2014 Jul 22	56860.86	19.85	0	0 – 2	0 – 2
15783	2014 Nov 20	56981.93	19.85	20	7 – 15	8 – 20
17558	2014 Dec 08	56999.85	19.78	4	0.7 – 5	0.8 – 5
17559	2014 Dec 15	57006.50	39.59	0	0 – 0.8	0 – 0.9

assume a standard cosmology with $H_0 = 73$ km s^{-1} Mpc^{-1}.

2.2 Observations, analysis and results

2.2.1 *Chandra*

We obtained one 10 ks *Chandra*/Advanced CCD Imaging Spectrometer (ACIS) (Garmire et al. 2003) observation of CXO J1225 in 2012 and five (4×20 ks and one 40 ks observation) in 2014 (see Table 2.1). These observations were done using ACIS-S in very faint mode. We reprocess the events with calibrations available in CALDB version 4.6.7, using version 4.7 of the *Chandra* X-ray centre CIAO tools (Fruscione et al. 2006). In all observations, we extract the source counts in a circular region with radius $2''$. For the background subtraction region we use an annulus centred on the source position with an inner radius of $5''$ and an outer radius of $20''$.

We detect the source in the observations with Obs. ID 16476, 15783 and 17558. In the observations with Obs. ID 13295, 16477 and 17559 the source is not detected (zero counts). We calculate 95% confidence limits for the count rates in these observations following Gehrels (1986) — for comparison we also calculated limits following Kraft et al. (1991), but we find that the differences are negligible. The count rates of the detections and upper limits of the non-detections, including the original detection in archival data from 2008, are listed in Table 2.1.

Of the 20 counts in observation 15783, several are detected above 2 keV. We use XSPEC version 12.8.2 and C-statistics (cstat; Cash 1979) modified to account for the subtraction of background counts, the so called W-statistics[1], to fit models to the data. We find that both a power law and a disc blackbody can describe the data. For the power law, we find a photon index $\Gamma = 1.4 \pm 0.5$, with a cstat value of 19.8 using 19 bins and 17 degrees of freedom. For a

[1] see http://heasarc.gsfc.nasa.gov/docs/xanadu/xspec/manual/

disc blackbody we find a temperature of 0.6 ± 0.1 keV, with a cstat value of 21.8 using 19 bins and 17 degrees of freedom. To ease comparison with Jonker et al. (2010), we assume a standard power law with photon index $\Gamma = 1.7$, a Galactic hydrogen column density $N_{\rm H} = 2.8 \times 10^{20}$ cm^{-2} (Dickey & Lockman 1990) and no local absorption to describe the spectrum.

We convert the detected count rates to (unabsorbed) fluxes in the 0.5-10 keV range using WEBPIMMS, the web version of PIMMS (Mukai 1993). The confidence intervals listed in Table 2.1 only take into account the uncertainties in the count rates, not the (unknown) additional uncertainty introduced by the model. To convert fluxes to luminosities we assume that the flux is isotropic and that CXO J1225 is at the distance of SDSS J1225 (182 Mpc). The highest luminosity that CXO J1225 reached in these new observations is 5×10^{40} erg s^{-1}, on 2014 November 20 (see Figure 2.1).

We align and stack all observations, using the point source at Right Ascension (R.A.) = 12:25:08.93, Declination (Dec) = 14:46:01.04 in observation 17559 for alignment, to search for X-ray emission from the nucleus of SDSS J1225. The total exposure time of the stacked image is 127.72 ks. In this deep image we detect eight counts in a circle with a radius of $1''$ centred on the position of the nucleus of SDSS J1225 (R.A. = 12:25:18.86, Dec = 14:45:47.7 [J2000], Abazajian et al. 2009). Assuming a power law with index 1.7 and $N_{\rm H} = 10^{21}$ cm^{-2} we find an unabsorbed $0.5 - 10$ keV flux of 8×10^{-16} erg cm^{-2} s^{-1} (absorbed flux = 7×10^{-16} erg cm^{-2} s^{-1}). At a distance of 182 Mpc this translates to a luminosity of 3×10^{39} erg s^{-1}.

Count rate in quiescence

The strongest limit on the count rate of CXO J1225 when it is in the low state is set by the 40 ks observation (17559), at $< 8 \times 10^{-5}$ cts s^{-1} ($L_{\rm X} < 3 \times 10^{39}$ erg s^{-1}). This is still consistent at the 95% confidence level with the count rates observed in observations 16476 and 17558, although alternately either one or both of these observations may have caught CXO J1225 fading after an outburst, in which case the quiescent level could be (much) lower.

Assuming the count rate is constant over observations 13295, 16476, 16477, 17558 and 17559 at a value so that only occasionally, because of Poisson fluctuations, three or four source counts are detected, we calculate the most likely value of the count rate in the following way. For a range of count rates ($10^{-5} - 5 \times 10^{-4}$ cts s^{-1}) we calculate the expected number of source counts in each observation. Then, taking into account the expected number of background counts and assuming both source and background follow a Poisson distribution, we calculate the probability to retrieve the observed number of counts in each observation. For each assumed count rate we then multiply the probabilities found for the five observations. We find that this value is maximal for a count rate of 5×10^{-5} cts s^{-1} ($L_{\rm X} \approx 2.5 \times 10^{39}$ erg s^{-1}).

If we repeat this calculation but without observation 17558 (as this detection could plausibly be due to a fading outburst) we find a most probable count rate of 2×10^{-5} cts s^{-1} ($L_{\rm X} \approx 10^{39}$ erg s^{-1}).

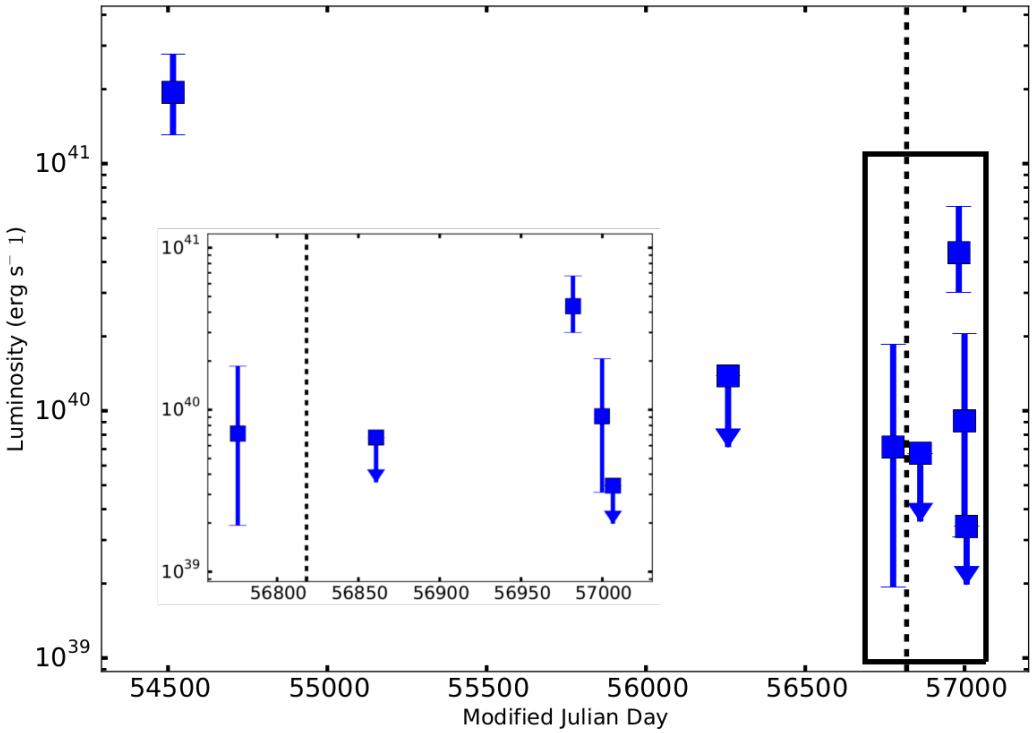

Figure 2.1: The 2008-2014 X-ray light-curve of CXO J1225. Blue squares are *Chandra* observations (detections with 95% confidence intervals and 95% confidence upper limits), the black dashed line indicates the date of our *HST*/WFC3 observation. The inset is zoomed-in on the 2014 data points, showing the decay of the outburst detected in November.

2.2.2 *HST*

On 2014 June 10 we obtained four dithered *HST*/Wide Field Camera 3 (WFC3) observations of CXO J1225 using the UVIS detector with the F475W (g'-band) filter (data set ICEF01010). The total exposure time is 2512 s. The optical counterpart that was reported by Jonker et al. (2010) is clearly visible in the multidrizzled image.

We use the WFC3 package (version 2.0) of DOLPHOT (version 2.0, Dolphin 2000) for the photometric analysis. Following the DOLPHOT/WFC3 user guide we run DOLPHOT on the flat-fielded, bias corrected *flt* images, excluding the ICEF01ohq frame because there is a cosmic ray hit close to the position of CXO J1225. We first process the *flt* files with *wfc3mask* to mask bad pixels. Then we split the multi-extension fits files into single extension files with *splitgroups* and calculate the sky background for each of them with *calcsky*. Finally we run *dolphot* to calculate the photometry. We use the parameter values recommended for WFC3/UVIS in the user guide. After trying several settings for the sky fitting we find that FitSky=1 and SkipSky=1 give the best results. The counterpart is significantly detected in all frames and has a g'-band magnitude of 27.1 ± 0.1 (Vega magnitude system; 27.0 ± 0.1 in AB magnitude). This corresponds to an absolute magnitude in the g'-band of -9.2 at the distance to SDSS J1225.

We follow the same procedure with the archival *HST*/ACS g'-band observation (data set J8FS34020, taken on 2003 June 16) using the ACS package (version 2.0) of DOLPHOT, excluding the J8FS34eqq frame because of a cosmic ray hit at the position of CXO J1225. We use the parameter values recommended for ACS in the user guide, with FitSky=1 and SkipSky=1. The counterpart is significantly detected at g'= 26.1 ± 0.1 (Vega magnitude system; 26.0 ± 0.1 in AB magnitude), corresponding to an absolute g'-band magnitude of -10.2 at the distance of SDSS J1225. This is 0.3 mag (3σ) brighter than the magnitude reported by Jonker et al. (2010). This difference is probably due to updated zeropoints and CTE corrections in the DOLPHOT ACS package.

We compare the magnitudes of six stars that are in the field of view of both the ACS and WFC3 observations and find that they are consistent with being constant within 2–σ, with an average difference between the ACS and WFC3 images of 0.07 ± 0.05 mag. Hence the difference of 1 ± 0.1 mag between the two epochs is not due to our use of different DOLPHOT packages or different settings for the photometric analysis, but to intrinsic variability of the source.

2.3 Discussion

We have collected new X-ray and optical data of CXO J1225, reported by Jonker et al. (2010) as a candidate HLX, recoiling SMBH or extremely X-ray bright SN. From the six new X-ray observations, we learn that the source varies by at least a factor 60 in count rate. After the initial detection in August 2008 at a luminosity of 2.2×10^{41} erg s^{-1}, CXO J1225 went undetected in a 10 ks observation in November 2012. In three 20 ks observations in 2014, the source is first barely detected at $7^{+4}_{-5} \times 10^{39}$ erg s^{-1} in April, then not detected in July, then brightens again to be detected at $(5 \pm 2) \times 10^{40}$ erg s^{-1} on November 20. Follow-up observations on December

8 (20 ks) and 15 (40 ks) show a rapid decline of the source luminosity to $< 3 \times 10^{39}$ erg s^{-1} (see Figure 2.1).

In our new *HST*/WFC3 image taken on 2014 June 10 the optical counterpart identified by Jonker et al. (2010) is still visible, but 1 ± 0.1 mag fainter in the g'-band than in the first *HST*/ACS image taken in 2003. The *HST* observations were not simultaneous with X-ray observations. The *HST*/ACS observation precedes the first *Chandra* observation by five years, so we do not know whether CXO J1225 was in outburst or not at that time. In 2014 *Chandra* observations were done ~ 6 weeks before and after the *HST* observation. The marginal detection (three counts) in April could either indicate the tail of an outburst that had completely faded at the time of the non-detection in July, or be the result of a random fluctuation of the quiescent flux. In either case it seems reasonable to assume that CXO J1225 was in a low state at the time of the second *HST* observation. If the 2003 observation was taken during an outburst, that would explain why the optical counterpart was brighter at that time than in the 2014 observation.

2.3.1 Supernova, recoiling BH or HLX?

With these new data we can determine which explanation for CXO J1225 is the most likely. The supernova scenario can be discarded — it is ruled out by the X-ray variability and the fact that the optical counterpart is still visible. The short time-scale of the X-ray variability rules out the possibility that CXO J1225 is a background AGN. This was already unlikely because of the blue colour of the counterpart and the high X-ray-to-optical flux ratio of the source (Jonker et al. 2010).

With the current data we cannot exclude the possibility that CXO J1225 is a recoiling massive BH, although — assuming that the outburst reaches the Eddington luminosity — the highest luminosity we have detected so far seems rather low for a supermassive BH. The detection of an X-ray source that is positionally consistent with the nucleus of SDSS J1225 casts further doubts on the recoiling BH scenario, as it seems to imply the presence of an SMBH in the centre of the galaxy. However, the luminosity of the X-ray source is low enough to be consistent with a low mass X-ray binary (LMXB) in the nuclear region of SDSS J1225.

2.3.2 Foreground object

Can CXO J1225 be a foreground object? It is located in the direction of the Virgo cluster and the elliptical galaxy NGC 4377 is at a distance of $1.5'$. If CXO J1225 is located at the distance of NGC 4377 (18 Mpc; Villegas et al. 2010), its peak X-ray luminosity would be $\sim 10^{39}$ erg s^{-1}, and it could be an outbursting LMXB in a globular cluster in the halo of NGC 4377. However, the limit on the absolute magnitude of the optical counterpart argues against this scenario. Based on the 2003 *HST*/ACS observations Jonker et al. (2010) report a limit on the z'-band magnitude of the counterpart of $z' > 25.7$. At 18 Mpc, this corresponds to an absolute z'-band magnitude > -5.5. This is fainter than any of the globular clusters in the Virgo cluster, and LMXBs are generally detected in the brighter globular clusters with $M_{z'} < -7$ (Sivakoff et al. 2007).

Another possibility is that CXO J1225 is a halo LMXB in NGC 4377 or an intra-cluster LMXB in Virgo, although currently no intra-cluster LMXBs are known. The absolute g'-band magnitude at that distance would be -5.2 for the brightest observation. Galactic LMXBs have been observed to reach $M_V \approx -4.0$ during outburst (cf. van Paradijs & McClintock 1994), so this would have to be an unusually bright LMXB.

If CXO J1225 were located in the halo of the Milky Way its maximum X-ray luminosity would be $\sim 10^{33}$ erg s^{-1} (assuming a distance of 10 kpc). This could be consistent with a very faint X-ray transient (cf. Heinke et al. 2015). However, the optical counterpart is more than 3 mag fainter than known optical counterparts to such sources (cf. Heinke et al. 2009).

Of the different foreground object scenarios for CXO J1225, a very bright LMXB in the halo of NGC 4377 or in the intra-cluster medium in the Virgo cluster is the only one not ruled out by the data, although it would stretch the parameter space of known LMXBs.

2.3.3 The second outbursting HLX

Taking all these considerations into account, the most likely scenario is that CXO J1225 is a bona fide HLX located in SDSS J1225. Its peak luminosity of 2.2×10^{41} erg s^{-1} makes it one of the most luminous HLXs known to date.

For the interpretation of the observations that clearly fall outside the outbursts, i.e. the non-detections and the detections with three or four counts, one can envisage two scenarios. First, one or both of the detections of a few counts can be seen as evidence for a decaying outburst. Especially for observation 17558 this seems a plausible scenario, as we know that an outburst occurred shortly before that observation. Secondly, all these (non-)detections can be due to random fluctuations of a source that has a luminosity such that the count rate lies just below our detection threshold.

We have seen evidence for two outbursts of CXO J1225, and the April 2014 detection might indicate the tail of another outburst. If the optical variability is connected to the outbursts, the ~ 1 mag brightening in the 2003 *HST* observation may indicate another one. The only other HLX that is known to show outbursts at such high luminosity is HLX-1. In that source, the X-ray flux varies by a factor ~ 50, and the V-band magnitude of its optical counterpart varies by ~ 1 mag over an outburst (Webb et al. 2014). These values are comparable to the ones we find for CXO J1225. The outbursts of HLX-1 occur with a recurrence time of $\sim 360 - 370$ days, although the last three outbursts were delayed by several weeks to months (Godet et al. 2014; Kong et al. 2015). We do not have sufficient data points to detect a recurrence pattern in the outbursts of CXO J1225.

The duration of the outbursts of CXO J1225 is poorly constrained. From our November-December 2014 observations we know that the source decays from 5×10^{40} erg s^{-1} to less than 3×10^{39} erg s^{-1} in three weeks, but we do not know what the peak luminosity was during that outburst, nor when it started. The quiescent luminosity of CXO J1225 is $\lesssim 3 \times 10^{39}$ erg s^{-1}. This is a factor ten fainter than the luminosity of HLX-1 in its low state (Servillat et al. 2011).

A strong indication for the presence of an IMBH in HLX-1 is the fact that its spectral state changes during its outbursts, in a similar fashion to Galactic LMXBs (Godet et al. 2009;

Servillat et al. 2011). Finding similar state changes during outbursts of CXO J1225 would confirm it as a strong IMBH candidate. However, in the observations we have obtained so far we do not detect enough counts to constrain the spectral shape during outburst and we have not yet detected CXO J1225 at all in quiescence.

2.4 Conclusions

New *Chandra* and *HST* observations of CXO J1225 show that the source is most likely a HLX with recurrent outbursts. This is only the second source for which such behaviour has been detected, after HLX-1. CXO J1225 is less luminous than HLX-1 and decays on a shorter time-scale. More observations are needed to determine whether its outbursts show a recurrence pattern similar to HLX-1. The characteristics of CXO J1225 make it a very interesting candidate IMBH.

Acknowledgements

We would like to thank T. Maccarone for interesting discussions and the anonymous referee for their useful and detailed comments that helped improve the Letter. The results reported in this Letter are based on observations made by the *Chandra* X-ray Observatory and the *Hubble Space Telescope*. We thank the *Chandra* X-ray Center's director Belinda Wilkes for granting us Director's Discretionary Time observations of CXO J1225.

CHAPTER 3

VLT/FORS2 OBSERVATIONS OF FOUR HIGH-LUMINOSITY ULX CANDIDATES[1]

M. Heida, P. G. Jonker, M. A. P. Torres, T. P. Roberts, G. Miniutti, A. C. Fabian and E. M. Ratti

Published in MNRAS, 433, 2013, p.681-687

Abstract

We obtained VLT/FORS2 spectra of the optical counterparts of four high-luminosity ($L_X \geq 10^{40}$ erg s^{-1}) ULX candidates from the catalogue of Walton et al. (2011b). We first determined accurate positions for the X-ray sources from archival *Chandra* observations and identified counterparts in archival optical observations that are sufficiently bright for spectroscopy with an 8 meter telescope. From the spectra we determine the redshifts to the optical counterparts and emission line ratios. One of the candidate ULXs, in the spiral galaxy ESO 306-003, appears to be a bona fide ULX in an H II region. The other three sources, near the elliptical galaxies NGC 533 and NGC 741 and in the ring galaxy AM 0644-741, turn out to be background AGN with redshifts of 1.85, 0.88 or 1.75 and 1.40 respectively. Our findings confirm the trend of a high probability of finding background AGN for systems with a ratio of $\log(F_X/F_{opt})$ in the range of -1 – 1.

3.1 Introduction

Ultraluminous X-ray sources (ULXs) are off-nuclear X-ray sources in galaxies with an X-ray luminosity above the Eddington luminosity of a 10 $M_\odot$ black hole, or $\sim 10^{39}$ erg s^{-1}. Several scenarios have been proposed to explain their high luminosities. Geometrical (King et al., 2001) or relativistic (Körding et al., 2002) beaming may allow for the observation of

[1]Observations based on ESO programme 088.B-0076A

super-Eddington luminosities. In some sources there is evidence for a new state with truly super-Eddington accretion rates (Gladstone et al., 2009). Recent investigations into the X-ray luminosity function (XLF) of ULXs suggest that the majority of ULXs are formed by the high-luminosity tail of X-ray binaries (XRBs) and contain stellar mass black holes (BHs) (Swartz et al., 2011; Mineo et al., 2012). The best-fitting XLF exhibits a cut-off around 10^{40} erg s^{-1}, suggesting that this may be the effective upper limit for the luminosity of the most massive objects in the sample.

However, Swartz et al. (2011) argue that if they extrapolate their best-fitting XLF, based on a complete sample of ULXs within 14.5 Mpc, to larger distances, they can not explain the relatively large number of ULXs with luminosities above 10^{41} erg s^{-1} that have been observed. Hence these ULXs may belong to a different class of objects. These sources would have to exceed the Eddington limit by more than a factor 100 if they contained stellar mass black holes. They may be good candidates to host the predicted but thus far elusive intermediate mass black holes (IMBHs). These IMBHs may form in the collapse of a dense stellar cluster (Portegies Zwart & McMillan, 2002), the collapse of population III stars in the early universe (Madau & Rees, 2001) or the direct collapse of massive gas clouds (Begelman et al., 2006). They may reside in globular clusters (Maccarone et al., 2007), but conclusive evidence for their existence there has not yet been found. For a review on IMBHs and their formation mechanisms see van der Marel (2004). The best candidate for an IMBH to date is the extremely bright source HLX-1 in ESO 243-49, which reaches maximum X-ray luminosities of $\sim 10^{42}$ erg s^{-1}(Farrell et al., 2009). The recent work by Sutton et al. (2012) provides more evidence for extreme ULXs as IMBHs.

Most ULX candidates are discovered by searching for off-nuclear X-ray point sources in galaxies (e.g. from the *Chandra* or XMM-*Newton* serendipitous source catalogues; see for example Walton et al. 2011b; Liu 2011). The ULX catalogues compiled in this way are contaminated with objects that also show up as off-nuclear, bright X-ray sources but are not accreting IMBHs or stellar mass BHs. Background active galactic nuclei (AGN) and quasars are obvious examples, but some X-ray bright supernovae (most likely Type IIn, Immler & Lewin 2003) and active foreground stars may also contaminate the catalogs. One way to identify these contaminants if the ULX candidate has a bright optical counterpart is to take an optical spectrum. If emission or absorption lines are present the redshift to the source can be measured. In this way we can determine whether the source is associated with the galaxy or is a background or foreground object (compare e.g. Gutiérrez 2013).

If the X-ray source is associated with the galaxy, optical spectra can give us additional information to classify the object. Some ULXs (Pakull & Mirioni, 2002; Kaaret & Corbel, 2009) are surrounded by bubbles of ionized gas, which can act as calorimeters and as such tell us if the emission is strongly beamed or not. The intensity ratios of the emission lines from these regions provide information on the source of the ionizing radiation, e.g. whether they are shock ionized or X-ray photo-ionized (e.g. Abolmasov et al. 2007).

We selected four high-luminosity ($L_X \geq 10^{40}$ erg s^{-1}) ULX candidates from the catalogue of Walton et al. (2011b) with accurate positions that we measured using archival *Chandra* observations and optical counterparts that are sufficiently bright for optical spectroscopy. Two of the ULX candidates are situated in elliptical galaxies (NGC 533 and NGC 741). ULX can-

Table 3.1: The *Chandra* observations of the four ULX candidates.

Galaxy	Obs. ID	Exp. time (kiloseconds)	Source on CCD	Off-axis angle (arcmin)	Obs. date (UT)
NGC 533	2880	38.1	ACIS S3	0.85	2002-07-28
NGC 741	2223	30.74	ACIS S3	2.74	2001-01-28
AM 0644-741	3969	39.97	ACIS S3	0.57	2003-11-17
ESO 306-003	4994	22.75	ACIS I3	6.60	2004-03-10

Notes: *Chandra* observation ID number, exposure time in kiloseconds, CCD on which the source was detected, the off-axis angle of the source in arcminutes and the observation date.

didates in elliptical galaxies have a higher chance to be background AGN (39%, compared to 24% for all sources in the catalogue of Walton et al. (2011b)). On the other hand, IMBHs may form in dense (globular) clusters (Portegies Zwart & McMillan, 2002; Miller & Hamilton, 2002) and the optical counterparts to these ULX candidates could well be just that, making them interesting targets for further investigation. AM 0644-741 is a ring galaxy with a ULX candidate situated in between the nucleus and the ring. ESO 306-003 is a spiral galaxy with a ULX in the outer edge of the disk, apparently associated with an extended optical source. We obtained optical spectra of these four sources with the FOcal Reducer and low dispersion Spectrograph (FORS2) mounted on the Very Large Telescope (VLT) (Appenzeller et al., 1998). The observations and data reduction steps are described in Section 2; Section 3 contains the results. In Section 4 we discuss our findings.

3.2 Observations and data reduction

3.2.1 X-ray observations

We use archival *Chandra* observations to get exact source positions for the ULX candidates in NGC 533, NGC 741, AM 0644-741 and ESO 306-003. Table 3.1 lists the details of all observations.

We use CIAO version 4.4 to process the *Chandra* observations, with the calibration files from caldb version 4.5.0. We treat the *Chandra* observations as follows: first we update the event files with *acis_process_events*, then we use *wavdetect* to find the position of the ULX candidate. Sources within $3'$ of one of the ACIS aimpoints have a 90% confidence error circle around the absolute position with a radius of $0.6''$; this is valid for the ULX candidates in NGC 533, NGC 741 and AM 0644-741. The candidate in ESO 306-003 has 25 counts and was observed at $6.6'$ off-axis, which means it has a 95% confidence error circle with a radius of $\sim 1.5''$ (Hong et al., 2005). For the sources in NGC 533, NGC 741 and AM 0644-741 we extract the source counts in a circle with 6 pixel radius (90% encircled energy fraction) around the source positions using *specextract*. For the ULX candidate in ESO 306-003 we use a circle with a radius of 10 pixels to get the same encircled energy fraction, since it was observed at

Table 3.2: The positions and unabsorbed 0.2 – 12 keV X-ray fluxes of the ULX candidates.

Source name	Host galaxy	Right Ascension	Declination	Source flux (erg cm^{-2} s^{-1})
CXOU J012533.3+014642	NGC 533	01:25:33.63	+01:46:42.6	$2.9 \pm 0.2 \times 10^{-14}$
CXOU J015616.1+053813	NGC 741	01:56:16.14	+05:38:13.2	$2.5 \pm 0.3 \times 10^{-14}$
CXO J064302.2-741411	AM 0644-741	06:43:02.24	−74:14:11.1	$3.5 \pm 0.2 \times 10^{-14}$
ESO 306-003 ULX	ESO 306-003	05:29:07.21	−39:24:58.4	$2.4 \pm 0.4 \times 10^{-14}$

Notes: the positions of the ULX candidates in NGC 533, NGC 741 and AM 0644-741 are accurate to within $0.6''$ (90% confidence level), for the source in ESO 306-003 this value is $1.3''$. We fit the fluxes assuming an absorbed powerlaw with photon index 1.7 and $N_H = 3 \times 10^{20}$ cm^{-2} for consistency with the method used by Walton et al. (2011b).

$6.6'$ off-axis. As background regions we use circles with 80 pixel radius on the same CCD but not containing any sources. We use XSPEC version 12.6.0 to fit an absorbed powerlaw (pegpwrlw) to the data in the 0.3 – 8 keV range. We then extrapolate to get the 0.2 – 12 keV flux to compare this with the values reported by Walton et al. (2011b). For consistency we adopt the same model parameters: a photon index of 1.7 and $N_H = 3 \times 10^{20}$ cm^{-2}, and allow only the flux to vary. We find that all *Chandra* fluxes are consistent with those from XMM-*Newton* as reported by Walton et al. (2011b). The positions of the X-ray sources and their fluxes are summarized in Table 3.2.

3.2.2 Optical images and photometry

To find the optical counterparts of the ULX candidates we use archival optical observations of their host galaxies. NGC 533 and NGC 741 were observed as part of the Sloan Digital Sky Survey (SDSS), and we use the SDSS r'-band images to identify the optical counterparts to the ULX candidates in these galaxies (Figure 3.1). There is no photometric information for the source in NGC 533, so we use the aperture photometry tool in GAIA to estimate the r'-band magnitude. SDSS does provide u', g', r', i' and z' magnitudes for the object in NGC 741, but these are incorrect because the source is too close to the edge of the frame. Therefore we also use GAIA to estimate the r'-band magnitude for this source. For both optical counterparts we find that $r' = 21 \pm 1$.

The *Hubble Space Telescope* (*HST*) archive contains several observations of AM 0644-741 made with the Advanced Camera for Surveys (ACS). We use the V-band (F555W) image with exposure identifier j8my05o2q, observed on 2004, January 16, with an exposure time of 2200 seconds (see Figure 3.1). We visually compare the position of point sources from the USNO CCD Astrograph Catalog (UCAC) 3 (Zacharias et al., 2009) with their counterparts in the *HST* image and find that the astrometric calibration of the image does not need to be improved. The ULX candidate has a counterpart that is in the DAOPHOT source list of this

HST image in the Hubble Legacy Archive (HLA[2]). It has a V-band magnitude of 21.79 ± 0.05.

We identify the optical counterpart to the ULX candidate in ESO 306-003 in a 480 seconds R-band observation made on 2004, January 25 UT with VLT/VIMOS that we retrieved from the ESO archive. Its R-band magnitude is approximately 21, with the caveat that this is an extended source in a region with a very high background level due to the galaxy, which means that this measurement is not very accurate. We also obtained a g'-band, 120 seconds exposure of this galaxy in our VLT/FORS2 run (see Figure 3.2), of which we visually inspected the astrometric solution by comparing the positions of bright stars with those in the UCAC 3.

3.2.3 Optical spectroscopy

We obtained VLT/FORS2 observations of NGC 741 (3×1800 s), AM 0644-741 (3×1800 s) and ESO 306-003 (2×2700 s) on 2011, December 3 UT under programme 088.B-0076A using the GRIS_600V grism and a $1''$ slit width. This configuration covers the wavelength range 4430 – 7370 Å with a dispersion of 0.74 Å/pixel, yielding a resolution of 4.25 Å for the $1''$ slit (measured at 6300 Å). This allows us to observe the Hα, [N II] complex and the Hβ and [O III] lines if the sources are located at the same distance as their apparent host galaxies, with high enough resolution to separate them. The night was photometric so we also observed several spectrophotometric standard stars to perform a flux calibration. The seeing varied from 0.7 – $1.1''$. The spectra of NGC 533 (3×1500 s) were made in service mode on 2012, January 16 UT with the GRIS_300V+10 grism and a $0.5''$ slit width, giving a wavelength coverage from 4450 – 8700 Å with a dispersion of 1.68 Å/pixel and a spectral resolution of 6.4 Å for the $0.5''$ slit (measured at 6300 Å). The seeing varied during the night and we have no observations of spectrophotometric standards.

To reduce the spectra we use the STARLINK software package FIGARO and the PAMELA package developed by Tom Marsh[3]. We follow the steps outlined in the PAMELA manual to extract the spectra, using Keith Horne's optimal extraction algorithm (Horne, 1986). We then use the software package MOLLY, also by Tom Marsh[3], to perform the wavelength calibration and, for the data taken on 2011, December 3, the flux calibration. We do not correct for telluric absorption. Because we have multiple spectra of each source we average them to get a better signal-to-noise ratio. The two observations of ESO 306-003 were taken under varying seeing conditions. Because of this the continuum level is different in the two spectra, so we normalize these spectra before averaging them. We use MOLLY's *mgfit* task to fit Gaussian profiles to the emission lines in the spectra to determine the full width at half maximum (FWHM) of the lines and the redshift to the sources.

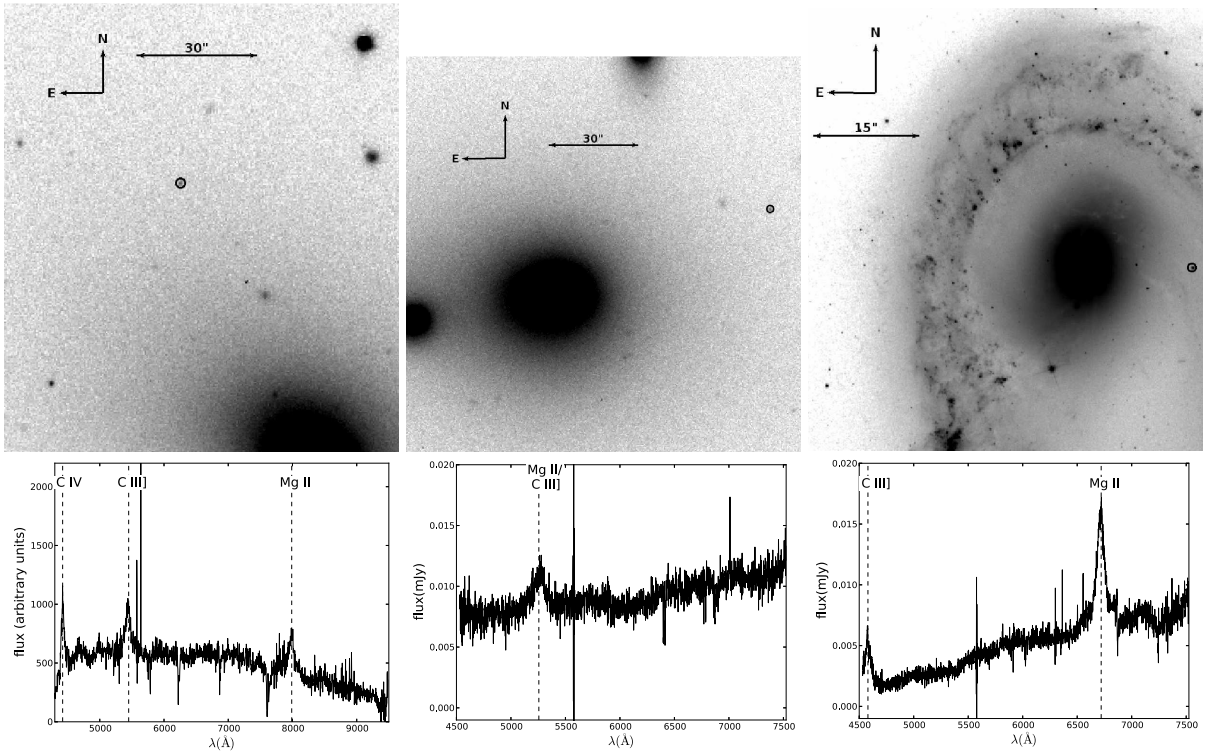

Figure 3.1: The finders and FORS2 spectra of the three ULX candidates that are background AGN. The 90% confidence error circles around the X-ray positions have a radius of $0.6''$, for NGC 533 and NGC 741 we plot a larger circle for visual clarity. *Left:* The SDSS *r'*-band image of NGC 533 with a $1.2''$ radius circle around the *Chandra* position of the ULX candidate and the spectrum in which the C IV, C III] and Mg II emission lines, redshifted by $z = 1.85$, are marked. The absorption features at 6200 Å are caused by interstellar absorption, and those at 6900 Å and 7600 Å are telluric in origin. *Middle:* The SDSS *r'*-band image of NGC 741 with a $1.2''$ radius circle around the *Chandra* position of the ULX candidate and the spectrum of the optical counterpart. The marked emission line can be either Mg II $\lambda 2798$ line redshifted by $z = 0.88$ or C III] at $z = 1.75$. *Right:* An *HST* ACS V-band image of AM 0644-741 with the $0.6''$ radius error circle around the *Chandra* position of the ULX candidate, and the spectrum with the Mg II and C III] lines, redshifted by $z = 1.40$, marked.

Table 3.3: Source properties of the background AGN

Apparent host galaxy	z	Line	FWHM km/s	Log(F_X/F_{opt})
NGC 533	1.8549 ± 0.0003	CIV	2300 ± 70	0.0 ± 0.5
		CIII]	7800 ± 200	
		Mg II	5700 ± 200	
NGC 741	0.8786 ± 0.0006 or	Mg II or	8400 ± 200	0.0 ± 0.5
	1.7535 ± 0.0009	C III]		
AM 0644-741	1.3993 ± 0.0001	C III]	5100 ± 70	0.7 ± 0.1
		Mg II	4220 ± 40	

Notes: Lines used for the redshift determination to the quasars, their FWHM in km/s and the X-ray-to-optical flux ratio of these sources. The X-ray-to-optical flux ratios are calculated using the XMM-*Newton* 0.2 – 12 keV fluxes from Walton et al. (2011b) and the *r'*-band (for NGC 533 and NGC 741) or V-band (for AM 0644-741) optical fluxes.

3.3 Results

3.3.1 NGC 533

NGC 533 is the dominant elliptical galaxy in a group with the same name at $z = 0.0185$ (Smith et al., 2000). The ULX candidate is located at $78''$ from the center of the galaxy that has a semi-minor axis of $90''$ (based on the D25 isophote, Nilson 1973). The X-ray source has an unresolved optical counterpart that is visible in the image of the SDSS, with $r' \approx 21$. Figure 3.1 shows the galaxy with the position of the ULX candidate and the FORS2 spectrum of the source.

Three broad emission lines are visible. We identify these as CIV, C III] and Mg II at $z = 1.8549 \pm 0.0003$. This proves the ULX candidate to be a background AGN, not associated with NGC 533. The 0.2 – 12 keV X-ray luminosity calculated for this source by Walton et al. (2011b) was $(2 \pm 1) \times 10^{40}$ erg s^{-1}, assuming a distance to the ULX of 73.8 Mpc. The true distance to this source is 4730 Mpc (using $H_0 = 75$ km/s/Mpc for consistency with Walton et al. 2011b), which gives this AGN an X-ray luminosity of $(7 \pm 4) \times 10^{43}$ erg s^{-1} using the flux as measured with XMM-*Newton*.

3.3.2 NGC 741

NGC 741 is an elliptical galaxy located at $z = 0.0185$ with a (D25) semi-major axis of $92.7''$ (de Vaucouleurs et al., 1991). The ULX candidate is located $78''$ West of the center of NGC 741 and has a counterpart that is unresolved in the SDSS image. Its r'-band magni-

[2]http://hla.stsci.edu

[3]http://deneb.astro.warwick.ac.uk/phsaap/software

tude is ~ 21. Figure 3.1 shows the SDSS r'-band image of NGC 741 with the position of the ULX candidate and the FORS2 spectrum of the counterpart.

The spectrum shows one broad emission line, with a FWHM of 147 Å. We cannot say with certainty which line this is. The most likely options are that it is either the Mg II $\lambda 2798$ line or the C III] $\lambda 1909$ line. In the first case this ULX candidate would be a background AGN at a redshift of $z = 0.8786 \pm 0.0006$ with an X-ray luminosity of $(1.6 \pm 0.6) \times 10^{43}$ erg s^{-1}. In the second case it would be at $z = 1.7535 \pm 0.0009$, with $L_X = (4.2 \pm 1.5) \times 10^{43}$ erg s^{-1}. In both cases the source is not a ULX but a background AGN, unconnected to NGC 741.

3.3.3 AM 0644-741

AM 0644-741 is a ring galaxy at $z = 0.022$ that shows signs of recent interaction with a smaller galaxy (Few et al., 1982; Lauberts & Valentijn, 1989). The ULX candidate in this galaxy is located in between the core of the galaxy and the ring. A point-like object with a V-band magnitude of 21.8 is visible at the position of the X-ray source in archival *HST* images (see Figure 3.1).

The FORS2 spectrum of the counterpart shows two emission lines that we identify as Mg II and C III] at $z = 1.3993 \pm 0.0001$. This ULX candidate is another background AGN with an 0.2 – 12 keV luminosity of $(8.1 \pm 0.8) \times 10^{43}$ erg s^{-1}.

3.3.4 ESO 306-003

The spiral galaxy ESO 306-003, at $z \approx 0.016$ (Couto da Silva & de Souza, 2006), contains a ULX candidate that is located on the edge of the spiral structure (see Figure 3.2). An optical source is visible on the edge of the error circle. Visual inspection shows the profile of the counterpart to be more extended than that of point sources in the same image, but because of the high background level and steep gradient it is not possible to perform an acceptable fit to the profile. The full width at half maximum (FWHM) of point sources in this image (provided by the seeing) is $0.8''$. At the distance of ESO 306-003 this yields a lower limit to the size of the source of 240 pc. The two spectra that we obtained of this source show slightly different line ratios and continuum levels (for example, the Hβ/Hα ratio changes by 10%). This can be explained by seeing variations if the optical counterpart to this source is extended: then slit losses can cause the small changes in the line ratios if there are intrinsic spatial variations in the line ratios in the extended source.

The spectrum is similar to that of an H II region, with narrow Hydrogen emission lines and strong forbidden lines. The redshift of the lines equals that of the center of the galaxy, indicating that if the X-rays are associated with this optical source, this is a bona fide ULX with a luminosity of $1.4 \pm 0.3 \times 10^{40}$ erg s^{-1} based on the XMM-*Newton* flux measured by Walton et al. (2011b). The X-ray flux is constant between the XMM-*Newton* and *Chandra* observations. The X-ray-to-optical flux ratio of the source is $\log(F_X/F_{opt}) = 0.3 \pm 0.5$, based on the XMM-*Newton* 0.2 – 12 keV flux from Walton et al. (2011b) and the r'-band flux. The line ratios, especially the [O I] $\lambda 6300$/Hα ratio, place the source among the transition objects in the diagnostic diagrams of Ho (2008) (see Figure 3.3). The He II $\lambda 4686$ emission line has been

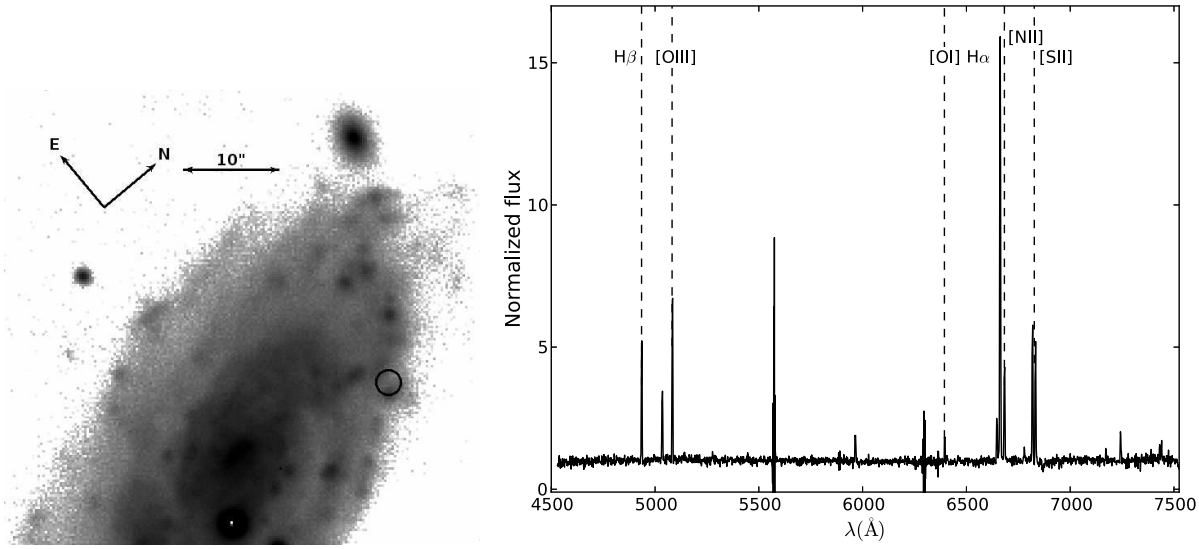

Figure 3.2: *Left:* The FORS2 g'-band acquisition image of ESO 306-003 with the $1.3''$ radius (90% confidence) error circle around the position of the ULX candidate. *Right:* The FORS2 spectrum of the candidate optical counterpart to the X-ray source. Several emission lines, redshifted by $z = 0.016$, are marked.

detected in several ULX nebulae (Pakull & Mirioni, 2002; Kaaret & Corbel, 2009), but we do not detect it here, possibly because the sensitivity of the detector drops off steeply towards the blue end. The 2-σ upper limit for the equivalent width of this line is 1.0 Å. This corresponds to a flux of $\sim 10^{-17}$ erg cm^{-2} s^{-1} or a luminosity of $\sim 5 \times 10^{36}$ erg s^{-1}.

3.4 Discussion

We obtained VLT/FORS2 spectra of the optical counterparts of four bright ULX candidates with accurate positions obtained by us from archival *Chandra* observations. Two of these are located in elliptical galaxies NGC 533 and NGC 741. Another candidate is situated in AM 0644-741, a ring galaxy that recently interacted with a small elliptical galaxy, and in the spiral galaxy ESO 306-003. Three of our four targets turn out to be background AGN with X-ray luminosities ranging from 1 – 8 $\times 10^{43}$ erg s^{-1}; one (in ESO 306-003) seems to be a bona fide ULX.

The fraction of background AGN in our sample is higher than the fraction estimated by Walton et al. (2011b) for their catalogue. Although this can be due to small number statistics since we only investigate four sources, it is in line with results from other spectroscopic studies of ULX candidates. Optical spectroscopy of a sample of 23 ULX candidates in total yielded 20 background AGN and three foreground stars (Gutiérrez & López-Corredoira 2005; Gutiérrez 2006; Gutiérrez & López-Corredoira 2007; Gutiérrez 2013). Another study that targeted 17 ULX candidates from the catalogue of Colbert & Ptak (2002) found that 15 were background AGN and the other two objects were foreground stars Wong et al. (2008).

All these studies mainly target ULX candidates that are relatively isolated and have a bright

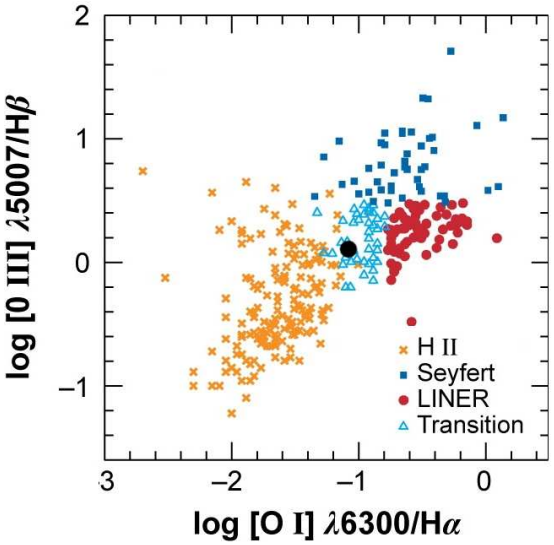

Figure 3.3: [O I] λ6300/Hα versus [O III] λ5007/Hβ line ratios for H II regions, AGN (LINERs and Seyferts) and transition objects (figure adapted from Ho 2008). The black dot represents the line ratios for the ULX in ESO 306-003.

optical counterpart, a selection effect induced by the relative ease with which spectroscopic observations can be carried out for these sources. Sources located in crowded areas, like the spiral arms of late type galaxies, are more difficult targets for ground based optical spectroscopic observations. This means that spectroscopic studies are aimed at ULX candidates that have a low X-ray-to-optical flux ratio and that are situated relatively far away from their suspected host galaxies. As the authors of these previous papers also note, these selection criteria introduce a bias towards background AGN.

A possible method to select ULX candidates that are most likely to be real ULXs is to calculate the expected contribution of background sources based on the known density of AGN in X-ray and optical observations (López-Corredoira & Gutiérrez 2006; Sutton et al. 2012). Alternatively it may be possible to use the X-ray-to-optical flux ratios of ULX candidates to select targets for future spectroscopic studies. All our sources have X-ray-to-optical flux ratios $\log(F_X/F_{opt})$ in the range between -1 and 1, typical for AGN (e.g. Barger et al. 2003). Most ULXs show values for $\log(F_X/F_{opt})$ ranging from 2 – 3 (Tao et al. 2011, 2012a; Sutton et al. 2012). The low value that we find for the ULX in ESO 306-003 can be explained if we assume that we do not resolve the ULX counterpart but instead observe the optical flux of the entire H II region that it resides in, thus lowering $\log(F_X/F_{opt})$.

However, if we were to select candidates for spectroscopy on the basis of their X-ray-to-optical flux ratios only we run the risk of missing interesting sources. For instance, ULXs may display different values for $\log(F_X/F_{opt})$ when observed in the high and low states, as was shown for M101 ULX-1 and M81 ULS1 (Tao et al. 2011). For both sources $\log(F_X/F_{opt})$ is between 2 and 3 during the high state, but around 0 during the low state, well inside the range of optical to X-ray flux ratios found for AGN. Therefore other source properties should be

taken into account as well, such as galaxy morphology, the distance of the ULX to its apparent host galaxy and the absolute magnitude of its optical counterpart. The source in AM 0644-741 is a good example of a candidate with such favorable properties: situated in a ring galaxy, which is a strong sign of a recent interaction phase that triggered star formation, often linked to ULXs (e.g. Swartz et al. 2004), and close to the center of its apparent host galaxy, decreasing the chance that it is a background AGN (Wong et al. 2008). It has an optical counterpart of such magnitude that it is consistent with being a bright globular cluster if it is at the distance of AM 0644-741. Nevertheless our optical spectrum showed it to be a background object.

The ULX in ESO 306-003

The X-ray source in ESO 306-003 is the only one of the four candidates in our sample that appears to be a bona fide ULX. The extended nature of the source is confirmed by the fact that the emission line spectrum is consistent with that of an H II region. However, the [O I]/Hα ratio indicates that some of the ionizing flux could come from an X-ray source. Potentially, we have found a ULX embedded in an H II region. Another possibility is that this ULX candidate is a background AGN shining through an H II region in ESO 306-003. The X-ray-to-optical flux ratio is similar to that of the other AGN in our sample, so we would expect to see a contribution of redshifted emission lines from the AGN in the optical spectrum. The fact that we do not detect this makes this scenario implausible.

We find a 2-σ upper limit for the flux of a HeII $\lambda4686$ line of 10^{-17} erg cm^{-2} s^{-1}. This corresponds to an upper limit to the luminosity in the line of $\sim 5 \times 10^{36}$ erg s^{-1}. The presence of this line would be a strong indication of ionization by an X-ray source. We can compare this upper limit with the strength of the HeII $\lambda4686$ line in other ULX nebulae. For Holmberg II X-1, Pakull & Mirioni (2002) report a luminosity of 2.5×10^{36} erg s^{-1}. Kaaret & Corbel (2009) report a flux for this line from the ULX in NGC 5408 of 3.3×10^{-16} erg cm^{-2} s^{-1}, which translates to a luminosity of 9×10^{35} erg s^{-1} at the distance to NGC 5408 (4.8 Mpc, Karachentsev et al. 2002). Both these ULXs have an X-ray luminosity of $\sim 10^{40}$ erg s^{-1} — similar to ESO 306-003 — and a HeII $\lambda4686$ to X-ray luminosity ratio of $\sim 10^{-4}$. If the same is true for ESO 306-003 then we would expect a HeII $\lambda4686$ flux of a few times 10^{-18} erg cm^{-2} s^{-1}, which is just below our 2-σ upper limit. New observations of this source with greater sensitivity at the wavelength of the HeII $\lambda4686$ line are needed to determine if the nebula is X-ray photo-ionized or not.

Acknowledgements

PGJ and MAPT acknowledge support from the Netherlands Organisation for Scientific Research. GM acknowledges support from the Spanish Plan Nacional de Astronomía y Astrofísica under grant AYA2010-21490-C02-02. This research is based on observations made with ESO Telescopes at the La Silla Paranal Observatory under programme ID 088B-0076A. This research has made use of software provided by the *Chandra* X-ray Center (CXC) in the application package CIAO and of the software package MOLLY provided by Tom Marsh.

CHAPTER 4

NEAR-INFRARED COUNTERPARTS OF ULTRALUMINOUS X-RAY SOURCES

M. Heida, P. G. Jonker, M. A. P. Torres, E. Kool, M. Servillat, T. P. Roberts, P. J. Groot, D. J. Walton, D.-S. Moon and F. A. Harrison

Published in MNRAS, 442, 2014, p.1054-1067

Abstract

In this paper we present the results of the first systematic search for counterparts to nearby ultraluminous X-ray sources (ULXs) in the near-infrared (NIR). We observed 62 ULXs in 37 galaxies within 10 Mpc and discovered 17 candidate NIR counterparts. The detection of 17 out of 62 ULX candidates points to intrinsic differences between systems that show and those that do not show infrared emission. For six counterparts we conclude from the absolute magnitudes and — in some cases — additional information such as morphology and previously reported photometric or spectroscopic observations, that they are likely background active galactic nuclei or ULXs residing in star clusters. Eleven counterparts have absolute magnitudes consistent with them being single red supergiant stars. Alternatively, these systems may have larger accretion discs that emit more NIR light than the systems that we do not detect. Other scenarios such as emission from a surrounding nebula or from a compact radio jet are also possible, although for Holmberg II X-1 the NIR luminosity far exceeds the expected jet contribution. The eleven possible red supergiant counterparts are excellent candidates for spectroscopic follow-up observations. This may enable us to measure the mass function in these systems if they are indeed red supergiant donor stars where we can observe absorption lines.

4.1 Introduction

Ultraluminous X-ray sources (ULXs) are point-like, off-nuclear X-ray sources with an X-ray luminosity above 10^{39} erg s^{-1} (Feng & Soria, 2011), the Eddington luminosity of a $\sim$10 $M_{\odot}$ black hole. The most luminous example reaches 10^{42} erg s^{-1} (HLX-1, Farrell et al. 2009). Several scenarios have been proposed to explain the high luminosities of these sources. Geometrical beaming could boost the observed luminosity by up to a factor $\sim$ 10 (King et al. 2001). Genuine super-Eddington accretion is another option (Begelman, 2002; Moon et al., 2003). Alternatively, if these systems contain black holes that are more massive than 100 $M_{\odot}$ (which is our working definition of intermediate mass black holes, IMBHs), that would naturally explain the high luminosities.

Observations indicate that ULXs at lower and higher luminosity may belong to different populations. The luminosity functions of ULXs and fainter extra-galactic X-ray binaries show a break around 2×10^{40} erg s^{-1} (Swartz et al. 2011; Mineo et al. 2012). At luminosities below this break, the identification of an 'ultraluminous' X-ray spectral state (e.g., Gladstone et al. 2009) added observational support to the idea that the majority of these ULXs are stellar-mass black holes accreting at super-Eddington rates, which are rarely observed in Galactic black hole X-ray binaries for reasons currently unknown. Alternatively, for a low-metallicity star it is possible to leave a black hole of $\lesssim 70$ $M_{\odot}$ (Belczynski et al., 2010). Accretion onto such a black hole could explain ULXs with luminosities up to a few times 10^{40} erg s^{-1} (Zampieri & Roberts, 2009). In this scenario only the brightest ULXs, with X-ray luminosities $\gtrsim 2 \times 10^{40}$ erg s^{-1}, remain as plausible IMBH candidates. Such a seemingly convincing case for an IMBH is provided by the ULX ESO 243-49 X-1 (Farrell et al., 2009).

Ultimately, the most reliable way to determine the nature of ULXs is to obtain dynamical mass measurements of their black hole masses using radial velocity curves of their companion stars, as well as measurements of the system inclination and binary mass ratio. Dynamical mass measurements of Galactic binary systems usually rely on optical spectroscopic observations of the motion of the companion star. Unfortunately, most attempts to use the same technique for ULXs have not met with success (c.f. Roberts et al. 2011; Liu et al. 2012; Cseh et al. 2013a, however, see the recent work of Liu et al. 2013). The reason for this failure is that most optical counterparts to ULXs are faint, and, in the cases where it has been possible to perform spectroscopic studies, the spectra show strong emission lines from the accretion disc, the irradiated companion star and/or from the surrounding nebulae but no absorption features from a stellar component. The emission lines can not be used for reliable dynamical mass measurements because their radial velocities vary erratically and on timescales that may be unrelated to the orbital period of the system.

Searches for photospheric lines from the donor stars in ULXs have thus far concentrated on the blue part of the spectrum because ULX donor stars were expected to be blue supergiants. This expectation is based on the fact that many ULXs are located in or near young star clusters (e.g. Fabbiano et al. 2001; Roberts et al. 2002; Gao et al. 2003; Swartz et al. 2009; Voss et al. 2011) and on the blue colours of many ULX counterparts (e.g. Roberts et al. 2001; Liu et al. 2002). However, these blue colours are also consistent with emission from an irradiated accretion disc (Soria et al., 2012; Grisé et al., 2012). And if ULX donor stars are indeed

massive young stars, some of them may very well be Wolf-Rayet stars (like the counterpart to M 101 ULX-1, Liu et al. 2013) or red supergiants (Copperwheat et al. 2005, 2007; Patruno & Zampieri 2008).

Red supergiant (RSG) stars are intrinsically bright in the NIR ($M_V \sim -6$, $V - H \sim 4$, $H - K \sim 0$) in contrast with the blue supergiants ($M_V \sim -6$, $V - -H \sim 0$, $H - -K \sim 0$; Elias et al. 1985; Drilling & Landolt 2000), and can outshine the accretion disc in that part of the spectrum. A Galactic analog is GRS1915+105, a black hole X-ray binary with a red giant companion star (not an RSG) with an orbital period of 33.5 days. A dynamical mass measurement of the black hole in this system was obtained from radial velocity studies in the NIR while the source was bright in X-rays, showing that irradiation of the companion star has little effect on long orbital period systems like this (Steeghs et al., 2013). A Roche-lobe overflowing red supergiant would have an even larger orbit than the red giant in GRS1915+105, so irradiation is not likely to produce strong effects in the companion atmosphere (Copperwheat et al. 2005, 2007). With the largest telescopes currently available, it is possible to perform time-resolved spectroscopy for sources with H- and K-band magnitudes up to ~ 20. This corresponds to the typical apparent magnitude of an RSG at a distance of ~ 10 megaparsec (Mpc).

In this paper we present the results of our search for candidate RSG companions to ULXs within 10 Mpc. The sample consists of sources from several catalogues of ULX candidates. We describe the sample in Section 2, the observations in Section 3 and the data reduction in Section 4. The results, including a table summarizing all detected counterparts and limiting magnitudes for the non-detections, can be found in Section 5. In Section 6 we discuss our findings.

4.2 Sample

Our sample consists mainly of ULX candidates from the catalogues of Swartz et al. (2004, 2011) and Walton et al. (2011b), supplemented with additional targets from other sources (see Tables 4.1 and 4.2). We only targeted ULX candidates within a distance of 10 Mpc, since this is the maximum distance at which it is still viable to take a NIR spectrum of an RSG with existing large telescopes. ULX candidates in very crowded regions, such as edge-on spiral galaxies and fields close to galactic centers, were excluded from the sample.

Five candidates had no reported accurate X-ray positions when we started our observing campaign. For these sources we determined an accurate X-ray position based on archival *Chandra*/ACIS observations. We used the CIAO task *acis_process_events* to reprocess the event files if the observations were conducted in very faint mode (Fruscione et al., 2006). Then we determined accurate positions for the ULX candidates using *wavdetect*. The sources and *Chandra* observation ID's are listed in Table 4.3. For the other sources X-ray positions and uncertainties were taken from the literature (see Table 4.1). Quoted error radii on the source location are at the 95% confidence level (2-σ).

The complete sample consists of 62 ULX candidates in 37 galaxies. We have collected recent distance measurements for these galaxies where available to compute absolute magni-

tudes and absolute magnitude limits for the NIR counterparts, assuming they are at the same distance as their host galaxies (see Table 4.4). These are generally different from the distance measurements used to compile catalogues of ULX candidates. For example, Walton et al. (2011b) use only distances from Tully (1988). Comparing these to the newer distance measurements showed that if there are significant differences, these older measurements generally underestimate the distance. Hence the true X-ray luminosities of these sources only go up with the new distance measurements and all sources in our sample are still ULX candidates.

Table 4.1: The ULX candidates of which we obtained NIR images, with their designation from Simbad, their best determined X-ray position with the radius of the 95% confidence error circle, and the catalogue ('this work' for sources for which we determined the position) and satellite that provided the position.

Galaxy	ULX name (SIMBAD)	R.A. (h:m:s)	Dec. (d:m:s)	Error	Source	Satellite
NGC 253	RX J004722.4-252051	00:47:22.59	-25:20:50.9	$1.0''$	Liu 2011	*Chandra*
NGC 253	RX J004742.5-251501	00:47:42.76	-25:15:02.2	$1.0''$	Liu 2011	*Chandra*
M74	[KKG2005] M74 X-1	01:36:51.06	15:45:46.8	$0.7''$	Liu 2011	*Chandra*
M74	XMMU J013636.5+155036	01:36:36.5	15:50:36.3	$0.8''$	Lin et al. 2012	XMM-*Newton*
NGC 855	[SST2011] J021404.08+275239.5	02:14:04.09	27:52:39.4	$1.0''$	Liu 2011	*Chandra*
NGC 925	[SST2011] J022721.52+333500.7	02:27:21.52	33:35:00.8	$1.0''$	Liu 2011	*Chandra*
NGC 925	[SST2011] J022727.53+333443.0	02:27:27.53	33:34:42.9	$1.0''$	Liu 2011	*Chandra*
NGC 1058	XMMU J024323.5+372038	02:43:23.27	37:20:42.1	$0.7''$	this work	*Chandra*
NGC 1313	RX J0318.3-6629	03:18:20.00	-66:29:10.9	$1.0''$	Liu 2011	*Chandra*
IC342	XMMU J034555.6+680455	03:45:55.61	68:04:55.3	$0.25''$	Feng & Kaaret 2008	*Chandra*
IC342	[SST2011] J034615.64+681112.2	03:46:15.61	68:11:12.8	$0.4''$	Lin et al. 2012	XMM-*Newton*
NGC 1637	[IWL2003] 68	04:41:32.97	-02:51:26.8	$1.0''$	Liu 2011	*Chandra*
NGC 2403	CXOU J073625.6+653539	07:36:25.55	65:35:40.0	$0.7''$	Swartz et al. 2004	*Chandra*
NGC 2403	2E 0732.2+6546	07:37:02.33	65:39:35.0	$0.7''$	this work	*Chandra*
NGC 2500	[SST2011] J080148.10+504354.6	08:01:48.11	50:43:54.6	$1.0''$	Liu 2011	*Chandra*
NGC 2500	CXO J080157.8+504339	08:01:57.84	50:43:39.4	$1.0''$	Liu 2011	*Chandra*
Holmberg II	Holmberg II X-1	08:19:28.99	70:42:19.4	$0.7''$	Swartz et al. 2004	*Chandra*
NGC 2903	CXOU J093206.2+213058	09:32:06.19	21:30:58.9	$0.6''$	Rosen et al. 2015	XMM-*Newton*
Holmberg I	[WMR2006] Ho I XMM1	09:41:30.15	71:12:35.7	$1.0''$	Rosen et al. 2015	XMM-*Newton*
Holmberg I	1WGA J0940.0+7106	09:39:59.44	71:06:40.2	$1.0''$	Rosen et al. 2015	XMM-*Newton*
Holmberg I	[WMR2006] Ho I XMM3	09:42:06.36	71:04:40.0	$1.4''$	Rosen et al. 2015	XMM-*Newton*
M81	[LM2005] NGC 3031 ULX1	09:55:32.95	69:00:33.6	$1.0''$	Liu 2011	*Chandra*
Holmberg IX	Holmberg IX X-1	09:57:53.31	69:03:48.1	$1.0''$	Liu 2011	*Chandra*

Continued on next page

Table 4.1 – *Continued*

Galaxy	ULX name (SIMBAD)	R.A. (h:m:s)	Dec. (d:m:s)	Error	Source	Satellite
NGC 3184	CXOU J101812.0+412421	10:18:12.05	41:24:20.7	$0.7''$	Swartz et al. 2004	*Chandra*
NGC 3239	[SST2011] J102506.98+170947.2	10:25:06.98	17:09:47.2	$1.0''$	Liu 2011	*Chandra*
NGC 3239	[SST2011] J102508.20+170948.3	10:25:08.20	17:09:48.4	$1.0''$	Liu 2011	*Chandra*
NGC 3486	XMMU J110022.4+285818	11:00:22.27	28:58:16.9	$0.7''$	this work	*Chandra*
NGC 3521	[SST2011] J110545.62+000016.2	11:05:45.63	00:00:16.5	$1.0''$	Liu 2011	*Chandra*
NGC 3621	[GSE2009] B	11:18:15.16	-32:48:40.6	$0.7''^{\dagger}$	Gliozzi et al. 2009	*Chandra*
NGC 3623	[LB2005] NGC 3623 ULX1	11:18:58.54	13:05:30.9	$1.0''$	Liu 2011	*Chandra*
NGC 3627	[SST2011] J112020.90+125846.6	11:20:20.89	12:58:46.0	$1.0''$	Liu 2011	*Chandra*
NGC 3627	[SST2011] J112018.32+125900.8	11:20:18.31	12:59:00.3	$1.0''$	Liu 2011	*Chandra*
NGC 3628	CXOU J112037.3+133429	11:20:37.37	13:34:29.2	$1.0''$	Liu 2011	*Chandra*
NGC 4136	CXOU J120922.6+295551	12:09:22.58	29:55:50.6	$1.0''$	Liu 2011	*Chandra*
NGC 4136	[SST2011] J120922.18+295559.7	12:09:22.19	29:55:59.7	$1.0''$	Liu 2011	*Chandra*
NGC 4204	[SST2011] J121510.91+203912.4	12:15:10.91	20:39:12.4	$1.0''$	Liu 2011	*Chandra*
NGC 4258	RX J121844.0+471730	12:18:43.88	47:17:31.7	$1.0''$	Liu 2011	*Chandra*
NGC 4258	RX J121857.7+471558	12:18:57.85	47:16:07.4	$1.0''$	Liu 2011	*Chandra*
NGC 4258	[WMR2006] NGC4258 XMM1	12:18:47.66	47:20:54.7	$0.8''$	Rosen et al. 2015	XMM-*Newton*
NGC 4258	RX J121845.6+472420	12:18:45.51	47:24:20.2	$1.0''$	Rosen et al. 2015	XMM-*Newton*
NGC 4395	IXO 53	12:26:01.53	33:31:30.6	$1.0''$	Liu 2011	*Chandra*
NGC 4449	RX J122818.0+440634	12:28:17.83	44:06:33.9	$1.1''$	Liu 2011	*Chandra*
NGC 4559	RX J123551+27561	12:35:51.71	27:56:04.1	$0.7''$	Swartz et al. 2004	*Chandra*
NGC 4618	[SST2011] J124129.14+410757.7	12:41:29.14	41:07:57.7	$0.7''^{\dagger}$	Swartz et al. 2011	*Chandra*
NGC 5128	1RXH J132519.8-430312	13:25:19.87	-43:03:17.1	$1.0''$	Kraft et al. 2001	*Chandra*
NGC 5128	CXOU J132518.2-430304	13:25:18.24	-43:03:04.5	$0.4''$	Sivakoff et al. 2008	*Chandra*
NGC 5204	CXOU J132938.6+582506	13:29:38.62	58:25:05.6	$1.0''$	Liu 2011	*Chandra*
M51	RX J132943+47115	13:29:43.31	47:11:34.8	$0.7''$	Terashima et al. 2006	*Chandra*

Continued on next page

Table 4.1 – *Continued*

Galaxy	ULX name (SIMBAD)	R.A. (h:m:s)	Dec. (d:m:s)	Error	Source	Satellite
M51	XMMU J132950.7+471153	13:29:50.68	47:11:55.2	$0.7''$	Terashima et al. 2006	*Chandra*
M51	XMMU J132953.3+471040	13:29:53.31	47:10:42.5	$0.7''$	Terashima et al. 2006	*Chandra*
M51	RX J132954+47145	13:29:53.72	47:14:35.7	$0.7''$	Terashima et al. 2006	*Chandra*
M51	XMMU J132957.6+471047	13:29:57.57	47:10:48.3	$0.7''$	Terashima & Wilson 2004	*Chandra*
M51	RX J133001+47137	13:30:01.01	47:13:43.9	$0.7''$	Terashima et al. 2006	*Chandra*
M51	RX J133006+47156	13:30:06.00	47:15:42.3	$0.7''$	Terashima et al. 2006	*Chandra*
M51	RX J133007+47110	13:30:07.55	47:11:06.1	$0.7''$	Terashima et al. 2006	*Chandra*
NGC 5408	NGC 5408 X-1	14:03:19.63	-41:22:58.7	$1.2''$	Kaaret et al. 2003	*Chandra*
NGC 5474	NGC 5474-X1	14:04:59.74	53:38:09.0	$1.0''$	Liu 2011	*Chandra*
M101	CXOU J140332.3+542103	14:03:32.38	54:21:03.0	$0.7''$	Swartz et al. 2004	*Chandra*
M101	2E 1402.4+5440	14:04:14.28	54:26:03.6	$0.7''$	Swartz et al. 2004	*Chandra*
M101	2XMM J140248.0+541350	14:02:48.19	54:13:50.7	$0.7''$	this work	*Chandra*
M101	CXOU J140314.3+541807	14:03:14.33	54:18:06.7	$0.7''$	this work	*Chandra*
NGC 5585	[SST2011] J141939.39+564137.8	14:19:39.39	56:41:37.8	$1.0''$	Liu 2011	*Chandra*

Notes - †: No positional error was given in the cited article, we assume the standard *Chandra* bore-sight error of $0.6''$ (90% confidence) and a localization error of less than $0.1''$ (90% confidence), which combine into an $0.7''$ total error (95% confidence).

Table 4.2: Entries (marked with •) and/or names of our sources in other catalogues. Sources are listed in the same order as in Table 4.1. (1): Swartz et al. (2004), (2): Liu & Bregman (2005), (3): Liu & Mirabel (2005), (4): Winter et al. (2006), (5): Walton et al. (2011b),(6): Swartz et al. (2011), (7): Barnard (2010).

ULX name (short)	(1)	(2)	(3)	(4)	(5)	(6)	Other
J004722-252051		NGC 253 X9		NGC 253 XMM2	•		NGC 253 ULX1[7]
J004742-251501		NGC 253 X6		NGC 253 XMM6			NGC 253 ULX3[7]
M74 X-1	•		NGC 628 ULX1		•		CXOU J013651.1+154547
J013636+155036			NGC 628 ULX2		•		
J021404+275239						•	CXOU J021404.0+275239
J022721+333500						•	CXOU J022721.5+333500
J022727+333443						•	CXOU J022727.5+333442
J024323+372038			NGC 1058 ULX1		•		CXOU J024323.2+372042
J0318-6629		NGC 1313 X2	NGC 1313 ULX1	NGC 1313 XMM1	•		CXOU J031820.0-662911
J034555+680455		PGC13826 X6	IC 342 ULX1	IC 342 XMM1	•	•	IC 342 X-1
J034615+681112		PGC13826 X7			•	•	2XMM J034615.6+681112
[IWL2003] 68							CXOU J044132.9-025126
J073625+653539	•	NGC 2403 X2	NGC 2403 ULX1	NGC 2403 XMM1	•	•	
J0732+6546		NGC 2403 X3		NGC 2403 XMM4	•		CXOU J073702.3+653935
J080148+504354						•	CXOU J080148.1+504354
J080157+504339						•	
Holmberg II X-1	•	PGC 23324 ULX1	Holmberg II ULX1	Ho II XMM1	•	•	
J093206+213058						•	3XMM J093206.1+213058
Ho I XMM1				Ho I XMM1			3XMM J094130.1+711235
J0940+7106				Ho I XMM2			3XMM J093959.4+710640
Ho I XMM3				Ho I XMM3			3XMM J094206.3+710444
NGC 3031 ULX1	•		NGC 3031 ULX1	M81 XMM1		•	CXOU J095532.9+690033

Continued on next page

Table 4.2 – *Continued*

ULX name (short)	(1)	(2)	(3)	(4)	(5)	(6)	Other
Holmberg IX X-1		PGC 28757 X2	NGC 3031 ULX2	Ho IX XMM1			CXOU J095753.3+690348
J101812+412421	•					•	
J102506+170947						•	CXOU J102506.9+170947
J102508+170948						•	CXOU J102508.2+170948
J110022+285818					•		CXOU J110021.7+285818
J110545+000016					•		CXOU J110545.6+000016
NGC3621 B							
NGC 3623 ULX1		NGC 3623 X2			•	•	CXOU J111858.5+130530
J112020+125846		NGC 3627 X2			•	•	CXOU J112020.8+125846
J112018+125900						•	CXOU J112018.3+125900
J112037+133429		NGC 3628 X2	NGC 3628 ULX2			•	
J120922+295551		NGC 4136 X1	NGC 4136 ULX1				
J120922+295559			NGC 4136 ULX2			•	CXOU J120922.1+29555
J121510+203912						•	CXOU J121510.9+203912
J121844+471730	•				•	•	CXOU J121843.8+471731
J121857+471558	•		NGC 4258 X3	NGC4258 XMM2	•	•	CXOU J121857.8+471607
NGC4258 XMM1				NGC4258 XMM1	•		3XMM J121847.6+472054
J121845+472420					•		3XMM J121845.5+472420
IXO 53		NGC 4395 X1	NGC 4395 ULX1	NGC4395 XMM1		•	CXOU J122601.5+333130
J122818+440634	•	NGC 4449 X5		NGC4449 XMM1		•	CXOU J122817.8+440633
J123551+27561	•	NGC 4559 X5	NGC 4559 ULX1		•	•	CXOU J123551.7+275604
J124129+410757						•	
J132519-430312		NGC 5128 X4	NGC 5128 ULX1				CXOU J132519.9-430317
J132518-430304							
J132938+582506	•	NGC 5204 X1	NGC 5204 ULX1	NGC5204 XMM1	•	•	

Continued on next page

Table 4.2 – *Continued*

ULX name (short)	(1)	(2)	(3)	(4)	(5)	(6)	Other
J132943+47115	•	NGC 5194 X4	NGC 5194-5 ULX2			•	
J132950+471153	•		NGC 5194-5 ULX3			•	
J132953+471040	•		NGC 5194-5 ULX4		•	•	
J132954+47145	•	NGC 5194 X9	NGC 5194-5 ULX5	M51 XMM7		•	CXOM51 J132953.7+471436
J132957+471047	•			M51 XMM6		•	
J133001+47137		NGC 5194 X6	NGC 5194-5 ULX7	M51 XMM3	•	•	
J133006+47156		NGC 5195 X2	NGC 5194-5 ULX9	M51 XMM4	•	•	
J133007+47110	•	NGC 5194 X8	NGC 5194-5 ULX8	M51 XMM2	•	•	CXOM51 J133007.6+471106
NGC 5408 X-1			NGC 5408 ULX1	NGC5408 XMM1	•		
NGC 5474-X1						•	CXOU J140459.7+533808
J140332+542103	•	NGC 5457 X5	NGC 5457 ULX7			•	
J1402+5440	•	NGC 5457 X23	NGC 5457 ULX3	M101 XMM3	•	•	CXOU J140414.3+542604
J140248+541350					•		CXOU J140248.1+541350
J140314+541807			NGC 5457 ULX2	M101 XMM1	•		
J141939+564137						•	CXOU J141939.3+564137

Table 4.3: The ULX candidates for which we calculated accurate X-ray positions from archival *Chandra* observations.

ULX candidate	*Chandra* obs. ID
J024323+372038	9579
J0732+6546	2014
J110022+285818	393
J140248+541350	14341
J140314+541807	14341

4.3 Observations

We obtained observations for this project using three different telescopes[1]. In the Northern hemisphere we used the William Herschel Telescope with the Long-slit Intermediate Resolution Infrared Spectrograph (WHT/LIRIS) and the MMT with the SAO Widefield InfraRed Camera (MMT/SWIRC) to obtain H- and/or *Ks*-band images of 51 and 16 sources, respectively. WHT/LIRIS provides a pixel scale of $0.25''$/pixel and a field of view of $4.27' \times 4.27'$, MMT/SWIRC has a pixel scale of $0.15''$/pixel and a field of view of $5.12' \times 5.12'$. For targets in the Southern hemisphere we were granted 8 hours of service mode observations with the Infrared Spectrometer And Array Camera on the Very Large Telescope (VLT/ISAAC, Moorwood et al. 1998) in period 89 (program 089.D-0663(A)) and 4 hours in period 90 (program 090.D-0417(A)). This yielded *Ks*-band images of 14 sources in total. We observed the 10 sources in p89 in one observing block (OB) per source. For the 4 sources in p90 we used two (shorter) OBs per source; for two sources (in NGC 1637 and NGC 3621), these OBs were executed in the same night, whereas the OBs for the two ULXs in NGC 253 were executed 14 (J004722-252051) and 42 (J004742-251501) days apart, respectively. We used the SW imaging mode of ISAAC, which gives a spatial scale of $0.148''$/pixel and a field of view of $152'' \times 152''$.

All observations were performed using multiple repetitions of a 5-point dither pattern. We used exposure times of 20 seconds in the H-band and 15 seconds in the *Ks*-band with WHT/LIRIS and MMT/SWIRC, and exposure times of 6 or 10 seconds with VLT/ISAAC. The ULXs were not necessarily centred on the detectors as the pointings were selected to minimize the background from the galaxy, maximize the number of reference stars in the field and avoid very bright stars. However, if the host galaxy covered more than half of the field of view of the image we alternated between the target and an off-target blank sky field to properly subtract the sky background.

A log of the observations including the total exposure time for each source, the size of the point spread function in the image as a measure of the image quality, the distance modulus to the galaxy and the uncertainty in the astrometry is shown in Table 4.4.

[1]The data are publicly available at http://archive.eso.org and http://casu.ast.cam.ac.uk/casuadc/ingarch/

Table 4.4: Log of the observations, with the distance modulus to the assumed host galaxy of the ULX candidates. The image number can be used to link details of the observations to the data on individual ULXs in Table 4.5. I.Q. is the image quality. The last column gives the 1-σ uncertainty in the astrometry of the image.

Im. no.	Galaxy	Filter	Instrument/ Telescope	Obs. date	Exp. time (seconds)	I.Q. (arcsec)	Distance modulus (magnitudes)	WCS uncertainty[‡] (arcsec)
1	NGC 253	Ks	ISAAC/VLT	2012-11-19*	750	0.7	27.7 ± 0.1[1]	0.26
2	NGC 253	Ks	ISAAC/VLT	2012-11-19*	750	0.4	27.7 ± 0.1[1]	0.48
3	M74	Ks	ISAAC/VLT	2012-07-06	260	1.0	30.0 ± 0.4[5]	0.5[§]
4	M74	Ks	LIRIS/WHT	2012-01-01	7125	0.8	30.0 ± 0.4[5]	0.36
5	M74	H	LIRIS/WHT	2013-01-29	3860	0.5	30.0 ± 0.4[5]	0.64
6	M74	Ks	LIRIS/WHT	2012-01-04	9105	0.7	30.0 ± 0.4[5]	0.14
7	NGC 855	Ks	LIRIS/WHT	2012-01-05	4350	0.8	29.94 ± 0.17[18]	0.33
8	NGC 925	Ks	LIRIS/WHT	2012-01-01	9285	0.7	29.3 ± 0.4[9]	0.17
9	NGC 925	H	LIRIS/WHT	2013-01-29	3000	0.6	29.3 ± 0.4[9]	0.28
10	NGC 1058	Ks	LIRIS/WHT	2012-01-05	5625	0.6	29.8 ± 0.4[7]	0.24
11	NGC 1058	H	LIRIS/WHT	2013-01-29	3000	1.0	29.8 ± 0.4[7]	0.27
12	NGC 1313	Ks	ISAAC/VLT	2012-07-05	160	0.6	28.2 ± 0.2[8]	0.42
13	IC342	Ks	LIRIS/WHT	2012-01-04	7410	0.8	27.72 ± 0.17[2]	0.21
14	IC342	Ks	LIRIS/WHT	2012-01-01	3975	1.7	27.72 ± 0.17[2]	0.22
15	IC342	H	LIRIS/WHT	2013-01-27	4000	0.9	27.72 ± 0.17[2]	0.23
16	NGC 1637	Ks	ISAAC/VLT	2012-11-22	750	0.3	30.0 ± 0.4[9]	0.4
17	NGC 2403	Ks	LIRIS/WHT	2012-01-01	6345	2.3	27.50 ± 0.05[8]	0.28
18	NGC 2403	H	LIRIS/WHT	2013-01-26	4000	0.7	27.50 ± 0.05[8]	0.29
19	NGC 2403	Ks	LIRIS/WHT	2012-01-04	7500	1.6	27.50 ± 0.05[8]	0.28
20	NGC 2500	Ks	LIRIS/WHT	2012-01-01	5580	1.5	30.0 ± 0.4[7]	0.06
21	NGC 2500	Ks	LIRIS/WHT	2012-01-07	6855	0.6	30.0 ± 0.4[7]	0.12

Continued on next page

Table 4.4 – *Continued*

Im. no.	Galaxy	Filter	Instrument/ Telescope	Obs. date	Exp. time (seconds)	I.Q. (arcsec)	Distance modulus (magnitudes)	WCS uncertainty‡ (arcsec)
22	Holmberg II	Ks	LIRIS/WHT	2012-01-05	3750	0.9	27.65 ± 0.03^{1}	0.22
23	Holmberg II	Ks	LIRIS/WHT	2013-01-27	3675	1.0	27.65 ± 0.03^{1}	0.39
24	Holmberg II	H	SWIRC/MMT	2011-05-17	1120	0.5	27.65 ± 0.03^{1}	0.23
25	NGC 2903	H	LIRIS/WHT	2013-01-29	3940	1.0	30.1 ± 0.4^{10}	0.13
26	Holmberg I	H	SWIRC/MMT	2011-05-17	900	0.8	27.95 ± 0.03^{1}	0.14
27	Holmberg I	H	SWIRC/MMT	2011-05-17	900	0.8	27.95 ± 0.03^{1}	0.17
28	Holmberg I	H	SWIRC/MMT	2011-05-17	600	1.0	27.95 ± 0.03^{1}	0.14
29	M81	Ks	LIRIS/WHT	2012-01-08	3375	0.9	27.86 ± 0.06^{6}	0.12
30	Holmberg IX	H	SWIRC/MMT	2011-05-17	1200	1.0	27.79 ± 0.08^{1}	0.25
31	NGC 3184	Ks	LIRIS/WHT	2012-01-07	3780	1.0	30.5 ± 0.5^{5}	0.47†
32	NGC 3239	Ks	LIRIS/WHT	2012-01-01	2085	1.7	29.5 ± 0.4^{7}	0.55
33	NGC 3239	H	LIRIS/WHT	2013-01-25	3820	0.7	29.5 ± 0.4^{7}	0.39
34	NGC 3486	Ks	LIRIS/WHT	2012-01-07	1695	0.7	31.1 ± 0.4^{11}	0.30
35	NGC 3521	Ks	ISAAC/VLT	2012-05-16	120	0.7	31.1 ± 0.4^{10}	0.5§
36	NGC 3621	Ks	ISAAC/VLT	2013-01-01	750	0.4	28.9 ± 0.4^{9}	0.23
37	NGC 3623	Ks	ISAAC/VLT	2012-06-09	120	0.6	30.5 ± 0.4^{10}	0.14
38	NGC 3627	Ks	ISAAC/VLT	2012-06-10	120	0.7	29.7 ± 0.4^{9}	0.24
39	NGC 3628	Ks	ISAAC/VLT	2012-06-10	120	0.9	30.7 ± 0.5^{12}	0.50†
40	NGC 4136	H	LIRIS/WHT	2013-01-25	3980	0.9	29.9 ± 0.4^{7}	0.34
41	NGC 4204	H	LIRIS/WHT	2013-01-29	2940	1.0	29.5 ± 0.4^{7}	0.62†
42	NGC 4258	H	LIRIS/WHT	2013-01-27	5000	0.8	29.29 ± 0.02^{13}	0.5§
43	NGC 4258	H	LIRIS/WHT	2013-01-27	4000	0.7	29.29 ± 0.02^{13}	0.31
44	NGC 4258	H	LIRIS/WHT	2013-01-27	4000	0.7	29.29 ± 0.02^{13}	0.27
45	NGC 4395	Ks	LIRIS/WHT	2012-01-04	5595	1.2	28.42 ± 0.02^{8}	0.32

Continued on next page

Table 4.4 – *Continued*

Im. no.	Galaxy	Filter	Instrument/ Telescope	Obs. date	Exp. time (seconds)	I.Q. (arcsec)	Distance modulus (magnitudes)	WCS uncertainty[‡] (arcsec)
46	NGC 4449	Ks	LIRIS/WHT	2012-01-04	3435	0.9	28.0 ± 0.1[14]	0.35
47	NGC 4559	H	LIRIS/WHT	2013-01-25	3400	0.8	29.6 ± 0.5[10]	0.28
48	NGC 4559	H	SWIRC/MMT	2011-05-17	6680	0.8	29.6 ± 0.5[10]	0.12
49	NGC 4618	Ks	LIRIS/WHT	2012-01-07	5265	0.9	29.3 ± 0.4[7]	0.62
50	NGC 5128	Ks	ISAAC/VLT	2012-04-22	120	0.3	27.77 ± 0.17[15]	0.16
51	NGC 5204	Ks	LIRIS/WHT	2011-05-16	5040	1.0	28.3 ± 0.3[16]	0.10
52	M51	H	LIRIS/WHT	2013-01-29	3460	1.2	29.6 ± 0.2[4]	0.28
53	M51	H	LIRIS/WHT	2013-01-29	3140	1.3	29.6 ± 0.2[4]	0.35
54	M51	H	LIRIS/WHT	2013-01-29	3500	1.5	29.6 ± 0.2[4]	0.23
55	NGC 5408	Ks	ISAAC/VLT	2012-04-22	120	0.3	28.4 ± 0.8[7]	0.26
56	NGC 5474	Ks	LIRIS/WHT	2012-01-05	4935	1.2	29.15[17]	0.46[†]
57	M101	H	SWIRC/MMT	2011-05-17	1160	1.2	29.04 ± 0.05[3]	0.36
58	M101	H	SWIRC/MMT	2011-05-17	1200	0.7	29.04 ± 0.05[3]	0.23
59	M101	H	SWIRC/MMT	2011-05-17	1200	0.7	29.04 ± 0.05[3]	0.15
60	M101	H	SWIRC/MMT	2011-05-17	1180	0.9	29.04 ± 0.05[3]	0.12
61	NGC 5585	Ks	LIRIS/WHT	2012-01-05	4950	1.1	29.9 ± 0.6[10]	0.06

Notes - [‡]: Rms error with respect to the reference catalogue. The 2MASS catalogue was used for the astrometric calibration, unless stated otherwise. [*]: Date of the first observation. The second observations were taken on 2012-12-03 (#1) and 2012-12-31 (#2). [†]: USNO B1.0 catalogue used for astrometric calibration. [§]: less than 4 sources available for astrometric calibration. [1]: Dalcanton et al. (2009), [2]: Herrmann et al. (2008), [3]: Shappee & Stanek (2011), [4]: Poznanski et al. (2009), [5]: Olivares E. et al. (2010), [6]: Durrell et al. (2010), [7]: Tully (1988), [8]: Jacobs et al. (2009), [9]: Tully et al. (2009), [10]: Springob et al. (2009), [11]: Theureau et al. (2007), [12]: Willick et al. (1997), [13]: Humphreys et al. (2008), [14]: McQuinn et al. (2010), [15]: Chattopadhyay et al. (2009), [16]: Karachentsev et al. (2003), [17]: Drozdovsky & Karachentsev (2000), [18]: Tonry et al. (2001)

4.4 Data reduction and analysis

The data obtained with VLT/ISAAC in period 89 were reduced with the ISAAC pipeline in the GASGANO environment, following the steps outlined in the ISAAC Data Reduction Guide[2]. The output of the pipeline is a co-added, sky-subtracted image without astrometric calibration. We used the astrometry tool 'fit to star positions' in the STARLINK program GAIA to calculate the astrometric solutions, using 2 Micron All Sky Survey (2MASS, Skrutskie et al. 2006) sources in the field of view if at least four were present. When this was not the case we used sources from the USNO B1.0 catalogue (Monet et al., 2003) for the calibration. We adopt the root-mean-square (rms) error of the fit as the 1-σ uncertainty on the positions of the NIR sources. We used the general data reduction software package THELI (Schirmer, 2013) to reduce the data obtained with WHT/LIRIS, MMT/SWIRC and the data obtained with VLT/ISAAC in p90. The greater flexibility of THELI makes it easier to immediately combine data taken on different nights, hence we decided to use it instead of the ISAAC pipeline for the reduction of the VLT/ISAAC data from p90. Because the final astrometric and photometric calibration was done in a uniform way for all images, we are confident that the use of different data reduction packages does not impact our results. Using THELI, we first produced master flats, applied them to the images and subtracted the sky background of the individual frames. THELI employs SEXTRACTOR (Bertin & Arnouts, 1996) and SCAMP (Bertin, 2006) to find sources in the individual images and determine an astrometric solution by matching their positions to sources from 2MASS or PPXML (Roeser et al., 2010) if not enough 2MASS sources are present. This astrometric solution is then used to coadd the images using SWARP (Bertin et al., 2002). We improved the astrometric accuracy of the final coadded images using the 'fit to star positions' tool in GAIA, again fitting to positions of sources from 2MASS or USNO B1.0. The rms errors on these fits are listed in Table 4.4 as a measure of the uncertainty in the astrometry of the NIR images. Three images (#20, 45 and 52) did not have a sufficient number of 2MASS or USNO B1.0 sources in the field of view. We calibrated these images using only three reference stars from 2MASS. With three reference stars and three degrees of freedom no rms error could be calculated. For these images we adopt a 1-σ uncertainty of $0.5''$.

We calculated the radius of the 95% confidence (2-σ) error circle around the position of the ULX candidates on the NIR images by quadratically adding the 2-σ uncertainty on the X-ray position and twice the rms error of the astrometric solution of the NIR images. There is an additional uncertainty in the 2MASS and USNO B1.0 positions with respect to the international celestial reference system (ICRS), but this error ($0.015''$ for 2MASS, $0.2''$ for USNO B1.0, Skrutskie et al. 2006; Monet et al. 2003) is negligible in the total error budget (that is dominated by the uncertainty in the X-ray position).

We used the tasks *daofind* and *phot* from the APPHOT package in IRAF[3] to calibrate the zeropoints of the images using 2MASS sources near the targets, detect counterparts within the

[2] ftp.eso.org/pub/dfs/pipelines/isaac/isaac-pipeline-manual-1.4.pdf

[3] IRAF is distributed by the National Optical Astronomy Observatory, which is operated by the Association of Universities for Research in Astronomy (AURA) under cooperative agreement with the National Science Foundation.

error circles and calculate their apparent magnitude. For the cases where we did not detect a counterpart we calculated the limiting magnitude at the position of the ULX by simulating stars at that position with a range of magnitudes using the IRAF task *mkobjects*. The magnitude of the faintest simulated star that was still detected at the three sigma level was taken as a robust lower limit for the magnitude of the ULX.

4.5 Results

Of the 62 ULX candidates in our sample, 17 have a candidate counterpart in one or more NIR images. The apparent and absolute magnitudes of the candidate counterparts are listed in Table 4.5. If a ULX has no detected counterpart, the limiting magnitude of the image at the position of the ULX is given. The errors on the apparent magnitudes reported in Table 4.5 are the 1-σ errors on the magnitude determination by IRAF and on the zeropoint calibration. For the absolute magnitudes there is an additional error that stems from the uncertainty in the distance modulus (listed in Table 4.4).

4.5.1 NIR counterparts

We detected candidate counterparts for 17 ULX candidates in our sample. Because some of these have been observed more than once, the total number of detections is 23. There are 11 sources in the *Ks*-band and 12 in the H-band. The absolute magnitudes of the candidate counterparts range from -7.1 to -13.88 in the H-band and from -8.1 to -14.3 in the *Ks*-band, with the majority of the sources lying between -9 and -11.5 in both bands (see Table 4.5).

4.5.2 Limiting magnitudes for non-detections

For the remaining 45 ULX candidates in our sample we only have lower limits on their NIR magnitudes, 29 in the *Ks*-band and 23 in the H-band. The apparent limiting magnitudes range from 17 to 21.25 in both NIR bands. Our aim was to reach a limiting magnitude of at least 20. Worse limits are mainly caused by bad seeing (although most of the sources that were observed under bad seeing conditions were subsequently repeated under better conditions) and crowding or high backgrounds from the host galaxies, especially in e.g. the spiral arms of M101 and M51.

The absolute limiting magnitudes vary from from -7.5 to -12 in the *Ks*-band and from -7.5 to -12.6 in the H-band.

Table 4.5: Apparent and absolute magnitudes of the candidate NIR counterparts to the ULX candidates, or upper limits for ULXs where we did not detect a source in the error circle around the X-ray position. The image number refers to the observation log (Table 4.4). The error radius is the radius of the 95% confidence circle around the position of the ULX within which we search for counterparts. It is derived by quadratically adding the positional error on the location of the X-ray sources and two times the rms error of the astrometric solution of fitting stellar positions on the NIR images.

Galaxy	ULX name	Im. no.	Error Radius	Det. y/n	Filter	Apparent magnitude†	Absolute magnitude†
NGC 253	J004722-252051	1	$1.1''$	y	Ks	$17.2 \pm 0.03 \pm 0.5$	$-10.5 \pm 0.03 \pm 0.5 \pm 0.10$
NGC 253	J004742-251501	2	$1.4''$	n	Ks	> 19.5	> -8.2
M74	M74 X-1	3	$1.2''$	n	Ks	> 20.0	> -10.0
		4	$1.0''$	n	Ks	> 20.0	> -10.0
		5	$1.5''$	n	H	> 21.25	> -8.8
M74	J013636+155036	6	$0.8''$	n	Ks	> 21.25	> -8.8
NGC 855	J021404+275239	7	$1.2''$	n	Ks	> 18.25	> -11.7
NGC 925	J022721+333500	8	$1.1''$	y	Ks	$18.0 \pm 0.03 \pm 0.2$	$-11.3 \pm 0.03 \pm 0.2 \pm 0.4$
		9	$1.1''$	y	H	$18.7 \pm 0.03 \pm 0.2$	$-10.6 \pm 0.03 \pm 0.2 \pm 0.4$
NGC 925	J022727+333443	8	$1.1''$	y	Ks	$19.5 \pm 0.08 \pm 0.2$	$-9.8 \pm 0.08 \pm 0.2 \pm 0.4$
		9	$1.1''$	y	H	$20.1 \pm 0.08 \pm 0.2$	$-9.2 \pm 0.08 \pm 0.2 \pm 0.4$
NGC 1058	J024323+372038	10	$0.8''$	y	Ks	$19.7 \pm 0.06 \pm 0.4$	$-10.1 \pm 0.06 \pm 0.4 \pm 0.4$
		11	$0.9''$	y	H	$20.8 \pm 0.2 \pm 0.3$	$-9.0 \pm 0.2 \pm 0.3 \pm 0.4$
NGC 1313	J0318-6629	12	$1.3''$	n	Ks	> 18.5	> -9.7
IC342	J034555+680455	13	$0.5''$	n	Ks	> 20.25	> -7.5
IC342	J034615+681112	14	$0.6''$	n	Ks	> 18.5	> -9.2
		15	$0.6''$	n	H	> 20.0	> -7.7
NGC 1637	[IWL2003] 68	16	$1.3''$	y	Ks	$16.3 \pm 0.005 \pm 0.5$	$-13.7 \pm 0.005 \pm 0.5 \pm 0.4$
NGC 2403	J073625+653539	17	$0.9''$	n	Ks	> 18.25	> -9.3
		18	$0.9''$	n	H	> 20.0	> -7.5

Continued on next page

Table 4.5 – *Continued*

Galaxy	ULX name	Im. no.	Error Radius	Det. y/n	Filter	Apparent magnitude†	Absolute magnitude†
NGC 2403	J0732+6546	19	$0.9''$	n	Ks	> 19.25	> -8.3
NGC 2500	J080148+504354	20	$1.0''$	n	Ks	> 19.75	> -10.3
NGC 2500	J080157+504339	20	$1.0''$	y	Ks	$15.7 \pm 0.002 \pm 0.2$	$-14.3 \pm 0.002 \pm 0.2 \pm 0.4$
		21	$1.0''$	y	Ks	$15.95 \pm 0.005 \pm 0.15$	$-14.1 \pm 0.005 \pm 0.15 \pm 0.4$
Holmberg II	Holmberg II X-1	22	$0.8''$	y	Ks	$19.30 \pm 0.08 \pm 0.10$	$-8.35 \pm 0.08 \pm 0.10 \pm 0.03$
		23	$1.0''$	y	Ks	$19.4 \pm 0.12 \pm 0.2$	$-8.2 \pm 0.12 \pm 0.2 \pm 0.03$
		24	$0.8''$	y	H	$20.6 \pm 0.3 \pm 0.10$	$-7.1 \pm 0.3 \pm 0.10 \pm 0.03$
NGC 2903	J093206+213058	25	$0.7''$	n	H	> 20.25	> -9.9
Holmberg I	Ho I XMM1	26	$1.0''$	y	H	$17.81 \pm 0.01 \pm 0.10$	$-10.14 \pm 0.01 \pm 0.10 \pm 0.03$
Holmberg I	J0940+7106	27	$1.1''$	n	H	> 19.25	> -8.7
Holmberg I	Ho I XMM3	28	$1.4''$	n	H	> 20.5	> -9.6
M81	NGC 3031 ULX1	29	$1.0''$	n	Ks	> 18.5	> -9.4
Holmberg IX	Holmberg IX X-1	30	$1.2''$	n	H	> 19.75	> -8.0
NGC 3184	J101812+412421	31	$1.2''$	n	Ks	> 20.5	> -10.0
NGC 3239	J102506+170947	32	$1.5''$	n	Ks	> 18.25	> -11.3
		33	$1.3''$	n	H	> 20.25	> -9.3
NGC 3239	J102508+170948	32	$1.5''$	n	Ks	> 17.5	> -12.0
		33	$1.3''$	n	H	> 20.25	> -9.3
NGC 3486	J110022+285818	34	$0.9''$	n	Ks	> 20.0	> -11.1
NGC 3521	J110545+000016	35	$1.4''$	n	Ks	> 19.25	> -11.9
NGC 3621	NGC3621 B	36	$0.8''$	n	Ks	> 18.0	> -10.9
NGC 3623	NGC 3623 ULX1	37	$1.0''$	n	Ks	> 19.75	> -10.8
NGC 3627	J112020+125846	38	$1.1''$	n	Ks	> 20.0	> -9.7
NGC 3627	J112018+125900	38	$1.1''$	y	Ks	$20.6 \pm 1.9 \pm 0.7$	$-9.1 \pm 1.9 \pm 0.7 \pm 0.4$

Continued on next page

Table 4.5 – *Continued*

Galaxy	ULX name	Im. no.	Error Radius	Det. y/n	Filter	Apparent magnitude†	Absolute magnitude†
NGC 3628	J112037+133429	39	$1.4''$	n	Ks	> 19.5	> -11.2
NGC 4136	J120922+295551	40	$1.2''$	y	H	$19.13 \pm 0.03 \pm 0.10$	$-10.78 \pm 0.03 \pm 0.10 \pm 0.4$
NGC 4136	J120922+295559	40	$1.2''$	y	H	$19.15 \pm 0.03 \pm 0.10$	$-10.75 \pm 0.03 \pm 0.10 \pm 0.4$
NGC 4204	J121510+203912	41	$1.6''$	n	H	> 20.25	> -9.3
NGC 4258	J121844+471730	42	$1.4''$	n	H	$17.79 \pm 0.02 \pm 0.10$	$-11.50 \pm 0.02 \pm 0.1 \pm 0.02$
NGC 4258	J121857+471558	43	$1.2''$	n	H	> 19.0	> -10.3
NGC 4258	NGC4258 XMM1	42	$1.3''$	n	H	> 19.5	> -9.8
NGC 4258	J121845+472420	44	$1.1''$	n	H	> 21.0	> -8.3
NGC 4395	IXO 53	45	$1.2''$	n	Ks	> 20.0	> -8.4
NGC 4449	J122818+440634	46	$1.3''$	n	Ks	> 18.25	> -9.8
NGC 4559	J123551+27561	47	$0.9''$	n	H	> 21.0	> -8.6
		48	$0.7''$	n	H	> 21.25	> -8.4
NGC 4618	J124129+410757	49	$1.4''$	n	Ks	> 20.25	> -9.1
NGC 5128	J132519-430312	50	$1.0''$	n	Ks	> 18.5	> -9.3
NGC 5128	J132518-430304	50	$0.5''$	n	Ks	> 19.25	> -8.5
NGC 5204	J132938+582506	51	$1.0''$	n	Ks	> 19.0	> -9.3
M51	J132943+47115	52	$0.9''$	n	H	> 17.5	> -12.1
M51	J132950+471153	52	$0.9''$	n	H	> 17.25	> -12.4
M51	J132953+471040	52	$0.9''$	y	H	$15.72 \pm 0.02 \pm 0.10$	$-13.88 \pm 0.02 \pm 0.10 \pm 0.2$
M51	J132954+47145	53	$1.0''$	n	H	> 20.5	> -9.1
M51	J132957+471047	52	$0.9''$	n	H	> 17.5	> -12.1
M51	J133001+47137	52	$0.9''$	n	H	> 17.0	> -12.6
M51	J133006+47156	53	$1.0''$	n	H	> 18.5	> -11.1
M51	J133007+47110	54	$0.8''$	n	H	> 19.5	> -10.1

Continued on next page

Table 4.5 – *Continued*

Galaxy	ULX name	Im. no.	Error Radius	Det. y/n	Filter	Apparent magnitude†	Absolute magnitude†
NGC 5408	NGC 5408 X-1	55	$1.3''$	y	Ks	$20.3 \pm 0.13 \pm 0.2$	$-8.1 \pm 0.13 \pm 0.2 \pm 0.8$
NGC 5474	NGC 5474-X1	56	$1.4''$	n	Ks	> 19.5	> -9.7
M101	J140332+542103	57	$1.0''$	n	H	> 18.5	> -10.5
M101	J1402+5440	58	$0.8''$	y	H	$19.3 \pm 0.04 \pm 0.2$	$-9.7 \pm 0.04 \pm 0.2 \pm 0.05$
M101	J140248+541350	59	$0.8''$	y	H	$17.72 \pm 0.01 \pm 0.05$	$-11.32 \pm 0.01 \pm 0.05 \pm 0.05$
M101	J140314+541807	60	$0.7''$	y	H	$18.35 \pm 0.03 \pm 0.10$	$-10.69 \pm 0.03 \pm 0.10 \pm 0.05$
NGC 5585	J141939+564137	61	$1.0''$	n	Ks	> 19.75	> -10.2

Notes - †: Magnitude and errors are as follows: Apparent/absolute magnitude ± statistical error on the magnitude as given by the *phot* routine ± statistical error on the zeropoint of the image ± error on the distance modulus (absolute magnitude only).

4.6 Discussion

We obtained NIR (H- and *Ks*-band) images of 62 ULXs in 37 nearby galaxies to search for NIR counterparts that could be red supergiant companions. For 17 ULXs, we detected a candidate counterpart in one or more images. Twelve of these have absolute magnitudes that are consistent with those of red supergiants (whose absolute magnitudes range from -8 (K0) to -10.5 (M5) in the K-band, Elias et al. 1985; Drilling & Landolt 2000). One of these, Ho I XMM1, we suspect to be a background active galactic nucleus (AGN; see Section 6.2); we can not exclude the possibility that other RSG candidates are also background AGN. The remaining five sources have an absolute magnitude < -11. These brightest sources are not likely to be single stars. They could be background AGN or (young) stellar clusters; see Section 6.2 for more details on the individual sources.

For the other 45 sources in our sample we obtained limiting magnitudes. Several of these ULX candidates have known optical counterparts, although in many cases it is not clear what is the source of the optical emission: a companion star or emission from an irradiated accretion disc.

The distribution of absolute magnitudes of the detected counterparts is plotted in Figure 4.1. At the faint end our sample is not complete, so nothing can be inferred from the shape of the distribution. At absolute magnitudes below -11, however, we expect to detect nearly all NIR sources. This is also the magnitude that the brightest single red supergiants can reach. The sharp drop in the number of detections below that magnitude therefore seems to imply that we do detect a population of possible single stars, the more so because the brightest sources are either confirmed background AGN or strong candidates to be background AGN or star clusters.

The fact that only a fraction of the ULXs has a bright NIR counterpart could reflect a difference between systems with blue supergiant or Wolf-Rayet donor stars and systems with red supergiant donor stars. The ratio of blue to red supergiants is not well known, and the ratio of non-detections to candidate RSG detections in our sample of $45/11 \approx 4.1$ is consistent with what has been observed (Langer & Maeder, 1995). Alternatively, the systems where we detected NIR counterparts might have larger accretion discs than the ones without a NIR detection, causing the excess NIR radiation. This scenario would suggest that the black holes in those ULXs have larger Roche lobes, either because they have a higher mass than the black holes in systems without bright NIR counterparts (assuming they have the same companion stars), or because the initial separation between the black hole and companion star was larger and hence, when the contact phase starts, the companion star is more evolved and both the disc and star are larger.

Another possibility is that the infrared radiation originates from a jet. We investigated this scenario for the only ULX in our sample with a NIR counterpart and an observed radio jet: Holmberg II X-1. We find that the counterpart that we detected is ~ 6 magnitudes brighter than what we would expect as contribution from the jet if it has a steep spectrum ($\alpha \approx -0.8$, for $S_\nu \propto \nu^\alpha$, as is common for jets from X-ray binaries accreting at high rates; Fender et al. 2009). If the radio emission is due to a steady jet with a flat spectrum ($\alpha = 0$) it would contribute significantly to the NIR emission, but such jets usually appear in the low/hard state

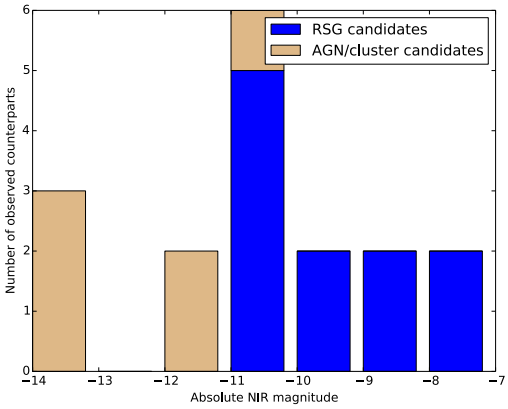

Figure 4.1: The distribution of absolute magnitudes of the detected candidate counterparts. For ULXs with both H- and *Ks*-band counterparts only the H-band magnitude is included.

(see Section 6.1: Holmberg II X-1). Finding a ULX in the low/hard state would be strong evidence for an IMBH. In principle the X-ray spectra of ULXs in the 'ultraluminous' state (showing a soft excess and a rollover in the spectrum above 3 keV, Gladstone et al. 2009) can be interpreted as a low/hard state with X-ray reflection from an ionized disc (Caballero-García & Fabian, 2010). However, this interpretation has been ruled out at least for a number of ULXs (e.g. Bachetti et al. 2013) by observations of their hard X-ray spectra with *NuSTAR* (Harrison et al., 2013), and thus far only HLX-1 has been observed in a state that is reminiscent of the low/hard state (Godet et al., 2009).

In Sections 6.1 and 6.2 we discuss the systems with NIR counterparts in more detail.

4.6.1 Candidate red supergiants

For twelve sources in our sample we have detected a NIR counterpart with an absolute magnitude consistent with that of a red supergiant, one of which we suspect to be a background AGN. The NIR images of the remaining eleven RSG candidates are shown in Figure 4.2.

Two sources, J080157+504339 in NGC 2500 and Holmberg II X-1, were observed twice in the *Ks*-band, J080157+504339 on 2012, January 1 and January 7, and Holmberg II X-1 on 2012, January 5, and 2013, January 27. In both cases, the source brightness was consistent with being the same at the two epochs.

We have measured $H-K$ colours for four of the eleven RSG candidates (J022721+333500 and J022727+333443 in NGC 925, J024323+372038 in NGC 1058 and Holmberg II X-1). The measured values are 0.7 ± 0.3, 0.6 ± 0.3, 1.1 ± 0.5 and 1.3 ± 0.3, respectively. With the caveat that the images in the two bands were taken several months apart (although if the NIR emission is indeed dominated by an RSG, it is not expected to vary significantly), and the errors are large, these are rather high values for red supergiants, whose $H - K$ colours range from 0 – 0.3 (Cox, 2000). It is unlikely that the red colours are caused by extinction, because the hydrogen column densities needed for this would be too high. For example, to

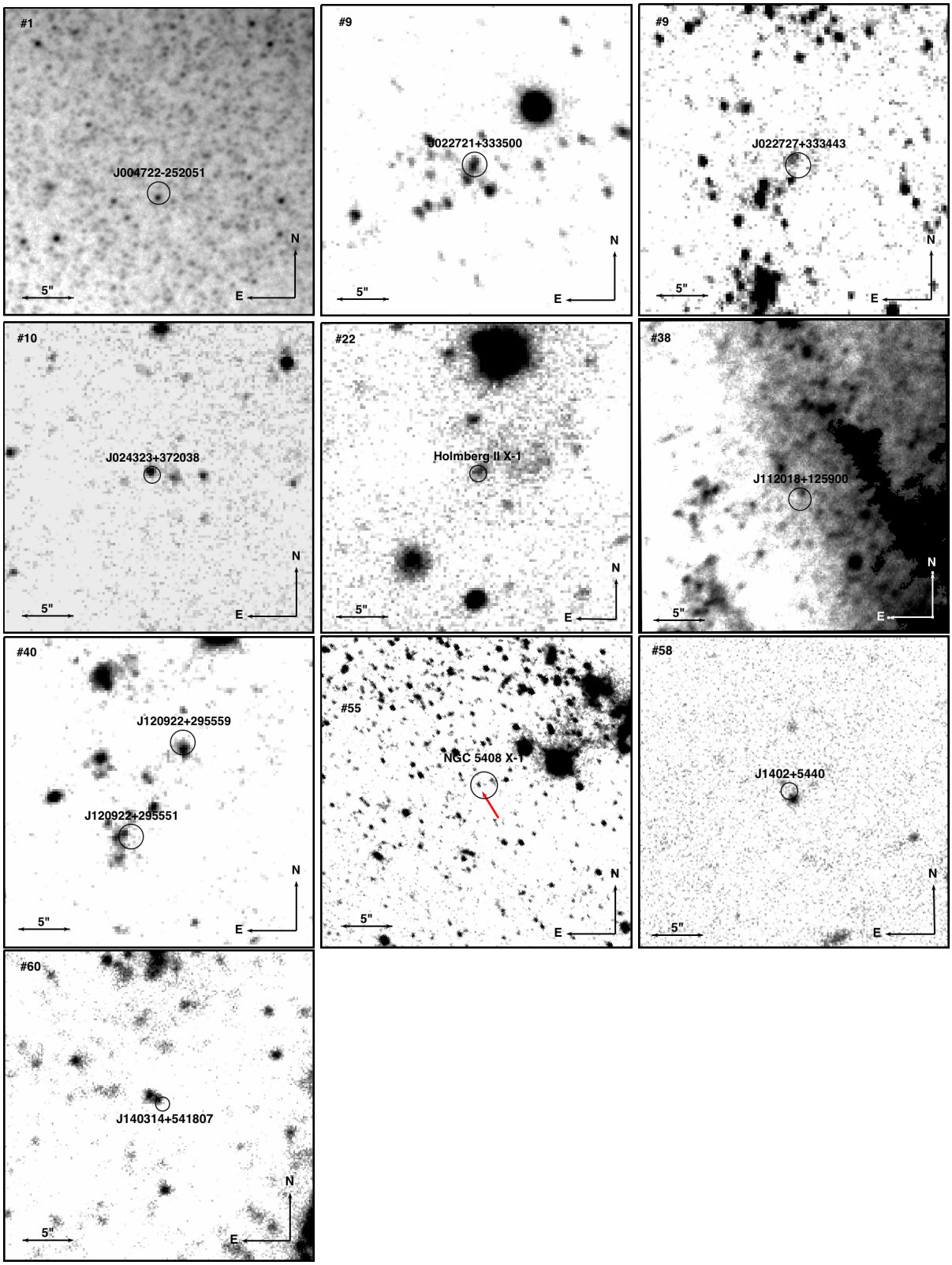

Figure 4.2: $0.5' \times 0.5'$ finder charts of all ULXs with a candidate counterpart that could be a RSG. The black circles are the 95% confidence error circles around the positions of the ULXs. The numbers in the upper left corners refer to the image numbers in Table 4.4.

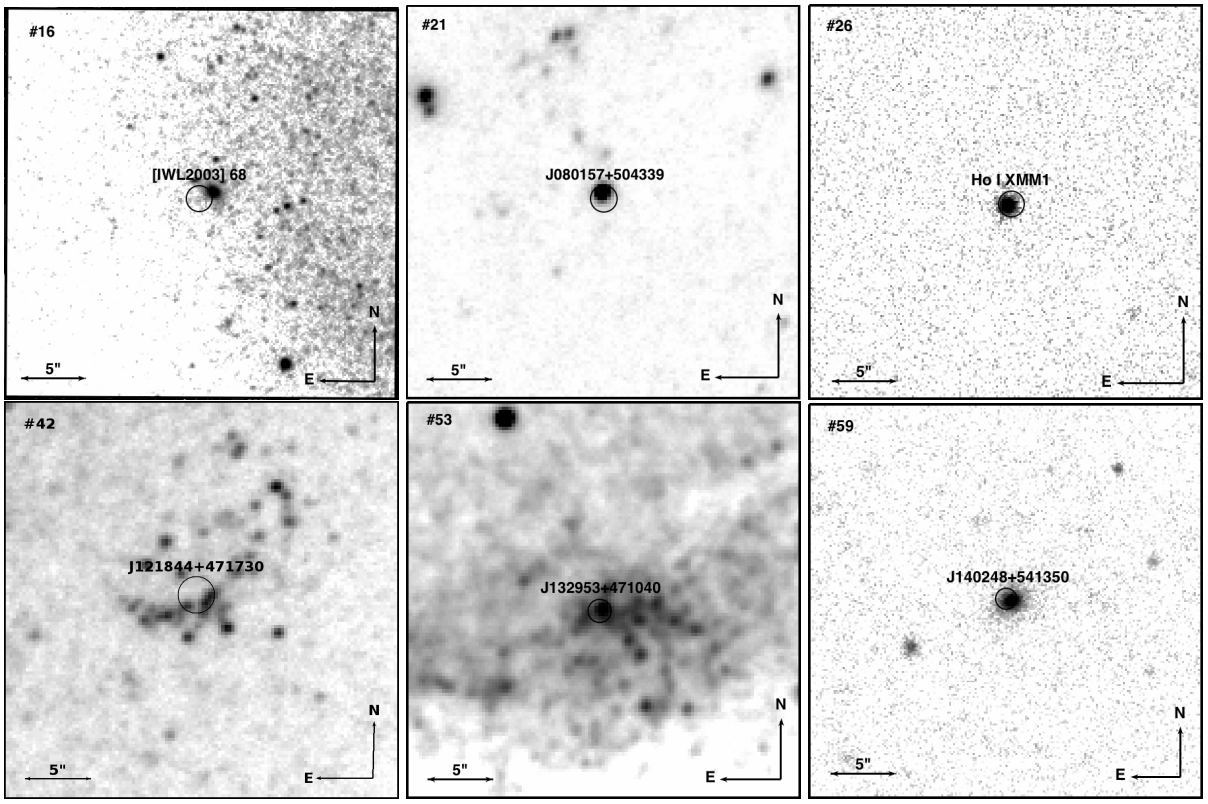

Figure 4.3: $0.5' \times 0.5'$ finder charts of all ULXs with a candidate counterpart that are likely or confirmed background AGN or (young) stellar clusters. The black circles are the 95% confidence error circles around the positions of the ULXs. The numbers in the upper left corners refer to the image numbers in Table 4.4.

cause a reddening of $H - K = 0.5$, one needs an extinction in the V-band $A_V \approx 8$ (based on relative extinctions from Cardelli et al. 1989). This corresponds to a hydrogen column density $N_H \approx 1.8 \times 10^{22}$ cm^{-2} (Güver & Özel, 2009). Although hydrogen column densities of ULXs can vary significantly, they do not usually reach such values. For instance for Holmberg II X-1, the hydrogen column density inferred from the X-ray spectrum is $N_H = 3.7 \times 10^{21}$ cm^{-2} (Kaaret et al., 2004). The ULX with one of the highest absorption columns known, M82 X-1, has $N_H = 1.12 \times 10^{22}$ cm^{-2} (Kaaret et al., 2006), still not nearly enough to account for a reddening of $H - K > 0.5$. Other possible mechanisms that could cause the red $H - K$ colours include a contribution from jets, although that seems unlikely based on the expected NIR contribution from the jet in Holmberg II X-1. It is also possible that there are strong (nebular) emission lines present that cause the red colours if those are stronger in the K- than in the H-band.

J004722-252051

This ULX candidate in NGC 253 has an X-ray luminosity of $(2.9 \pm 0.12) \times 10^{39}$ erg s^{-1} (90% confidence). The X-ray source is variable on short timescales (Barnard 2010, their ULX1). We detected a counterpart to this X-ray source in our *Ks*-band image with an absolute magnitude of *Ks* = $-10.5 \pm 0.03 \pm 0.5 \pm 0.10$ (the errors are the statistical error on the magnitude, the error on the zeropoint of the image and the error on the distance modulus, respectively). This absolute magnitude is consistent with that of an M-type supergiant; spectroscopic observations may shed more light on the nature of this source.

J022721+333500

We detected the counterpart to this ULX candidate in NGC 925 in both the H- and the *Ks*-band, with absolute magnitudes $H = -10.6 \pm 0.03 \pm 0.2 \pm 0.4$ and $Ks = -11.3 \pm 0.03 \pm 0.2 \pm 0.4$. The source is rather bright for a single star, but within the uncertainties the absolute magnitudes are still consistent with an M-type supergiant. The counterpart is extended in both the H- and *Ks*-band image (see Figure 4.2). If it indeed consists of two sources of about equal brightness, one of them could be the true counterpart of the ULX and that single source would be fainter than the absolute magnitudes that we find for the combined sources.

J022727+333443

The second ULX candidate in NGC 925 has a higher X-ray luminosity than most sources in our sample, reaching $\sim 2.5 \times 10^{40}$ erg s^{-1} (Swartz et al., 2011). A candidate counterpart is detected in both our H- and *Ks*-band image, with absolute magnitudes of *Ks* = $-9.8 \pm 0.08 \pm 0.2 \pm 0.4$ and $H = -9.2 \pm 0.08 \pm 0.2 \pm 0.4$. These magnitudes are consistent with those of a red supergiant.

J024323+372038

This ULX candidate is located in the outskirts of NGC 1058. It has a candidate counterpart with absolute magnitudes of *Ks* = $-10.1 \pm 0.06 \pm 0.4 \pm 0.4$ and $H = -9.0 \pm 0.2 \pm 0.3 \pm 0.4$, if it is at the distance to NGC 1058. These absolute magnitudes are compatible with the source being a red supergiant. Because the ULX candidate is not located in a spiral arm and no signs of recent star formation are visible in the NIR images, we have to take into account the possibility that this is a foreground star or background AGN. Spectroscopic observations are necessary to determine the true distance to this source.

Holmberg II X-1

Holmberg II X-1 is a ULX with an X-ray luminosity of $\sim 10^{40}$ erg s^{-1}. It has an optical counterpart with a $V-$band magnitude of 21.86 ± 0.09 surrounded by an ionized nebula (Kaaret et al. 2004; Pakull & Mirioni 2002; Moon et al. 2011) and its UV and optical emission are best fitted by an irradiated disc model (Tao et al., 2012b). The source has also been detected in radio observations, and recently Cseh et al. (2013b) reported the discovery of recurrent radio jets from the ULX. Taking the flux density of the radio core and the spectral index of $\alpha = -0.8 \pm 0.2$ reported by Cseh et al. (2013b), the NIR emission expected from the central component has an apparent *Ks*-band magnitude of ~ 25.3, 6 mag fainter than the counterpart that we detected. This spectrum is consistent with optically thin synchrotron emission, as expected for intermittent jets occurring at high accretion rates (Fender et al., 2009). If we assume a flat spectrum (expected for steady jets in the low/hard state) then the *Ks*-band magnitude would be ~ 16.5, 3.5 mag brighter than what we detect. The spectral index needed to explain the *Ks*-band emission is $\alpha \approx -0.25$. Note that the X-ray spectrum of Holmberg II X-1 indicates that it is not in the low/hard state but instead in an 'ultraluminous' state, possibly accreting above the Eddington limit (e.g. Gladstone et al. 2009; Sutton et al. 2013). It is therefore unlikely that the radio emission is due to a steady jet with a flat spectrum and we do not expect jet emission to contribute significantly to the NIR light.

The absolute magnitude of the counterpart of *Ks* = $-8.35 \pm 0.08 \pm 0.10 \pm 0.03$, $H = -7.1 \pm 0.3 \pm 0.10 \pm 0.03$ indicates that the infrared excess might be due to a red supergiant companion. It could also be related to the nebula surrounding the ULX.

J112018+125900

J112018+125900 is a ULX candidate located on the edge of a spiral arm in NGC 3627. Its absolute *Ks*-band magnitude of $-9.1 \pm 1.9 \pm 0.7 \pm 0.4$ puts it in the magnitude range of red supergiants, but its apparent magnitude ($20.6 \pm 1.9 \pm 0.7$ in the *Ks*-band) and its location in a crowded region will make it difficult to observe it spectroscopically with current instrumentation.

J120922+295551

This ULX candidate in NGC 4136 was detected by the ROSAT High Resolution Imager (HRI) at 2.5×10^{39} erg s^{-1} (Lira et al., 2000), and subsequently at much lower luminosity in a *Chandra* observation by Roberts et al. (2004). We detected a counterpart with an absolute H-band magnitude of $-10.78 \pm 0.03 \pm 0.10 \pm 0.4$. Within the uncertainties this is compatible with an M-type RSG companion.

J120922+295559

The second ULX candidate in NGC 4136 was discovered by Roberts et al. (2004) in a *Chandra* observation, at $\sim 11''$ from J120922+295551 with a maximum unabsorbed X-ray luminosity of 2.6×10^{39} erg s^{-1}. Its NIR counterpart has an absolute H-band magnitude of $-10.75 \pm 0.03 \pm 0.10 \pm 0.4$. Within the uncertainties this is compatible with an M-type RSG companion.

NGC 5408 X-1

Lang et al. (2007) discovered an optical counterpart to this ULX in *Hubble Space Telescope* (*HST*) images with a V- and I-band magnitude of 22.4. The counterpart has also been studied by Grisé et al. (2012), who discovered it in 6 *HST* filters from the near UV to the NIR. They find that the flux of the source drops continuously with increasing wavelength to $\sim 0.13 \times 10^{-18}$ erg s^{-1} cm^{-2} Å^{-1} in the H-band and concluded that the companion star was either a blue (O- or B-type) supergiant or the optical emission was dominated by the accretion disc. Optical spectra obtained with the VLT show a blue continuum superimposed with emission lines from the surrounding nebula (Kaaret & Corbel 2009; Cseh et al. 2011).

Radio emission from the nebula has also been detected by Lang et al. (2007); since the emission is resolved in their VLA images, they conclude that it can not originate in a relativistic jet. The flux density and spectral index of this radio source are similar to those of the compact radio jet in Holmberg II X-1, so assuming that the spectrum continues into the NIR we would expect a similar magnitude for NGC 5408 X-1 of *Ks* ≈ 25, 5 mag fainter than what we detect.

The error circle in our image actually contains two sources, but comparison with the *HST* image of Lang et al. (2007) shows that the most Eastern source (indicated with an arrow in Figure 4.2) is the counterpart. This source has an apparent *Ks*-band magnitude of $20.3 \pm 0.13 \pm 0.2$. At the distance of NGC 5408 this corresponds to an absolute *Ks*-band magnitude of $-8.1 \pm 0.13 \pm 0.2 \pm 0.8$. Interestingly, this corresponds to a higher flux ($\sim 0.3 \times 10^{-18}$ erg s^{-1} cm^{-2} Å^{-1}) than Grisé et al. (2012) measured in the H-band, while none of their models predict an increase in flux towards the *Ks*-band. It is possible that this excess infrared radiation is emitted by the companion star, while most of the optical emission originates from the disc. However, RSGs typically have $H - K \approx 0$, while for this source we find $H - K \approx 2$ (based on the H-band magnitude reported by Grisé et al. 2012). Since the *Ks*-band image was not taken simultaneously with the optical and H-band data, variability of the source is also a possible explanation.

J1402+5440

One of the four ULX candidates that we observed in M101, this source has a reported X-ray luminosity of 2.4×10^{39} erg s^{-1} (Swartz et al., 2011). The counterpart that we detected in our H-band image has an absolute magnitude of $-9.7 \pm 0.04 \pm 0.2 \pm 0.05$. This places it in the magnitude range of red supergiants.

J140314+541807

J140314+541807 is another ULX in M101 with an X-ray luminosity of 2.9×10^{39} erg s^{-1} as reported by Winter et al. (2006). We detected a counterpart in the H-band with an absolute magnitude of $-10.69 \pm 0.03 \pm 0.10 \pm 0.05$. Within the uncertainties this is compatible with an M-type RSG companion.

4.6.2 Candidate star clusters and background AGN

Five of the candidate counterparts that we discovered have absolute magnitudes that are incompatible with them being single stars. Some of these can be classified as background AGN; others might be bona fide ULXs located in stellar clusters (cf Voss et al. 2011; Jonker et al. 2012). Additionally, two of the ULX candidates near Holmberg I are likely not real ULXs but background AGN. We discuss these sources in more detail below; the NIR images of these sources are shown in Figure 4.3.

[IWL2003] 68

The absolute magnitude of the *Ks*-band counterpart to this ULX candidate in NGC 1637 is $-13.7 \pm 0.005 \pm 0.5 \pm 0.4$. This is much brighter than a single red supergiant. The source is resolved in our *Ks*-band image. The counterpart has also been detected in *HST* images of the galaxy by Immler et al. (2003), who report apparent magnitudes $m_V \sim 22.8$ and $m_I \sim 21.1$ and a full width at half maximum (FWHM) of $0.45''$, more than twice as large as the size of the point sources in the image. At the distance to NGC 1637 this corresponds to a physical size of ~ 25 pc. The counterpart could be a star cluster in NGC 1637, or a background galaxy containing an AGN.

J080157+504339

This ULX candidate, situated in NGC 2500, has a bright counterpart that we detected in two *Ks*-band observations at an absolute magnitude of $-14.3 \pm 0.002 \pm 0.2 \pm 0.4$ and $-14.1 \pm 0.005 \pm 0.15 \pm 0.4$, respectively, if the distance to NGC 2500 is assumed. However, optical spectroscopic observations by Gutiérrez (2013) have shown this source to be a background AGN.

Ho I XMM1

The ULX candidate Ho I XMM1 is situated at $5'$ from the centre of the dwarf irregular galaxy Holmberg I. The galaxy has a diameter (semimajor axis) of $3.6'$ (Gil de Paz et al., 2007); the X-ray source is thus located outside the galaxy itself. The H-band counterpart that we detected has an absolute magnitude of $-10.14 \pm 0.01 \pm 0.10 \pm 0.03$. This in itself does not exclude the possibility that the counterpart is a red supergiant. However, it has also been detected by the Wide-Field Infrared Survey Explorer (WISE) and its colours in the WISE bands are [3.4]-[4.6] = 0.8, [4.6]-[12] = 2.5, placing it firmly among the AGN in WISE colour-colour diagrams (cf Stern et al. 2005; D'Abrusco et al. 2012). Thus it is likely that this ULX candidate is a background AGN like J080157+504339 in NGC 2500.

J0940+7106

J0940+7106 is another ULX candidate $5'$ from the centre of Holmberg I. It does not have a counterpart within the 95% confidence error circle of $1.1''$, but a single NIR point source is located just outside it. This NIR source was also detected by WISE. Its colours are [3.4]-[4.6] = 1.35, [4.6]-[12] = 2.4, which place the source among the Seyfert galaxies in the diagram of D'Abrusco et al. (2012). Therefore we expect that the X-ray source and the NIR source are related, and that this ULX candidate is also in fact a background AGN.

J121844+471730

This ULX candidate in NGC 4258 is located in the centre of a cluster of stars. The counterpart has an absolute H-band magnitude of $-11.50 \pm 0.02 \pm 0.1 \pm 0.02$ and is thus too bright to be a single star.

J132953+471040

The counterpart to J132953+471040 in M51 has an absolute H-band magnitude of $-13.88 \pm 0.02 \pm 0.10 \pm 0.2$. Comparing to the *HST* image of Terashima et al. (2006), we find that this source is at the centre of the star cluster in which the ULX is located. Even in the higher resolution *HST* image this source is unresolved, although extended, and it is not possible to distinguish single stars.

J140248+541350

This ULX candidate in M101 is associated with an optical counterpart in the Sloan Digital Sky Survey (SDSS) catalogue (Pineau et al., 2011). The SDSS source is classified as a galaxy in all Sloan filters except the u'-band. We also detected the counterpart in our H-band image, where it is clearly extended (see Figure 4.3). This source is likely to be a background galaxy harbouring an AGN.

4.6.3 Non-detections of sources with known optical counterparts

Several ULX candidates in our sample have known optical counterparts, and optical spectra are available for a few. Some of these we did detect in our NIR images (see Sections 5.1 and 5.2), but the majority were not detected by us. Ptak et al. (2006), Tao et al. (2011) and Gladstone et al. (2013) found (sometimes multiple) candidate optical counterparts in archival *HST* data for 11 ULXs that we do not detect in our images (J004742-251501, J0318-6629, J034555+680455, J034615+681112, J073625+653539, NGC 3031 ULX1, Holmberg IX X-1, J112020+125846, IXO 53, J123551+27561, J132519-430312 and J132938+582506). Optical spectra are available for Holmberg IX X-1, J132938+582506 in NGC 5204 (both in Roberts et al. 2011) and J140332+542103 in M101 (Liu et al., 2013).

The V-band apparent magnitudes for these counterparts lie between 22 and 25. Holmberg II X-1 and NGC 5408 X-1, the only two RSG candidates that we detect in the NIR that have also been detected in the optical, have values for $V - K \sim 2.1 - 2.5$ (not taking into account possible variability). Typical $V - K$ values for RSGs range from ~ 2 – 4, but in ULXs there will also be a contribution from the accretion disc to the optical light, which lowers $V - K$. For the ULXs with $V-$band magnitude up to ~ 22 we can state that they have $V - K$ closer to 0, because otherwise we would have detected them in our NIR images. Indeed, for Holmberg IX X-1 (with a $V-$band magnitude of ~ 22.8, Grisé et al. 2006) there is also an *HST* H-band observation in which the counterpart is detected at a magnitude of 22.56 (Grisé et al., in prep.). These $V - K$ values are in line with what would be expected for early type companion stars (Elias et al., 1985). The ULXs with $V \approx 23 - 24$ we would not have detected in our NIR images if they have $V - K \approx 2.5$, but we can exclude that they have $V - K$ values that are even higher. The ULXs with the very faintest optical counterparts, with $V \gtrsim 25$, we could not detect even if they had $V - K \approx 4$.

4.7 Conclusions

We have performed the first systematic search for near-infrared counterparts to nearby ULXs. We observed 62 ULXs in the H- and/or *Ks*-band and detected candidate counterparts for 17 of them. For the other 45 ULXs we determined limiting magnitudes. Of the 17 ULXs with NIR counterparts, eleven had no previously reported optical or NIR counterpart. We detected eleven candidate counterparts with absolute magnitudes that are consistent with them being single red supergiants. Two of these (Holmberg II X-1 and NGC 5408 X-1) also have known optical counterparts. Holmberg II X-1 has a radio jet, but the NIR emission that we detect is 6 mag brighter than the emission expected from the jet. In NGC 5408 X-1, we detect excess *Ks*-band emission compared to the models tested by Grisé et al. (2012). This excess infrared radiation could be emitted by the companion star, while most of the optical emission originates from the disc. However this would not explain the large value for $H - K$ in this ULX. It is also possible that the source is variable.

Six counterparts are too bright to be single stars and in some cases extended; they are likely star clusters or background galaxies.

The fact that we detect only a fraction of the ULXs in our NIR images points towards differences between ULX systems: the systems that show relatively strong NIR emission might have larger accretion discs than the ones that do not, or there may be strong nebular lines present that are absent in other sources. Alternatively, these systems may contain red supergiant donor stars that are intrinsically bright in the NIR. If the NIR emission indeed originates from a late-type donor star, these systems are excellent candidates for future spectroscopic studies to find dynamical masses for their black holes.

Acknowledgements

EK thanks Mischa Schirmer for his help with the data reduction software THELI. We thank the anonymous referee for their comments that helped improve the paper. TPR's contribution to this paper was funded as part of STFC consolidated grant ST/K000861/1. Based on observations collected at the European Southern Observatory, Chile, programmes 089.D-0663(A) and 090.D-0417(A). The William Herschel Telescope is operated on the island of La Palma by the Isaac Newton Group in the Spanish Observatorio del Roque de los Muchachos of the Instituto de Astrofísica de Canarias. Observations reported here were obtained at the MMT Observatory, a joint facility of the Smithsonian Institution and the University of Arizona.

CHAPTER 5

DISCOVERY OF A RED SUPERGIANT COUNTERPART TO RX J004722.4-252051, A ULX IN NGC 253[1]

M. Heida, M. A. P. Torres, P. G. Jonker, M. Servillat, S. Repetto, T. P. Roberts, D. J. Walton, D.-S. Moon and F. A. Harrison

Published in MNRAS, 453, 2015, p.3510-3518

Abstract

We present two epochs of near-infrared spectroscopy of the candidate red supergiant counterpart to RX J004722.4-252051, a ULX in NGC 253. We measure radial velocities of the object and its approximate spectral type by cross-correlating our spectra with those of known red supergiants. Our VLT/X-shooter spectrum is best matched by that of early M-type supergiants, confirming the red supergiant nature of the candidate counterpart. The radial velocity of the spectrum, taken on 2014, August 23, is 417 ± 4 km s^{-1}. This is consistent with the radial velocity measured in our spectrum taken with Magellan/MMIRS on 2013, June 28, of 410 ± 70 km s^{-1}, although the large error on the latter implies that a radial velocity shift expected for a black hole of tens of $M_{\odot}$ can easily be hidden. Using nebular emission lines we find that the radial velocity due to the rotation of NGC 253 is 351 $\pm$ 4 km s^{-1} at the position of the ULX. Thus the radial velocity of the counterpart confirms that the source is located in NGC 253, but also shows an offset with respect to the local bulk motion of the galaxy of 66 $\pm$ 6 km s^{-1}. We argue that the most likely origin for this displacement lies either in a SN kick, requiring a system containing a $\gtrsim 50\ M_{\odot}$ black hole, and/or in orbital radial velocity varia-

[1]Observations based on ESO programme 093.D-0256

tions in the ULX binary system, requiring a $\gtrsim 100\ M_{\odot}$ black hole. We therefore conclude that RX J004722.4-252051 is a strong candidate for a ULX containing a massive stellar black hole.

5.1 Introduction

Ultraluminous X-ray sources (ULXs) are defined as off-nuclear X-ray sources with a luminosity greater than the Eddington luminosity of a 10 $M_{\odot}$ black hole (BH); in practice a limit for the 0.3 – 10.0 keV luminosity $\geq 10^{39}$ erg s^{-1} is used (for a review see e.g. Feng & Soria 2011). The two main scenarios to explain these high luminosities are (1) super-Eddington accretion on to stellar mass BHs or neutron stars (Begelman 2002) and (2) sub-Eddington accretion on to intermediate mass BHs (IMBHs; Colbert & Mushotzky 1999).

A growing body of evidence indicates that the group of sources we call ULXs may contain objects of both kinds. A recent discovery of X-ray pulses from M82 ULX-2 proves that the accretor in the system is a neutron star (Bachetti et al. 2014). Yet this ULX sometimes reaches an X-ray luminosity of 1.8×10^{40} erg s^{-1}, which is clearly orders of magnitude above its Eddington limit. Liu et al. (2013) use optical spectroscopic observations of the donor star of M101 ULX1 and Motch et al. (2014) use optical spectroscopic and photometric observations of the donor star of NGC 7793 P13 to calculate a dynamical limit on the BH masses in these systems. In both cases they find the accretor is most likely a stellar mass BH. These recent discoveries support the suggestion of Gladstone et al. (2009) and others that the peculiar X-ray spectral state, seen in several ULXs with high-quality X-ray data (e.g. Bachetti et al. 2013; Sutton et al. 2013; Pintore et al. 2014), is an 'ultraluminous' state and that many ULXs are stellar mass BHs emitting above their Eddington limit.

However, the brightest ULXs, with luminosities above 10^{41} erg s^{-1} (also known as hyperluminous X-ray sources [HLXs]), are still good candidates to host IMBHs (eg. Farrell et al. 2009; Jonker et al. 2010; Sutton et al. 2012). The brightest known ULX and strongest candidate for hosting an IMBH is ESO 243-49 HLX1, with an estimated BH mass of $\sim 20000\ M_{\odot}$ (Farrell et al. 2009). M82 ULX-1 and NGC 2276-3c are two other ULXs that are candidate IMBHs (Pasham et al. 2014; Mezcua et al. 2015).

The most reliable, model-independent method to measure the mass of the accretors in ULXs is through dynamical mass measurements. The first attempts to do so (Roberts et al. 2011; Liu et al. 2012) used optical emission lines from the accretion discs in these systems. However, these do not show periodic motion. A more promising approach is to measure the radial velocity curve of the donor star, as has been done for several Galactic X-ray binaries (e.g. McClintock & Remillard 1986).

The optical spectra of many ULX counterparts do not show stellar features, as they are dominated by emission from the accretion disc (cf. Grisé et al. 2012; Tao et al. 2012b; Sutton et al. 2014). Some ULXs may however have red supergiant (RSG) donor stars. Since RSGs are intrinsically very bright in the near-infrared (NIR) it is possible to measure their radial velocities spectroscopically out to ~ 10 Mpc. An additional advantage is that in the NIR the contribution from the accretion disc is lower than in the optical regime. Also, because of the large orbital separations in such systems, irradiation of the donor star is not expected to play

an important role (Copperwheat et al. 2007). Therefore, we performed a photometric survey of nearby ($D < 10$ Mpc) ULXs in the NIR to search for ULXs with RSG donor stars (see Chapter 4).

In this paper we present the results of NIR spectroscopic follow-up of the ULX with the brightest candidate NIR counterpart (*Ks* = 17.2 ± 0.5) in the sample presented in Chapter 4 of this thesis: RX J004722.4-252051 in NGC 253 (hereafter J0047), at a distance of 3.4 Mpc (Dalcanton et al. 2009). The counterpart is also listed in the catalogue by Bailin et al. (2011) (source ID 47620), with $V = 21.58$ and $I = 19.96$. Given this V-band magnitude and the *Ks*-band magnitude reported in Chapter 4, we derive that the $V - K = 4.4 \pm 0.5$ colour is consistent with that of an RSG, assuming both the V and K magnitudes do not vary strongly in time.

The ULX has been studied in X-rays by for example Barnard (2010) (NGC 253 ULX1), Sutton et al. (2013) (NGC 253 XMM2), Pintore et al. (2014) (NGC 253 X-1) and Wik et al. (2014) (source 7). It is not a particularly bright ULX, with a peak luminosity in the 0.3 – 10 keV band of 2.4×10^{39} erg s^{-1}(Pintore et al. 2014), and it has been observed to drop well below the ULX threshold in other observations. Additionally, it shows unusually high variability for a disc-like object (Sutton et al. 2013). The spectrum was classified by Sutton et al. (2013) as a 'broadened disc', an ultraluminous state associated with sources accreting around their Eddington limit (Gladstone et al. 2009). This would imply a mass of $\lesssim 20\ M_\odot$ for the BH in this system.

5.2 Observations and data reduction

We obtained two spectra of J0047 separated by about one year: one with the MMT and Magellan Infrared Spectrograph (MMIRS; McLeod et al. 2012) on the Magellan Clay telescope at Las Campanas Observatory, and the other with X-shooter (Vernet et al. 2011) on the Very Large Telescope (VLT) UT3 at Cerro Paranal.

Magellan/MMIRS

The MMIRS spectrum (proposal ID 2013A-CFA-3) was taken on the night of 2013, June 28, with a 2-pixel ($0.4''$) slit, the HK grism and the HK filter. This setup yields a spectrum from 1.25 to 2.45 μm, with an average spectral resolution ($\frac{\Delta\lambda}{\lambda}$) of R ≈ 1400. We used an ABBA nodding pattern with a dither offset step of $20''$. We obtained 16 spectra with exposure times of 300 s each, for a total time on source of 4800 s. The data were reduced through the CfA MMIRS pipeline (v0.9.7RC7-20140301; Chilingarian et al. 2013). This pipeline subtracts the two exposures of one dither pair, performs a flat-field and residual sky correction and rectifies the 2D spectra. The spectra are wavelength-calibrated using the positions of telluric OH-emission lines; the rms of the residuals of the wavelength solution is 0.6 Å. The dither pairs are then co-added and telluric absorption lines are removed using a telluric standard star observed close in time to and at similar airmass as the target. These corrected 2D spectra still have both a positive and a negative trace of the object. We use the STARLINK program

FIGARO for the further data reduction steps: use the optimal extraction algorithm by Horne (1986) to extract the spectrum of the positive trace from the pipeline-reduced 2D spectrum, the spectrum of the negative trace from the inverted 2D spectrum, and then add the two to obtain the final spectrum. The nodding pattern unfortunately projected the positive trace of J0047 on top of the fainter, extended negative trace of another region of NGC 253. We use a narrow extraction region for the positive trace to minimize the effects of this configuration. We correct the wavelength calibration of the MMIRS pipeline (that is done using wavelengths in vacuum) to match the calibration of our other spectra (that are calibrated using wavelengths in air).

VLT/X-shooter

The X-shooter spectrum (programme ID 093.D-0256) was taken in service mode on the night of 2014, August 23. X-shooter has three spectroscopic arms that operate simultaneously, providing spectral coverage from the near UV to the near-IR. We used slit widths of $0.8''$ in the UVB arm, $0.7''$ in the VIS arm and $0.6''$ in the NIR arm, resulting in resolutions of 6200, 10600 and 7780, respectively. We used X-shooter in nodding mode, with an ABBA nodding pattern and a nod throw of $5''$. The integration times for the UVB, VIS and NIR arms were 260, 210 and 285 seconds, respectively. The total exposure times for the three arms are 2600, 2100 and 2850 seconds.

In the NIR arm, the signal-to-noise ratio (S/N) per spectral resolution element in the *J*- and *H*-bands is ~ 10 in regions that are not affected by atmospheric emission lines. Because the throughput of X-shooter drops rapidly towards the K-band, that part of the spectrum is not useful.

We process the NIR observations of the ULX counterpart and a telluric standard star at similar airmass observed close in time to the target with the X-shooter pipeline workflow in the REFLEX environment (Freudling et al. 2013). The pipeline produces flat-fielded, sky-subtracted, rectified, wavelength- and flux-calibrated 1D and 2D spectra. The rms amplitude of the residuals of the wavelength solution is 0.1 Å. The wavelength calibration is done with arcs that are taken during the day, not at the same airmass as the observations. This can introduce a small offset with respect to the real wavelength solution. We check this by comparing the positions of sky emission lines to the line list of Rousselot et al. (2000) and find an offset of ≈ 0.3 Å, that we correct for. We then use the SPEXTOOLS-task XTELLCOR_GENERAL (Vacca et al. 2003) to correct the spectrum for telluric absorption features.

The *H*-band spectra of RSGs contain several strong absorption edges from CO and lines from neutral metals that can be used to derive the effective temperature of the star.The *J*-band also contains absorption lines from neutral metals such as Fe, Ti and Mg that can be used to derive abundances, but they are not very sensitive to temperature (Davies et al. 2010). We have verified that these absorption lines are present in the *J*-band, but in the remainder of this paper we focus our analysis on the *H*-band.

In the data from the UVB and VIS arms the S/N of the counterpart is very low (< 1). However, there are spatially extended emission lines visible that appear centred on a source at $\sim 5''$ East from the ULX counterpart (not detectable in the NIR arm) that is present in one of

the nod positions (the 'B' position). From inspection of archival VLT/FORS1 R and I-band images taken in the night of 2004, July 23 we know that there is a blue ($V-I=0$; Bailin et al. 2011) source that lies partially in the slits at that position. The presence of this source makes it impossible to process the data in nodding mode. We follow the X-shooter pipeline manual and use the *xsh_wkf_stare.oca* file to process the data in stare mode. We extract the emission line spectrum at the position of the counterpart from the exposures without the blue source in the slit (the 'A' position), and at a position close to the blue source from the exposures in the 'B' nod position. For each exposure, the pipeline produces bias-subtracted, flat-fielded, sky-subtracted, rectified, wavelength- and flux-calibrated 1D and 2D spectra. It also produces 1D and 2D spectra of the subtracted sky emission. For the VIS arm, where there are many strong sky emission lines, we use these sky lines to check the wavelength calibration and find no systematic offset. The rms amplitude of the residuals of the wavelength solution for both the VIS and UVB spectra is 0.06 Å.

5.3 Analysis and results

5.3.1 Cross-correlation analysis

We are primarily interested in two properties of the candidate counterpart: its spectral type, to give us an indication of the temperature and (via the observed absolute magnitude) the radius of the star, and its radial velocity to confirm that it is a donor star in a binary that belongs to NGC 253 and is not a foreground or background object. Therefore, we cross-correlate our X-shooter spectrum with high S/N spectra of known RSGs of different spectral types (ranging from K1 to M4.5) and metallicities.

The set of RSG spectra that we use contains one Galactic RSG, CD-60 3621, whose heliocentric radial velocity is -17.7 ± 0.4 km/s (Mermilliod et al. 2008; however, as their individual radial velocity measurements of the star show intrinsic variations from -16.0 to -19.0 km/s, we adopt a larger uncertainty of 3 km/s. All uncertainties quoted in this paper are 1-σ errors). Its spectral type is M1.5 I (Levesque et al. 2005). This star was observed with X-shooter as part of the X-shooter Spectral Library on the night of 2010, February 3 (see Chen et al. 2014 for a description of the library). We retrieved the pipeline-reduced spectrum from the ESO phase 3 archive. The spectrum has been wavelength calibrated, but not corrected for telluric absorption. The observations were done with the $0.6''$ slit in the NIR-arm, so the resolution of the spectrum is the same as for our X-shooter spectrum (observations for both J0047 and CD-60 3621 were done with seeing $> 0.6''$, so the resolution is set by the slit width).

The other RSGs in our comparison sample are those described by Davies et al. (2013). They observed 19 RSGs of a range of spectral types in the LMC and SMC with X-shooter. These spectra have been corrected for telluric absorption, but their radial velocities are not as accurately known as that of CD-60 3621. Since these observations were done with a wide ($5''$) slit, they have a lower resolution than our X-shooter spectrum ($R\approx5000$).

We use the program MOLLY for the analysis of the data. After reading the spectra into MOLLY, we first use *hfix* to calculate and subsequently apply heliocentric corrections. We

prepare the spectra for cross-correlation following the recommendation in the MOLLY user guide[2], first normalizing with a second-order polynomial fit and then subtracting a fourth-order spline fit to the normalized spectra. We resample the spectra to a common velocity spacing (10.85 km s^{-1} pix^{-1} for our X-shooter spectrum, 118.4 km s^{-1} pix^{-1} for our MMIRS spectrum) with *vbin* and then run *xcor* to calculate the cross-correlation functions of J0047 with the comparison sample. *xcor* also calculates the radial velocity offset from the cross-correlation function by fitting a parabola to the three peak pixels. This is a generally robust estimate but it underestimates the uncertainty on the radial velocity. To get a better estimate of the uncertainty we fit a polynomial plus Gaussian curve to the cross-correlation functions using *mgfit*. As a sanity check we also calculate the cross-correlation functions of CD-60 3621 with the LMC/SMC RSGs. The parts of the spectrum of J0047 that are most affected by noise from strong telluric emission lines are masked out during the cross-correlation.

The cross-correlation between the *H*-band X-shooter spectrum of J0047 and CD-60 3621 yields a velocity shift of 434.4 ± 1.0 km s^{-1}. This uncertainty is the statistical error on the determination of the position of the peak of the cross-correlation function. The total uncertainty includes the uncertainty on the wavelength calibration of X-shooter (2 km s^{-1} for both spectra) and the uncertainty in the radial velocity of CD-60 3621 (3 km s^{-1}). Quadratically adding all these uncertainties and adding the radial velocity of CD-60 3621 gives a velocity shift of 417 ± 4 km s^{-1}. The cross-correlations of J0047 with the SMC/LMC sample yield consistent results.

We obtain the highest values of the cross-correlation function for CD-60 3621 and LMC-136042 (the latter is an M3-type RSG). In addition, following the procedure described by Origlia et al. (1993), we measure the equivalent widths of the CO (1.62 μm) bandhead and the Si I (1.59 μm) absorption line using the *light* command in MOLLY (see Figure 5.1 where parts of the spectra are plotted, shifted to zero radial velocity with respect to the heliocentric frame). The ratio of these lines is sensitive to the temperature of the star. We find a ratio of $\log(W_{1.62}/W_{1.59}) = 0.15 \pm 0.1$, which is consistent with an effective temperature in the range 3000 – 4000 K [Förster Schreiber 2000; with the caveat that our spectrum has a higher resolution than those of Förster Schreiber (2000) and Origlia et al. (1993), and it is not known if this will affect the line ratio].

The cross-correlation functions for the SMC RSGs all have lower values than those for the LMC RSGs. From this we conclude that J0047 is an early M-type RSG, with a metallicity closer to that of the LMC and Milky Way RSGs than to that of those in the SMC, which have a lower metallicity. This is not unexpected, as abundance measurements of H II regions in NGC 253 yield values for 12 + log(O/H) in the range 8.5 – 9.0 (Webster & Smith 1983), comparable to abundance ratios found in H II regions in the Milky Way (e.g. Balser et al. 2011). Values found for H II regions in the LMC and SMC are 8.4 ± 0.12 and 7.98 ± 0.09, respectively (Pagel et al. 1978).

The Magellan/MMIRS spectrum of J0047, due to its much lower resolution and lower S/N, can not be used to constrain the spectral type of the RSG. Therefore, we cross-correlate

[2] http://deneb.astro.warwick.ac.uk/phsaap/software/molly/html/USER_GUIDE.html

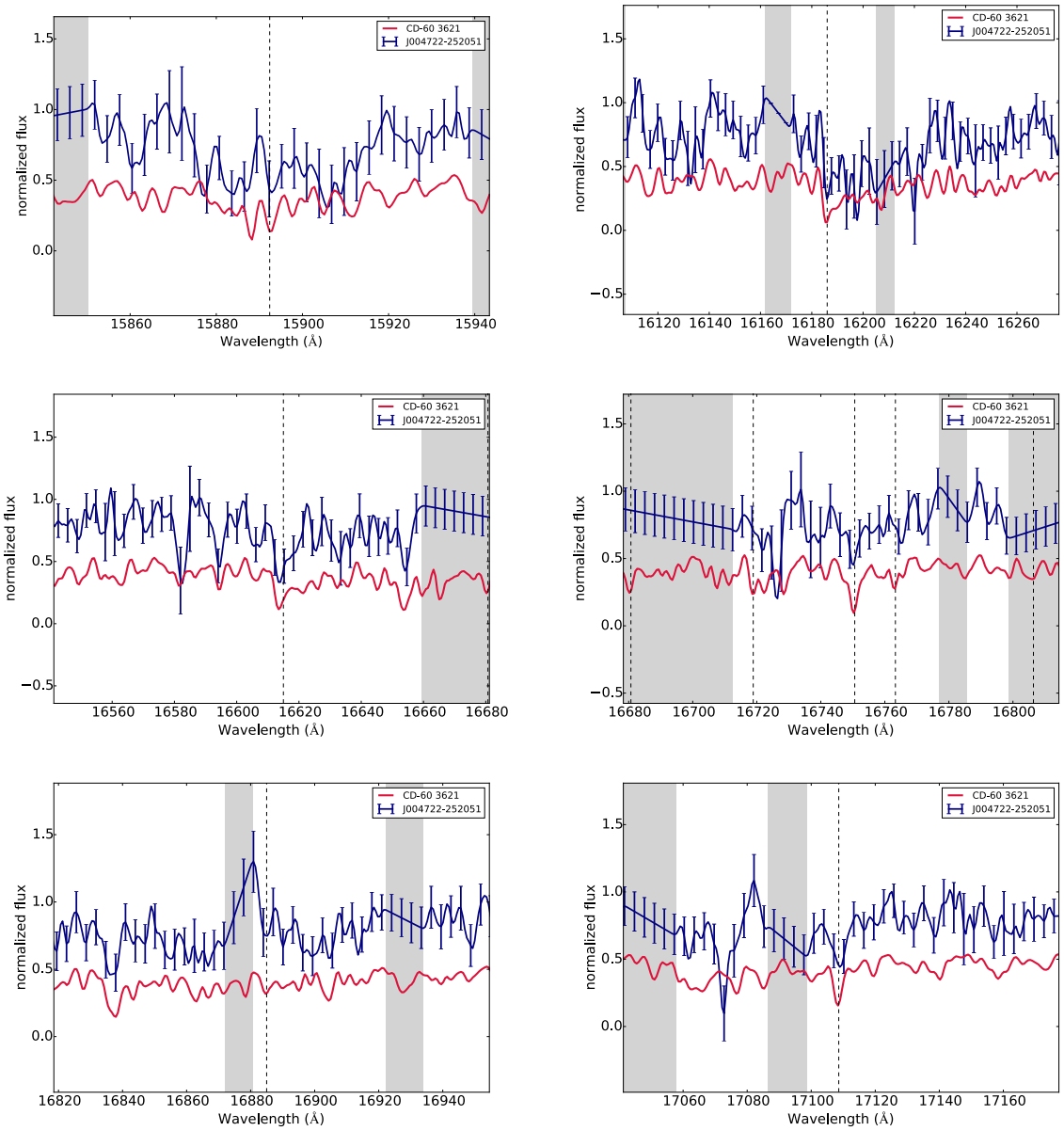

Figure 5.1: Sections of the *H*-band X-shooter spectrum of J0047 (upper, blue line) and the X-shooter spectrum of CD-60 3621 (lower, red line). Both spectra are normalized and smoothed to the resolution of X-shooter. For presentation purposes only, we interpolated the spectrum of J0047 over areas that are strongly affected by telluric emission (grey shaded areas). Error bars are plotted for every fifth data point. The spectrum of CD-60 3621 is shifted vertically by -0.5. The J0047 spectrum is shifted by -417 km s^{-1} and the CD-60 3621 spectrum is shifted by 17 km s^{-1}. The dashed vertical lines indicate the positions of atomic and molecular lines (left to right, top to bottom: Si I (1.59 μm), CO bandhead (1.62 μm), CO bandhead (1.66 μm), Al I triplet (1.672, 1.675, 1.676 μm), OH (1.69 μm), Mg I (1.71 μm).

this spectrum only with CD-60 3621, resampled to the velocity resolution of the MMIRS spectrum. We initially mask only those pixels that are strongly affected by residuals from telluric emission lines. This leaves 169 pixels (from a total of 463) for the cross-correlation. The peak of the cross-correlation function is found at a shift of 3.5 ± 0.2 pixels, or 410 ± 20 km s^{-1}. As a consistency check we also cross-correlate the spectra using only regions where we could visually identify absorption lines. This leaves us with 63 pixels. The shift found in this way is consistent with the first: 3.6 ± 0.3 pixels, or 430 ± 30 km s^{-1}. Correcting these shifts for the radial velocity of CD-60 3621 gives values of 400 ± 20 and 410 ± 30 km s^{-1}, respectively. However, the uncertainty on the position of the peak of these cross-correlation functions is calculated assuming they have a Gaussian profile. This is the case for the X-shooter data but not for the MMIRS data. Therefore, the error on the radial velocity of the MMIRS spectrum is underestimated.

To gain more insight in the uncertainties on the radial velocities, we perform a bootstrap analysis. We use the MOLLY command *boot* to produce 1000 resampled copies of the MMIRS and X-shooter spectra. We then cross-correlate these with the spectrum of CD-60 3621 using *xcor*, and fit a Gaussian to the resulting distribution of radial velocities. The width of this Gaussian is a good measure of the uncertainty on the radial velocity. After correcting for the radial velocity of CD-60 3621 we find a value of 416.6 ± 1.6 km s^{-1} for the X-shooter spectrum. As we expected, this value is consistent with the one we obtained directly from the cross-correlation. For the MMIRS spectrum, we find a radial velocity of 410 ± 70 km s^{-1} if we use the 169-pixel mask (see Figure 5.2), and 410 ± 30 km s^{-1} with the 63-pixel mask. We conservatively adopt that the radial velocity of J0047 as measured from the MMIRS spectrum is 410 ± 70 km s^{-1}.

5.3.2 Nebular emission lines

Although the UVB and VIS spectra have very weak continua (UVB: S/N < 1, VIS: S/N ≈ 1) there are several emission lines visible in the data. In the UVB data, these are the [O II]$\lambda\lambda 3727, 3729$, H$\beta$ and [O III]$\lambda\lambda 4956, 5007$ lines. In the VIS spectrum we detect [N II]$\lambda 6548$, Hα, [N II] $\lambda 6583$ and the [S II] $\lambda\lambda 6716, 6731$ doublet. Inspection of the 2D spectra reveals that these lines do not fill the whole slit but are extended in the direction of — and peak around — the bright source that dominates the unused nod position B (this source is located $\sim 5''$ East of the RSG, but is not visible in our NIR image due to its blue colour; for the 1 and 2D VIS spectra see Figure 5.3). After reading the spectra of the single exposures into MOLLY and applying *hfix*, we average them using the task *average*. We then measure the radial velocity of the emission line region in the UVB and VIS spectra separately by using the *mgfit* function to fit a set of Gaussian curves with a common velocity offset to the above-mentioned lines. The average radial velocity we find in this way is 351 ± 4 km s^{-1}.

From the fits to the spectra we also obtain line ratios of log([O III]/Hβ), log([N II]/Hα) and log([S II]/Hα). These ratios are plotted in Figure 5.4, adapted from Ho (2008). Close to the blue source the line ratios are fully consistent with a H II region, while at the position of the ULX the line ratios are more like those seen in Seyferts.

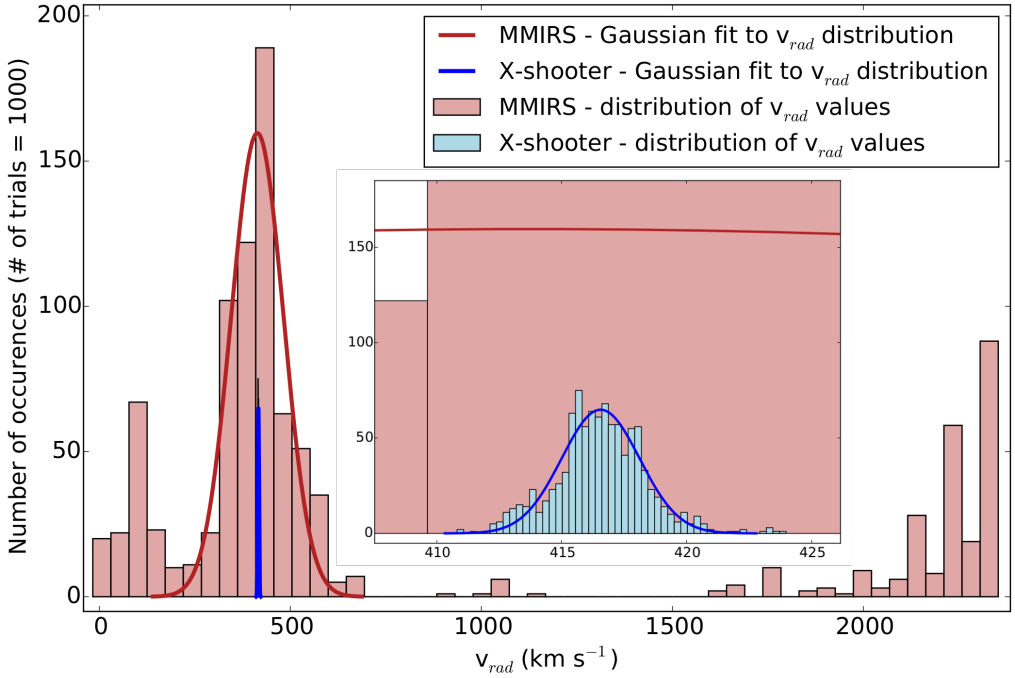

Figure 5.2: The histograms show the distribution of radial velocities obtained by cross-correlating 1000 bootstrapped copies of the MMIRS spectrum (red) and the X-shooter spectrum (blue) with CD-60 3621. The systemic velocity of CD-60 3621 of 17 km s^{-1} is already subtracted. The best-fitting Gaussian curves to the data are also plotted (red/blue lines). Inset is a zoom-in of the image around 415 km s^{-1} to show the X-shooter data more clearly.

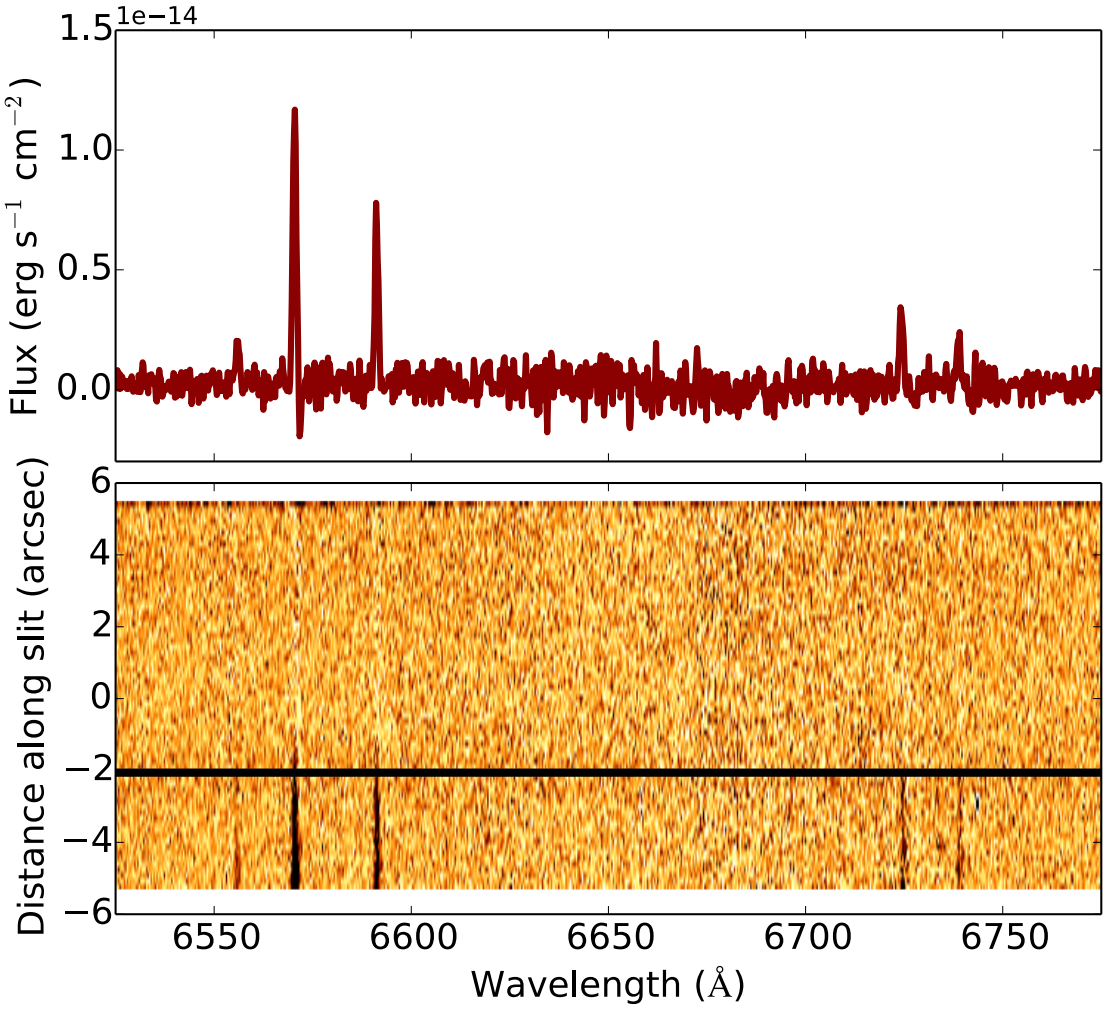

Figure 5.3: Part of the VIS spectrum with the [N II]λ6548, Hα, [N II] λ6583 complex and the [S II] $\lambda\lambda$6716, 6731 doublet. Upper figure: the flux-calibrated spectrum extracted at the position of the ULX. Lower figure: the 2D image of the spectrum. Here it can clearly be seen that the emission lines are extended. The black horizontal line indicates the position of the RSG (not visible) on the detector.

The He II λ4686 line, which acts as a photon counter for photons in the 54 – 200 eV band (Pakull & Angebault 1986), has been observed in several ULX nebulae (cf. Pakull & Mirioni 2002; Kaaret & Corbel 2009; Moon et al. 2011; Gutiérrez & Moon 2014). We do not detect it in our X-shooter spectrum, with a $2-\sigma$ (99.7 % confidence) upper limit of 8.8×10^{-17} erg cm^{-2} s^{-1} (corresponding to a luminosity of 1.2×10^{35} erg s^{-1}).

5.3.3 Probability of chance superposition

J0047 is located close to one of the spiral arms of NGC 253 (see Figure 5.5). In such an environment, the probability of a chance superposition of an unrelated object may not be negligible. Using the IRAF task *daofind* we search for point sources in our VLT/ISAAC *Ks*-band image (see Chapter 4) that are equally bright or brighter than the apparent magnitude of the

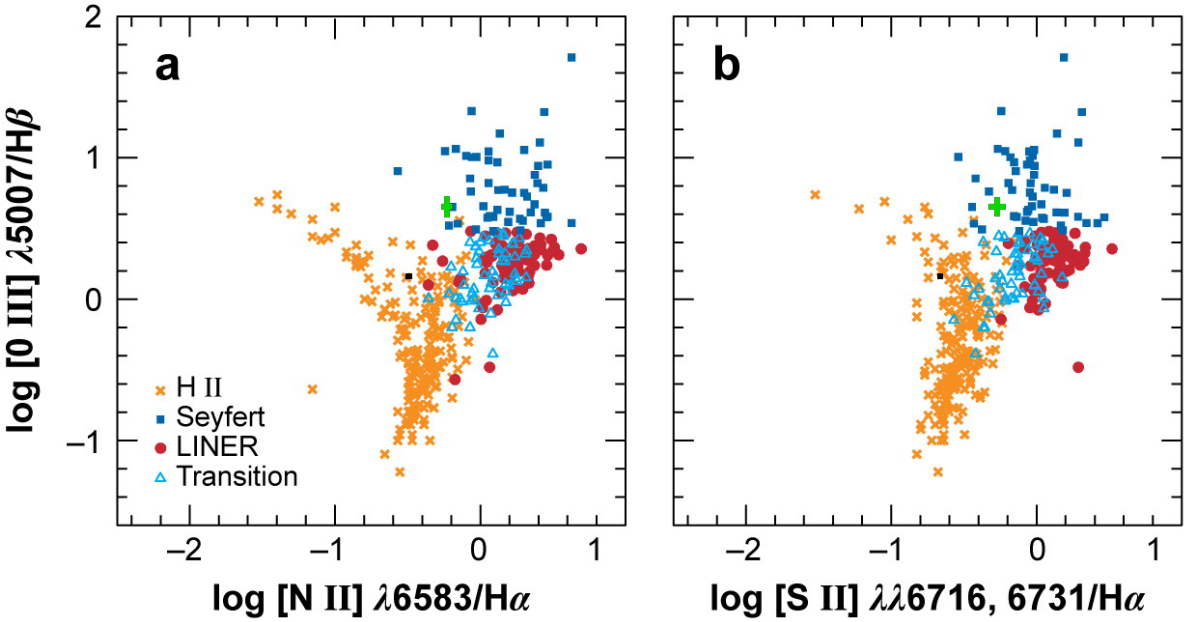

Figure 5.4: The position and error bars of the line ratios in diagnostic diagrams, indicated by black squares (for the spectrum extracted close to the blue source) and green pluses (for the spectrum extracted at the position of the ULX; figure adapted from Ho 2008). Close to the blue source the line ratios are fully consistent with a H II region, while at the position of the ULX the line ratios are more like those seen in Seyferts, indicating that the ULX might play a role in ionizing the part of the nebula that surrounds it.

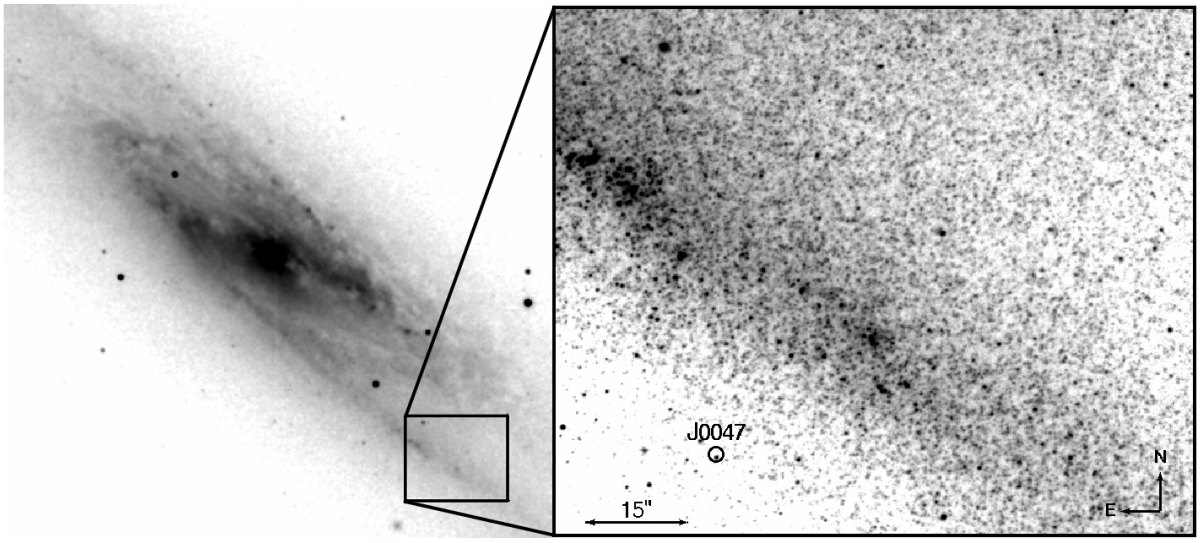

Figure 5.5: NIR image of the region around J0047. Left: 2MASS image of NGC 253. Right: Our VLT/ISAAC *Ks*-band image with the X-ray position of the ULX indicated by the black circle (radius $1.1''$, 95% confidence).

candidate RSG ($Ks = 17.2 \pm 0.5$). We find that there are 50 such sources in our image, that has a total area of 7200 arcsec^2. The error circle around the X-ray position of the ULX has a radius of $1.1''$, or an area of 3.8 arcsec^2 (see Chapter 4 for the calculation of the size of the error circle and details of the ISAAC NIR image). This means the probability of finding a source as bright as the RSG in the error circle by chance superposition is 2.6%. However, this image includes part of a spiral arm of NGC 253 while the ULX is located just outside this arm, where the point source density is lower. Therefore, 2.6% is a conservative upper limit. Due to the inhomogeneous distribution of stars, the value for the chance superposition probability depends strongly on the part of the image that is selected for the calculation. Therefore, it is not possible to find an accurate value for the chance superposition probability. With an upper limit of 2.6% we cannot exclude the possibility that the RSG and ULX are unrelated. Only a robust measurement of radial velocity variations will prove whether the RSG is orbiting the compact object responsible for the ULX emission.

5.4 Discussion and conclusions

We obtained low- and medium-resolution *H*-band spectra of the counterpart of J0047, a ULX in NGC 253. From a cross-correlation with spectra of RSGs in the Milky Way, LMC and SMC we conclude that the candidate counterpart is most likely an early M-type supergiant.

In the near-UV and visible parts of our X-shooter spectrum we detect several emission lines with line ratios that are in between those of H II regions and Seyferts (see Figure 5.4). The 2D profile of the emission lines shows that they are extended in the direction, and peak at the position, of a bright and blue optical source at $\sim 5''$ (corresponding to ~ 85 pc at the distance of NGC 253) from the RSG. This source is not visible in our NIR image but was

reported by Bailin et al. (2011) to have $M_V = -8.1$ and $V - I = 0$, consistent with a late B or early A supergiant. Close to this blue source the ratios of the emission lines are different from the ratios found at the position of the ULX, and fully consistent with a H II region. We do not detect the He II $\lambda 4686$ line that is indicative of X-ray illuminated nebulae, with a $2-\sigma$ upper limit of 8.8×10^{-17} erg cm^{-2} s^{-1} (corresponding to a luminosity of 1.2×10^{35} erg s^{-1}). For comparison, Moon et al. (2011) report a luminosity in this line of $\sim 8.8 \times 10^{34}$ erg s^{-1}for M81 X-6, a ULX with an X-ray luminosity similar to J0047. We propose that the nebula is excited both by young stars and the ULX, tracing a region with recent star formation where also the RSG was formed. A detection of - or a stronger limit on - the He II $\lambda 4686$ line could (dis)prove this scenario.

We use these lines to measure the projected radial velocity of NGC 253 at the position of the ULX and find a value of 351 ± 4 km s^{-1}. This is compatible with the value of 350 ± 30 km s^{-1} reported by Hlavacek-Larrondo et al. (2011), who measured the rotation curve of the galaxy using Hα observations. The radial velocity of the counterpart, as measured from our VLT/X-shooter spectrum taken in August 2014, is 417 ± 4 km s^{-1}. This proves that it is not a foreground or background object but is located in NGC 253, confirming its absolute *Ks*-band magnitude of -10.5 ± 0.5 and its identification as an RSG. This absolute magnitude is too bright for asymptotic giant branch (AGB) stars, that have absolute K-band magnitudes between -6.4 and -8.2 (Knapp et al. 2003). This makes J0047 a very strong candidate for a ULX with an RSG donor star. The ultimate proof for this would be the detection of periodic radial velocity variations in the RSG.

With an effective temperature in the range of 3000 – 3900 K (spectral types M0–3, Tokunaga 2000), the expected radius of the RSG based on its absolute *Ks*-band magnitude of -10.5 is $\approx 600 - 1600\ R_\odot$. Assuming Roche lobe filling RSG with a mass of 10 $M_\odot$, the orbital period expected for such an RSG orbiting a BH is 4.5 – 20 years. The apparent radial velocity amplitude depends on this period as well as on the mass ratio and the inclination of the system. For instance, for an inclination of 60°, this velocity amplitude varies from ~ 20 km s^{-1} in the case of a stellar mass BH, to hundreds km s^{-1} for an IMBH (see Figure 5.6). We do not detect a significant difference in radial velocity between our June 2013 and August 2014 spectra (Δv = 10 ± 70 km s^{-1}). The large uncertainty is due entirely to the June 2013 low resolution, low S/N MMIRS spectrum, and prevents us from putting strong limits on the mass of a possible BH companion. We calculate the probability of detecting a velocity shift larger than 80 km s^{-1} (our 1-σ upper limit on the velocity shift) for a range of black hole masses and orbital periods, taking into account that the orbital phase is unknown. For a system inclination of 60°, we find that if the orbital period is 4.5 years, we have a $< 50\%$ chance of detecting a velocity shift if $M_{BH} < 100\ M_\odot$. If the orbital period is more than 10 years we would not detect RV variations even if the RSG orbits a 1000 $M_\odot$ BH.

However, we do measure a radial velocity offset of 66 ± 6 km s^{-1} between the RSG and its surroundings (as traced by the emission lines). We consider three possible explanations for this offset:

1: The RSG and the X-ray source are unrelated, and the RSG is a single runaway star. In this scenario the ULX has another, fainter donor star that we do not detect. Eldridge et al. (2011) calculated the runaway fraction of RSGs in a simulated stellar population; at solar

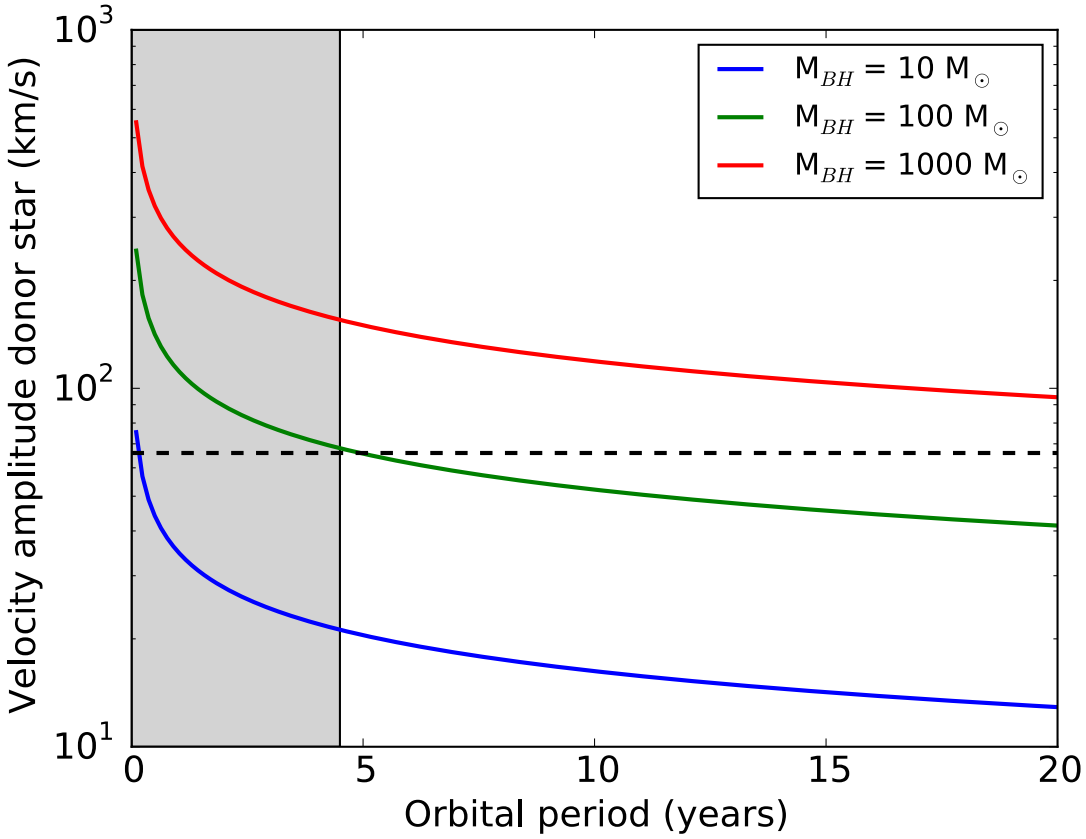

Figure 5.6: The radial velocity amplitude for a 10 $M_\odot$ mass donor in orbit around a 10, 100, or 1000 $M_\odot$ black hole (lower, middle and upper line, respectively) as a function of orbital period. A system inclination of 60° is assumed. Assuming a Roche lobe filling RSG, the expected orbital period is between 4.5 and 20 years. Smaller donor radii give shorter orbital periods; a higher donor mass requires a higher BH mass to reach the observed velocity. The black dashed line indicates a velocity of 66 km s^{-1}; the hashed area is ruled out based on the necessary radius of the RSG.

metallicity, they find that 7.2% of RSGs have a space velocity > 30 km s^{-1} (their table 4). Of those runaway RSGs, $\sim 10\%$ have a space velocity > 60 km s^{-1} (the 1-σ lower limit to our velocity offset; their figure 2). We combine this with the upper limit of 2.6% that we find for the chance superposition probability of the RSG with the ULX. Using these conservative estimates (since we only measure the radial velocity of the RSG and the space velocity is likely larger) we find that the probability of a chance superposition of the ULX with a runaway RSG is $\lesssim 0.02\%$.

2: The RSG is the donor of the ULX and the offset of 66 ± 6 km s^{-1} is the systemic velocity of the binary: the BH (or neutron star) received a large natal kick (NK) and dragged the RSG (or its progenitor) with it (Repetto et al. 2012). Some Galactic BH binaries show high peculiar velocities (cf. Miller-Jones 2014). However, these are all BHs with low-mass companions. Instead, Cyg X-1, a binary containing a stellar mass BH with an $\sim 30\ M_\odot$ donor star (which is of the same magnitude as the RSG mass), has a peculiar velocity of only ~ 20 km/s. The difficulty with this scenario is that the probability of kicking a BH/NS plus 10 $M_\odot$ donor in a wide orbit to a high systemic velocity, while keeping the binary intact, is very small.

In order to quantify this we simulate a population of binaries containing the progenitor of the BH with a 10 $M_\odot$ star as companion, calculating the effect of the BH formation event on the orbital and kinematical properties of the binary. The distribution of initial binary separations is taken to be flat between a minimum value $a_{\rm min}$, corresponding to the orbital separation at which either one of the two components fills its Roche lobe, and a maximum value of $1000\ a_{\rm min}$. We model the BH formation event assuming a mass equal to half the mass of the BH is ejected instantaneously from the binary. In the most standard formation scenario, BHs are thought to be produced via fallback on to the nascent neutron stars. In such a scenario, BHs are then expected to receive a NK, as neutron stars do. The NK will be however reduced by the ratio $M_{\rm NS}/M_{\rm BH}$, simply by conservation of linear momentum: $V_{\rm NK,\,BH} = V_{\rm NK,\,NS}(M_{\rm NS}/M_{\rm BH})$, where $V_{\rm NK,\,NS}$ is drawn from a Maxwellian distribution as in Hobbs et al. (2005). The NK has a random orientation with respect to the binary orbital plane. Through the laws of conservation of energy and orbital angular momentum, we calculate the orbital parameters (a, e) of the binary right after the BH is formed. We select among those binaries which stay bound in the process, those ones which satisfy two constraints.

The first constraint is that the systemic velocity acquired by the binary in the BH formation event, i.e. the velocity of the new centre of mass with respect to the old one, has to be larger than 60 km s^{-1}. The second constraint comes from the spectral and photometric properties of the companion star. The orbital separation after the BH is formed has to allow for mass transfer to happen on the nuclear time-scale of the companion when it fills its Roche lobe as an RSG. This is done making sure that the Roche lobe radius of the companion in the circularized orbit is in the interval $600 - 1600\ R_\odot$.

We show the results of this simulation in Figure 5.7. The solid line shows the probability for the binary to stay bound in the BH formation event. The dashed line shows the probability for such a surviving binary to acquire a systemic velocity larger than 60 km s^{-1}. Both probabilities are shown as a function of the BH mass. We also show in the plot the range of possible systemic velocities acquired by the surviving binary; the minimum and maximum value for the systemic velocity are calculated at the 99.7% probability. These simulations were done

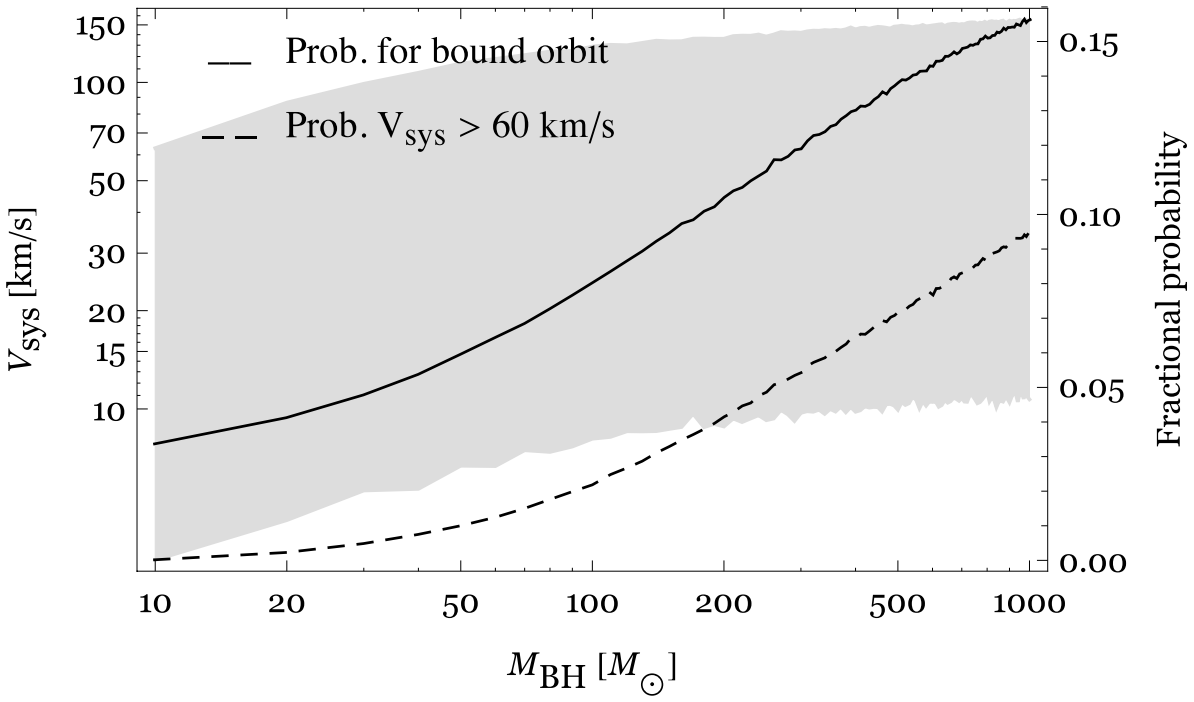

Figure 5.7: Probability fraction for the binary to stay bound in the BH formation event (solid line), and probability fraction that such a surviving binary acquires a systemic velocity greater then 60 km s^{-1} (dashed line), both as a function of the BH mass. The shaded area corresponds to the range of possible systemic velocities acquired by the binary as a function of the BH mass.

conservatively assuming an RSG of 10 $M_\odot$; if the donor star is more massive, the probabilities will be lower.

Projection effects lower the probability even further. The chance that v_{sys} is pointed within a degree from our line of sight is of the order of 10^{-5}, so the space velocity of the RSG with respect to its environment is likely larger than what we measure in the radial direction. Bearing in mind that BH formation is still very uncertain, we also tested a more conservative formation scenario for the BH, in which the BH does not receive any NK at birth, and the peculiar velocity at birth is a consequence of the mass ejection only (Blaauw kick, Blaauw 1961). In such a case, none of the surviving binaries acquire a velocity greater than 60 km/s.

These simulations show that if the velocity difference is due to the systemic velocity only, a BH of $\gtrsim 50\ M_\odot$ is necessary to explain the measured offset.

3: The RSG is the donor of the ULX and (part of) the offset of 66 km s^{-1} is due to the binary motion of the RSG around the BH. It is difficult to explain the offset as the systemic velocity of the binary, but the velocity amplitude of an RSG orbiting a BH can be hundreds km s^{-1}. This requires a BH mass of $\gtrsim 100\ M_\odot$ for a system inclination $\leq 60°$ (see Figure 5.6).

Such a high BH mass seems at odds with what is expected based on analysis of the X-ray spectra of this ULX. However, Pintore et al. (2014) suggest this ULX may be viewed at high inclination, which would mean a lower mass BH is sufficient to explain the RV offset (Figure 5.6 shows the RV amplitude assuming an inclination of 60°). If beaming plays a role

in creating the high X-ray luminosities observed in ULXs, a high inclination might explain the relatively low X-ray luminosity of this source. The combination of these two effects might be enough to reconcile the two mass estimates.

With the current data we cannot distinguish among these scenarios for J0047. New, high quality (X-shooter) spectra will allow us to measure radial velocity shifts if they are present. This will allow us to decide whether this ULX is a good target for dynamical measurements of its BH mass.

Acknowledgements

We thank the anonymous referee for their comments that helped improve the paper. We want to thank Ben Davies for sharing his X-shooter RSG spectra and Tom Marsh for developing MOLLY. This paper uses data products produced by the OIR Telescope Data Center, supported by the Smithsonian Astrophysical Observatory. Based on observations made with ESO Telescopes at the La Silla Paranal Observatory under programme ID 093.D-0256. TPR's contributions were funded as part of the STFC consolidated grant award ST/L00075X/1.

CHAPTER 6

KECK/MOSFIRE SPECTROSCOPY OF FIVE ULX COUNTERPARTS

M. Heida, P. G. Jonker, M. A. P. Torres, T. P. Roberts, D. J. Walton, D.-S. Moon, D. Stern and F. A. Harrison

To be submitted to MNRAS

Abstract

We describe *H*-band spectra of the candidate counterparts of five ULXs (two in NGC 925, two in NGC 4136, and Holmberg II X-1) obtained on 2013 December 22, 2014 January 10 and 2014 November 5 with Keck/MOSFIRE. The candidate counterparts of two ULXs (J022721+333500 in NGC 925 and J120922+295559 in NGC 4136) have spectra consistent with those of (M-type) red supergiants (RSGs). We obtained two epochs of spectroscopy of the candidate counterpart to J022721+333500, separated by 10 months, but discovered no radial velocity variations with a 2-σ upper limit of 40 km s^{-1}. If the RSG is the donor star of the ULX, the most likely options are that either the system is seen at low inclination ($< 40^{\circ}$), or the BH mass is less than 100 $M_{\odot}$, unless the orbital period is longer than 6 years, in which case the obtained limit is not constraining. The spectrum of the counterpart to J120922+295559 shows emission lines on top of its stellar spectrum, and the remaining three counterparts do not show absorption lines that can be associated with the atmosphere of a star; their spectra are instead dominated by emission lines. Those counterparts with RSG spectra may be used in the future to search for radial velocity variations, and, if those are present, determine dynamical constraints on the mass of the accretor.

6.1 Introduction

Ultraluminous X-ray sources (ULXs) are point-like, off-nuclear X-ray sources with a luminosity in the 0.3–10 keV band $> 10^{39}$ erg s^{-1} (see Feng & Soria 2011 for a review). This is higher than the Eddington luminosity of a 10 $M_{\odot}$ black hole (BH), which raises the question how ULXs attain their high luminosities. The majority of (candidate) ULXs, with $L_{\rm X}< 10^{41}$ erg s^{-1}, likely contain stellar mass BHs accreting at or above their Eddington limit (Middleton et al. 2015 and references therein), although some of these ULXs could still contain massive stellar or even intermediate mass BHs (Colbert & Mushotzky 1999). The most luminous ULXs, with $L_{\rm X}> 10^{41}$ erg s^{-1} (referred to as hyperluminous X-ray sources or HLXs) are hard to explain as stellar mass BHs, and are strong candidates to host BHs more massive than those found in X-ray binaries in our Galaxy (Farrell et al. 2009; Strohmayer & Mushotzky 2003; Pasham et al. 2014; Casares & Jonker 2014).

To date, there are only two ULXs with mass estimates that do not depend on modelling of their X-ray spectra (Motch et al. 2014; Liu et al. 2013). In both cases, although the uncertainties on the masses are large, a stellar mass BH is favoured as the accretor. In addition, Bachetti et al. (2014) discovered X-ray pulsations from M82 X-2, proving that the accretor in that ULX is a neutron star.

Improved model-independent mass measurements of ULX accretors are necessary to prove that the so-called 'ultraluminous state' (Gladstone et al. 2009) is indeed a sign of super-Eddington accretion onto stellar mass BHs, to see if neutron star accretors are common among ULXs, and to find out if some ULXs contain massive stellar or intermediate mass BHs. Dynamical mass measurements would be the most reliable. Through phase-resolved spectroscopic observations of the donor star (preferably using photospheric absorption lines to measure the radial velocity), it is possible to trace the radial velocity curve of the donor and measure the mass function, setting a lower limit on the mass of the compact object. In the optical regime, attempts to measure the mass function in this way have been hampered by the presence of bright accretion discs in these systems (Roberts et al. 2011; Liu et al. 2012). However, some ULXs may have red supergiant (RSG) donor stars and these can outshine the disc in the near-infrared (NIR) part of the spectrum (Copperwheat et al. 2005).

In Chapter 4 we describe our systematic search for NIR counterparts to nearby ULXs. We discovered 11 candidate counterparts that could be RSG donor stars. NIR spectroscopy with the Very Large Telescope (VLT) has shown that one of these candidate counterparts, RX J004722.4-252051 in NGC 253, is indeed an M-type RSG, with a peculiar velocity suggestive of a massive stellar BH accretor (Chapter 5). In this paper we describe the results of our observations with the Keck telescope that yielded NIR spectra of five other ULX counterparts from our sample. Two of the ULXs are situated in NGC 925 and two in NGC 4136. The last ULX whose NIR counterpart we observed is Holmberg II X-1 (hereafter Ho II X-1). Three of these ULXs (J022721+333500 in NGC 925 and J120922+295551 and J120922+295559 in NGC 4136) have been observed to reach maximum X-ray luminosities of a few times 10^{39} erg s^{-1}; J022727+333443 in NGC 925 and Ho II X-1 are brighter, reaching X-ray luminosities of a few times 10^{40} erg s^{-1}.

The goal of this campaign was to characterize the NIR counterparts. Hence we initially

Table 6.1: Description of the Keck/MOSFIRE observations. Apparent and absolute *H*-band magnitudes from Chapter 4 are also provided.

Source	H	M_H	Observation date (UT)	Exposure time (h)
J022721+333500	18.7	-10.6	2013 Dec 22& 2014 Jan 10	5.4
			2014 Nov 4	3
J022727+333443	20.1	-9.2	2013 Dec 22 & 2014 Jan 10	5.4
J120922+295551	19.1	-10.8	2014 Jan 10	2.4
J120922+295559	19.2	-10.7	2014 Jan 10	2.4
Ho II X-1	20.6	-7.1	2014 Jan 10	2.6

obtained only one epoch of data per source. Based on these observations, we obtained a second epoch for one source in NGC 925, J022721+333500, to search for radial velocity shifts. This paper is organised as follows: in Section 2 we describe the setup of our observations. Section 3 describes our data reduction and analysis. In Section 4 we present the results for the separate counterparts and in Section 5 we discuss our findings and conclude.

6.2 Observations

We obtained *H*-band spectra of five ULX counterparts with the Multi-Object Spectrometer for Infra-Red Exploration (MOSFIRE; McLean et al. 2010, 2012), mounted on the Keck I telescope on Mauna Kea. MOSFIRE has a field of view of $6.1' \times 6.1'$ with a pixel scale of $0.18''$ per pixel and a robotic slit mask system with up to 46 slits. The data were taken on 2013 December 22, 2014 January 10 (program ID C241M), and 2014 November 4 (program ID C201M; all dates are in UT). We used slit masks with $0.7''$ wide slits which give us, in combination with the *H*-band filter and the fixed MOSFIRE diffraction grating, a spectral resolution $R \approx 3000$ and spectral coverage from ~ 14500 – 18000 Å. The seeing on all nights was $> 0.7''$ ($\sim 0.8''$ – $1.0''$), so that the resolution is set by the slit width. The integration time per exposure was 119.3 s on all nights. On 2013 December 22 and 2014 January 10 we used an ABBA nodding pattern with a nod amplitude of $1.5''$ along the slit. On 2014 November 4, we used a different slit orientation than we did for the observations of NGC 925 in December 2013 and January 2014 (see also Figure 6.1). The orientation used in the first observations was chosen to avoid other nearby objects — the new orientation was chosen to better separate the two components of the elongated counterpart of J022721+333500; however, the seeing was not good enough to distinguish the two components. As a result there were multiple sources in the slit containing J022721+333500, so we used an ABBA nodding pattern with a larger nod amplitude ($2.9''$ for the first 20 exposures and $3.4''$ for the remaining 71 exposures). The total exposure times are listed in Table 6.1. We observed telluric standard stars at similar airmass as the science targets before and after every series of exposures. No flux standards were observed. For every slit mask configuration we obtained flats and arc spectra in the afternoon before the observing run.

6.3 Data reduction and analysis

We use the MOSFIRE Data Reduction Pipeline version 2014.03.14 (MOSFIRE-DRP; described in detail by Steidel et al. 2014) to reduce the raw data. The pipeline handles the background subtraction and combines the separate exposures to produce a 2D, rectified and wavelength calibrated spectrum for every slit. The wavelength calibration is done by fitting a polynomial to the night sky lines, using wavelengths in vacuum. The typical standard deviation of the residuals after fitting is 0.1 Å ($\sim$ 2 km s^{-1}). For every observing night and target, we split the science exposures into two groups of at most 1.5 hours and reduce them separately.

We then use the STARLINK program FIGARO to extract the spectra with the *profile* and *optextract* tasks (Horne 1986). In the November 2014 observation of J022721+333500 we extract spectra of three objects that are visible in the slit. To correct for telluric absorption, we use the IDL routine XTELLCOR_GENERAL (Vacca et al. 2003).

For the final analysis (characterization of the spectra and — if possible — cross-correlation with template spectra to measure radial velocities) we use Tom Marsh's programme MOLLY. We load the wavelength-calibrated spectra into MOLLY and first run the task *hfix* to calculate the heliocentric velocity. Because the spectra are not flux-calibrated, we normalize them by fitting a 3rd order polynomial and dividing by it. This removes any systematic flux offsets, which is important to do before we average the spectra of every target. The only exception is J022727+333443, since it has no continuum that can be used for the normalization. After normalizing the spectra we rebin them to a common velocity scale of 30.25 km s^{-1} pixel^{-1} using *vbin*, which also moves the spectra to the heliocentric frame. Finally we average the spectra into one spectrum per target (two for J022721+333500), after checking that there are no velocity shifts between the spectra taken in December 2013 and January 2014.

For J022721+333500 and J120922+295559, we use *xcor* to cross-correlate the spectra with template spectra of a range of spectral types (that have been normalized in the same way as our science spectra). As templates we use model RSG spectra from Lançon et al. (2007), with solar abundances, a mass of 15 $M_\odot$ and temperatures ranging from 2900 – 5000 K. With *xcor* we apply shifts to the spectrum of -10 to +30 pixels, with steps of 1 pixel, and calculate the value of the cross-correlation function for each pixel shift. *xcor* then computes the radial velocity difference between spectrum and template by fitting a parabola to the cross-correlation function at the peak pixel and its two neighbouring pixels. To obtain a more robust measure of the uncertainty on the radial velocity measurements, we use the MOLLY command *boot* to produce 1000 bootstrapped copies of the spectra, and use *xcor* to cross-correlate them with one of the model spectra of Lançon et al. (2007) (with $T_{\rm eff}$ = 3500 K). We then fit a Gaussian curve to the resulting distribution of radial velocities and adopt the centroid and width of this Gaussian as a robust estimate of the radial velocity and its uncertainty.

For the other spectra, where we detect emission lines, we use the MOLLY command *mgfit* to fit Gaussian lines to the positions of [Fe II] and/or hydrogen Brackett lines in the spectra, and calculate their offset with respect to their rest wavelengths.

6.4 Results

NGC 925: J022721+333500

In the NIR image of NGC 925 (see Figure 6.1) the counterpart to J022721+333500 appears elongated. Due to the orientation of the slits that we used for the observations in December 2013 and January 2014, only one object (source 2 in Figure 6.1) is visible in those observations. In the November 2014 observations we used a different slit orientation to better separate the components of the counterpart, but the seeing was not good enough to distinguish them. In these observations, spectra of three objects are visible. Source 2 (see Figure 6.1) corresponds to the elongated counterpart. All three spectra (sources 1 to 3) show a continuum with many absorption lines from neutral metals. The CO bandheads at 1.62 and 1.66 μm are also detected, proving that the objects are all K- or M-type stars (see Figure 6.2 for the spectrum of source 2).

From the cross-correlation with template spectra we find a radial velocity of 495 ± 11 km s^{-1} for source 1 and 502 ± 8 km s^{-1} for source 3. For source 2 we find a radial velocity of 506 ± 9 km s^{-1} for the Dec 2013/Jan 2014 spectrum and 500 ± 14 km s^{-1} for the Nov 2014 spectrum. However, source 3 is not centred on the slit, which causes an offset in the radial velocity. The sources are too faint to be visible in our through-slit alignment images. However, brighter stars selected to check the slit alignment were detected and we use the comparison of their locations on the through slit image with that of the deep WHT/LIRIS image to determine the actual location of the slit on the sky. From this we derive a best estimate of the offset between the location of source 3 and the centre of the slit of $0.5'' \pm 0.05''$ (see Figure 6.1). This corresponds to 2.8 ± 0.3 pixels on the MOSFIRE detector, or a velocity offset of 85 ± 10 km s^{-1}. Because the source is not a perfect point source, this value is an upper limit on the the velocity offset. If we correct for this we find a radial velocity $\geq 420 \pm 15$ km s^{-1} for source 3. The radial velocities of sources 1 and 2 are in agreement with what is expected from the radial velocity field of NGC 925 (de Blok et al. 2008). This proves that the objects are located in NGC 925, confirming the absolute magnitude reported for source 2 in Chapter 4. That absolute magnitude is such that even if source 2 consists of two equally bright sources, they are both RSGs. The radial velocity of source 3 is somewhat offset with respect to the local radial velocity, but that source is still most likely located in NGC 925. The highest values for the cross-correlation function for all sources are found when cross-correlating with the templates with the lowest temperatures, indicating that these are probably M-type stars.

NGC 925: J022727+333443

The counterpart to J022727+333443 shows no continuum emission at all. The spectrum is dominated by a single strong emission line due to [Fe II] ($\lambda 1.644$). Many weaker emission lines are visible, due to [Fe II], H (Brackett lines), He I, He II and H_2. These are indicated in Figure 6.3. We fitted Gaussian profiles to these emission lines to calculate the radial velocity of the counterpart. The [Fe II], hydrogen and helium lines are well fitted by a Gaussian, but

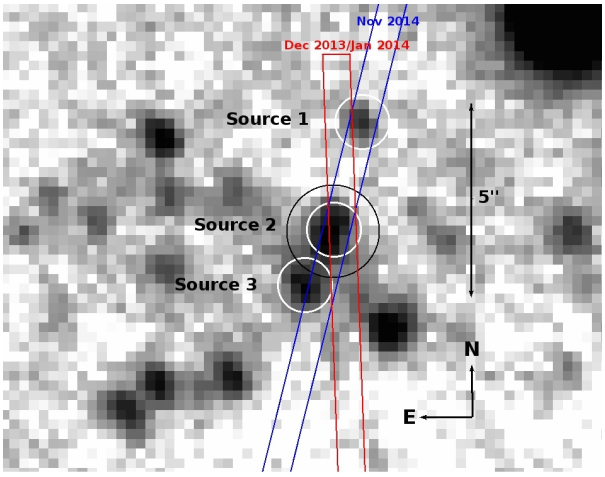

Figure 6.1: WHT/LIRIS *H*-band image of J022721+333500 in NGC 925, with the MOSFIRE slit positions indicated by red (December 2013/January 2014 observations) and blue (November 2014 observations) boxes. The black circle indicates the *Chandra* X-ray localisation of the ULX. The white circles indicate the sources visible in our November 2014 MOSFIRE observation. Sources 3 is not centred on the slit, causing an offset $\leq 85 \pm 10$ km s^{-1} in its measured radial velocity.

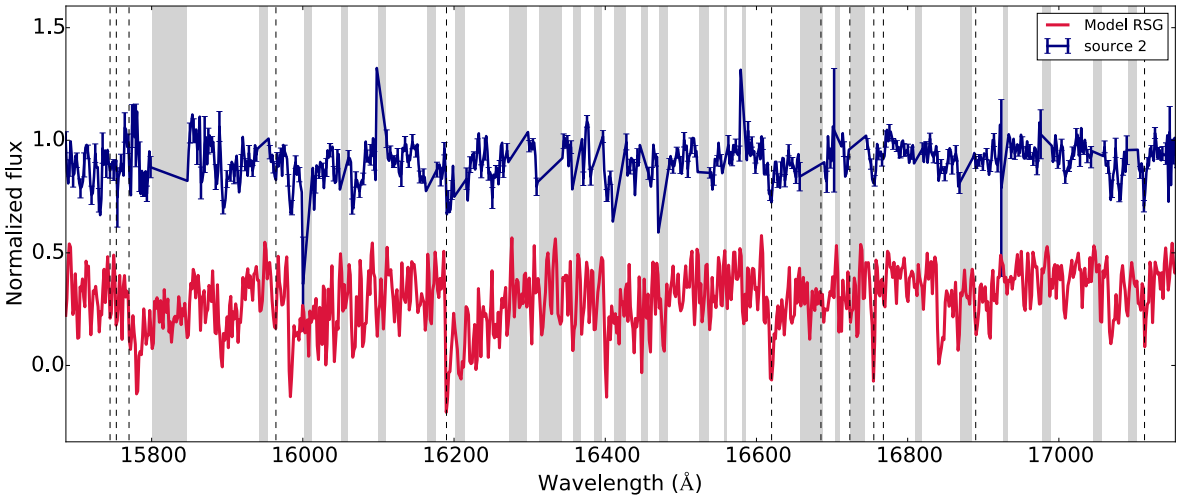

Figure 6.2: The normalized spectra of J022721+333500 (source 2, from the Dec 2013/Jan 2014 observation, blue line) and a 3500 K model from Lançon et al. (2007) (red line, shifted downwards by 0.5 for clarity). The spectrum of J022721+333500 has been shifted by -506 km s^{-1} and has been interpolated over wavelength ranges that were strongly affected by noise from telluric emission lines (grey shaded areas). The dashed lines indicate the positions of absorption lines that are indicative of late-type stars — from short to long wavelength: Mg I triplet (1.574, 1.575, 1.577 μm), Si I (1.59 μm), CO bandhead (1.62 μm), CO bandhead (1.66 μm), Si I (1.67 μm), Al I triplet (1.672, 1.675, 1.676 μm), OH (1.69 μm), and Mg I (1.71 μm).

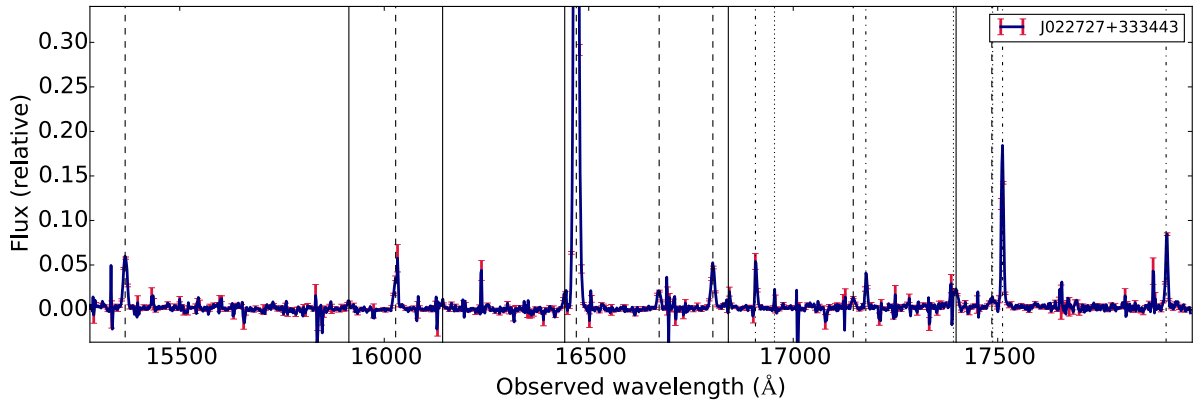

Figure 6.3: The MOSFIRE spectrum of J022727+333443. Error bars (in red) are plotted for every third data point. Dotted lines indicate positions of He lines, dashed lines indicate positions of [Fe II] lines, solid lines indicate the H Brackett series, dot-dashed lines indicate positions of H_2 lines. The vertical lines representing spectral transitions are redshifted by 540 km s^{-1}. The peak of the [Fe II] ($\lambda 1.644$) line lies at 1.35 (relative units).

the H_2 lines are asymmetric. The radial velocity of the lines is 540 ± 2 km s^{-1}, proving that the source is part of NGC 925 and not a foreground or background object.

Ho II X-1

Ho II X-1 is a well-studied nearby ULX. It is surrounded by a nebula powered by the X-ray source that was discovered in optical observations (e.g. Pakull & Mirioni 2002; Lehmann et al. 2005). Our NIR spectrum shows a weak continuum with emission lines, most notably the [Fe II] ($\lambda 1.644$) line and the hydrogen Brackett lines (see Figure 6.4). From the positions of the emission lines we calculate a radial velocity of 165 ± 3 km s^{-1}, consistent with the radial velocity of the galaxy and earlier observations of the nebula.

NGC 4136: J120922+295551

The spectrum of the counterpart of J120922+295551 resembles that of Ho II X-1, with a weak continuum and emission lines (see Figure 6.5). The 2D spectrum shows spatially extended emission around the position of the ULX, with stronger Brackett emission lines further from the ULX. The radial velocity of the counterpart as measured from the shifts of the emission lines is 550 ± 5 km s^{-1}, proving that the source is located in NGC 4136. The continuum emission could be due to an RSG. The signal to noise ratio in the continuum is ~ 5, and the strongest absorption line in an RSG, the CO-bandhead at 1.62 μm, lies in a region that is heavily affected by noise from telluric emission lines, precluding us from detecting this feature. Other RSG absorption lines would not be significant at this signal to noise ratio.

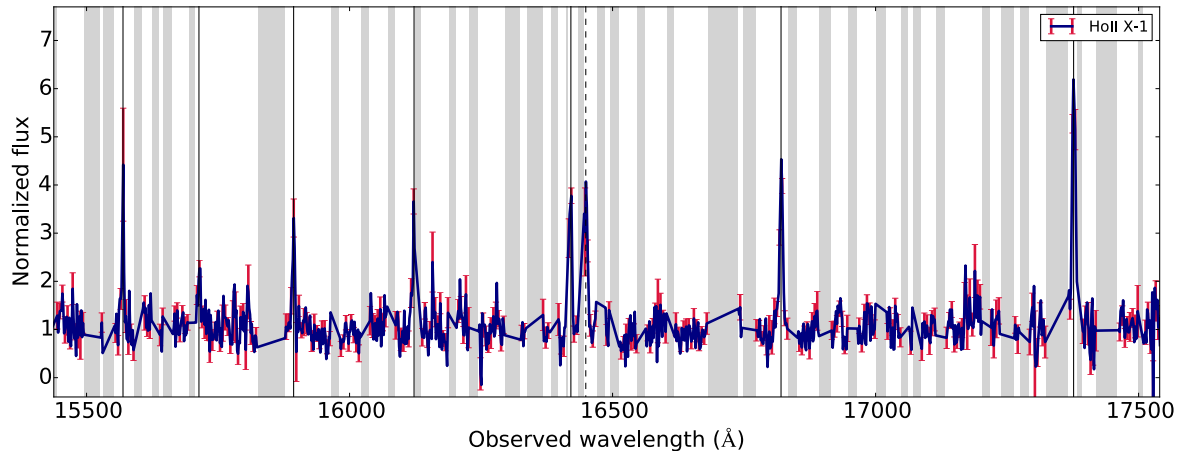

Figure 6.4: The normalized MOSFIRE spectrum of Ho II X-1. The spectrum has been interpolated over wavelength ranges that were strongly affected by noise from telluric emission lines (grey shaded areas). Error bars (in red) are plotted for every third data point. The dashed line indicates the [Fe II] ($\lambda 1.644$) line, the solid lines indicate the positions of the hydrogen Brackett lines. The vertical lines representing spectral transitions are redshifted by 165 km s^{-1}.

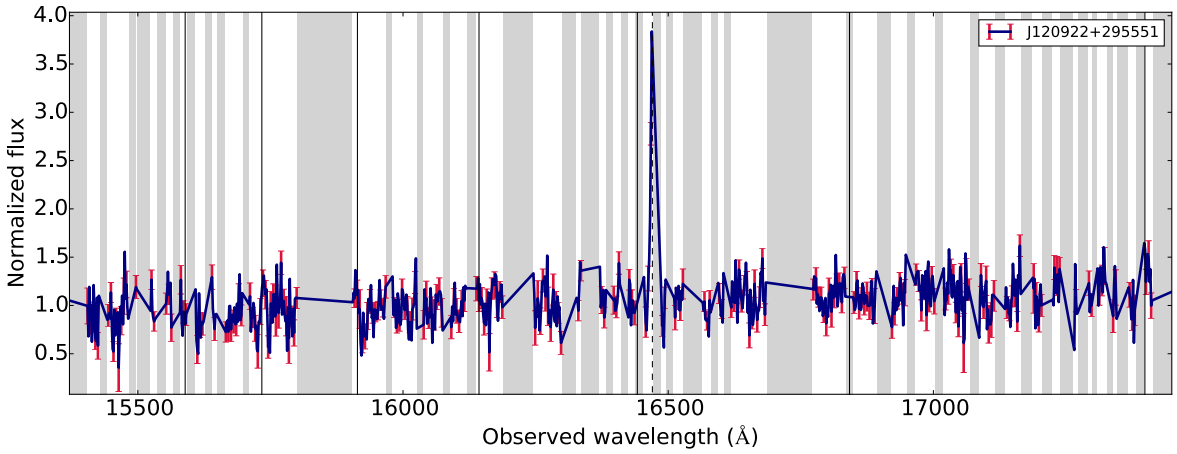

Figure 6.5: Part of the normalized MOSFIRE spectrum of J120922+295551. The spectrum has been interpolated over wavelength ranges that were strongly affected by noise from telluric emission lines (grey shaded areas). Error bars (in red) are plotted for every third data point. The dashed line indicates the [Fe II] ($\lambda 1.644$) line, the solid lines indicate the positions of the hydrogen Brackett lines. The vertical lines representing spectral transitions are redshifted by 550 km s^{-1}.

NGC 4136: J120922+295559

The spectrum of J120922+295559 shows continuum emission with absorption lines due to neutral metals and CO, indicative of late-type stars (see Figure 6.6). However, the strongest feature in the spectrum is the [Fe II] (λ1.644) emission line (dash-dotted line), similar to J022727+333443 and J120922+295551. Weaker emission lines are visible at the positions of the hydrogen Brackett lines that are in regions uncontaminated by noise from telluric emission lines, most notably at the position of the Br (10-4) line at 1.74 μm. Visual inspection of the 2D spectrum reveals that the peak of the [Fe II] emission is spatially offset by $\sim 0.8''$ with respect to the continuum emission, corresponding to a distance of ~ 45 pc. The Br (10-4) line does not show this spatial offset.

In late type stars, the CO bandhead at 1.62 μm is the strongest absorption feature, but in the J120922+295559 spectrum this bandhead is redshifted into a region heavily contaminated by noise from telluric emission lines, precluding us from reliably detecting this absorption feature. There is an absorption feature visible at the position of the CO bandhead at 1.66 μm, as well as at the positions of the Si I line at 1.59 μm, the Al I triplet (1.672, 1.675, 1.676 μm), the OH line at 1.69 μm, and the Mg I line at 1.71 μm. The cross-correlation with model RSGs yields a radial velocity of 586 ± 22 km s^{-1}, consistent with the radial velocity of NGC 4136 at the location of the ULX (Fridman et al. 2005) and thus proving that the source is indeed located in that galaxy. The highest values for the cross-correlation function are achieved with the templates with temperatures of 2900 – 4000 K, pointing towards an M-type RSG.

We measure the radial velocity offset of the emission lines by fitting Gaussian profiles to the [Fe II] (λ1.644) and Br (10-4) lines while masking the rest of the spectrum. Fitting the two lines separately we find that their radial velocities are consistent with being the same within the error bars. Fitting them simultaneously to reduce the uncertainty, we find a radial velocity of 570 ± 4 km s^{-1}, consistent with the velocity of the RSG.

6.5 Discussion and conclusions

We obtained Keck/MOSFIRE *H*-band spectra of five ULX counterparts, two located in NGC 925, two in NGC 4136 and Ho II X-1. Two of these, J022721+333500 in NGC 925 and J120922+295559 in NGC 4136 are consistent with being M-type supergiants. The absorption lines in such spectra can in principle be used to measure the radial velocity curve of the counterpart and obtain a lower limit on the BH mass.

The counterpart of J022721+333500 is elongated in our *H*-band image, but during our Keck/MOSFIRE observations, seeing conditions were not good enough to allow us to separate the spectra of the two putative components. The peak-to-peak distance of the elongated core in our LIRIS image is $\sim 0.7''$. An adaptive optics-assisted or *Hubble Space Telescope* NIR image at $\sim 0.1''$ resolution would be useful to confirm whether or not the counterpart in our LIRIS image consists of two individual sources. If this is the case, a bore-sight corrected *Chandra* position of the ULX, with a localization error of $\sim 0.2''$, could distinguish which one is the counterpart of the ULX. We obtained two epochs of spectroscopy of the candidate counterpart and found no change in the radial velocity, with a 2-σ upper limit of 40 km s^{-1}. Assuming that

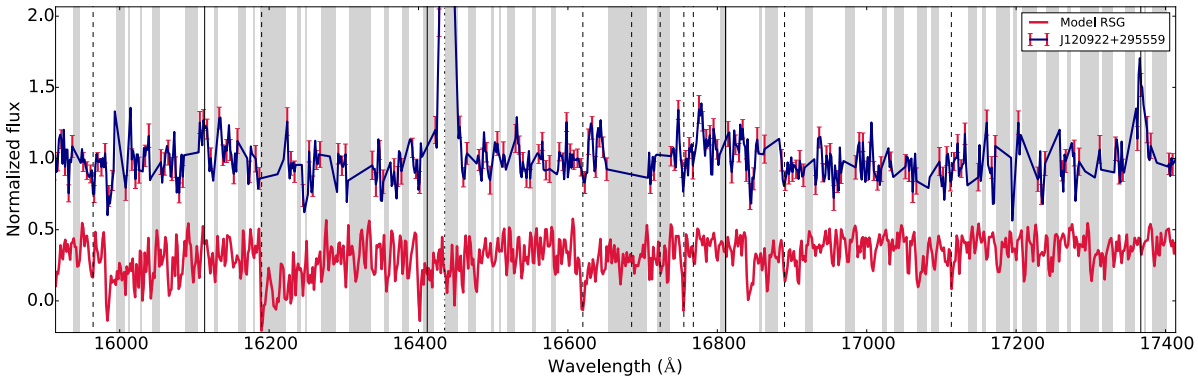

Figure 6.6: The normalized spectra of J120922+295559 (blue line, with error bars — in red — plotted at every third data point), and a 3500 K model from Lançon et al. (2007) (red line, shifted downwards by 0.5 for clarity). The spectrum of J120922+295559 has been shifted by -586 km s^{-1} and has been interpolated over wavelength ranges that were strongly affected by noise from telluric emission lines (grey shaded areas). Solid lines indicate the positions of hydrogen Brackett lines, dashed lines indicate the positions of absorption lines that are indicative of late-type stars — from short to long wavelength: Si I (1.59 μm), CO bandhead (1.62 μm), CO bandhead (1.66 μm), Si I (1.67 μm), Al I triplet (1.672, 1.675, 1.676 μm), OH (1.69 μm), and Mg I (1.71 μm). The dash-dotted line indicates the position of the [Fe II] (1.644 μm) emission line, the peak of which lies at 4.7 (relative units).

the RSG is the donor star in a binary system, the probability that we would not detect a velocity shift between two measurements depends on the orbital period, ratio of the mass of the donor star to the mass of the BH, and the inclination of the system. We calculate this probability by drawing 10000 random values for the orbital phase at the time of the first observation, and calculating how many of these result in a velocity shift smaller than our observed upper limit for a range of BH masses, orbital periods and system inclinations. The results of this calculation are shown in Figure 6.7 for system inclinations of 20°, 40° and 60°. The upper limit of 40 km s^{-1}, with the measurements taken 308 days apart, puts very weak restraints on the orbital period or BH mass if the system inclination is $< 40°$. For $i = 40°$, BH masses larger than $\sim 100\ M_{\odot}$ in combination with orbital periods shorter than ~ 4 years would likely (probability $> 50\%$) have led to a velocity difference larger than 40 km s^{-1} and would thus have been detected. For $i \geq 60°$, the same BH masses in combination with orbital periods shorter than ~ 6 years would likely have led to a detection. Given the expected radius of an M-type RSG, orbital periods shorter than 3 years can be ruled out as the Roche-radius would then be too small to contain the RSG. If the RSG is the donor star of the ULX, the most likely options are that either the system is seen at low inclination, or the BH mass is less than 100 $M_{\odot}$, unless the orbital period is longer than 6 years.

In the spectrum of J120922+295559, both stellar features, most likely due to an M-type RSG, and emission lines are visible. The absorption lines from the RSG may be used to search for radial velocity variations.

The RSG candidate counterpart of RX J004722.4-252051 in NGC 253 (see Chapter 5) shows a radial velocity that is offset with respect to its environment by 66 ± 6 km s^{-1}. The candidate donor stars of J022721+333500 and J120922+295559 do not show such an offset,

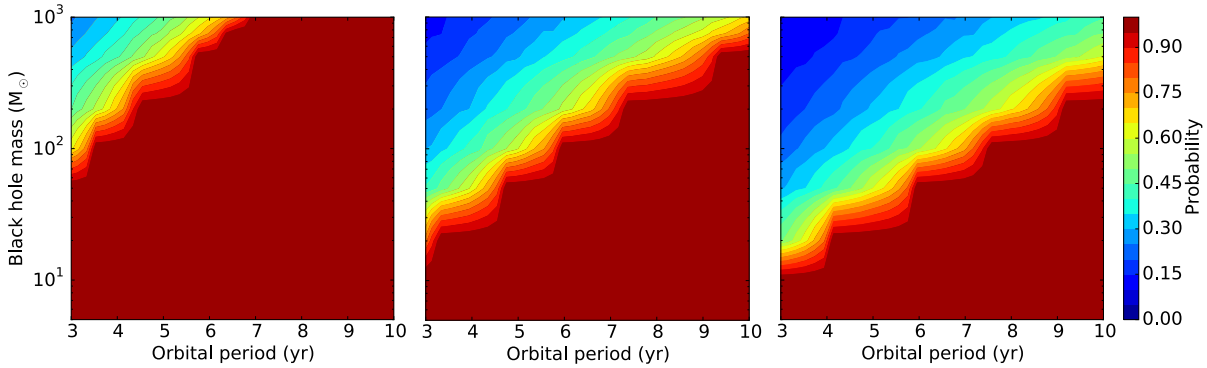

Figure 6.7: The probability that we would not detect a velocity shift smaller than 40 km s^{-1} between our two epochs of spectroscopy of J022721+333500, as a function of BH mass and orbital period, for system inclinations of 20°, 40° and 60° (left to right). We assume a mass of 10 $M_\odot$ for the RSG. Orbital periods shorter than 3 years are ruled out given the expected radius of an M-type RSG.

although source 3 in our *H*-band image of the environment of J022721+333500 may show a velocity offset, with an upper limit of 80 km s^{-1}, with respect to sources 1 and 2. Analogous to RX J004722.4-252051 in NGC 253, this offset could be due to binary motion of the RSG around a massive stellar BH or to a natal kick imparted on the BH in the supernova explosion, if source 3 would be the donor star of the ULX. However, this seems unlikely based on the 95% confidence error circle of the X-ray position of the ULX in Figure 6.1. Alternatively, it may be a runaway RSG (e.g. Eldridge et al. 2011).

Among these three RSGs, J120922+295559 is the only one that also shows emission lines in its NIR spectrum. Optical emission lines from an H II region close to the ULX are visible in the spectrum of RX J004722.4-252051, but no emission lines were detected in the NIR part of its spectrum.

The emission lines in the spectra of J022727+333443, Ho II X-1, J120922+295551 and J120922+295559 can have several origins. They may originate in a nebula, or in the accretion disc — although the latter is ruled out for the [Fe II] line in J120922+295559, as it is spatially offset from the spectrum of the counterpart. These emission lines cannot be used for dynamical mass measurements. We will discuss them in more detail in a forthcoming paper.

The apparent and absolute magnitudes mentioned in Table 6.1 are those of the combined flux in the emission lines and the continuum emission. To estimate the magnitude due to the continuum (and hence a possible donor star) only, we compare the signal to noise level for the continuum emission to values calculated with the MOSFIRE exposure time calculator[1] for our observing conditions and a range of magnitudes. We find that for Ho II X-1, the flux in the emission lines does not contribute significantly to the magnitude of the counterpart. For J022727+333443 in NGC 925, we find a limit on the apparent magnitude of $H \gtrsim 22.5$, corresponding to an absolute magnitude $M_H \gtrsim -7$. This makes it unlikely that the donor star is a supergiant of spectral type F or later (Tokunaga 2000). For J120922+295551 in NGC 4136, we find an apparent magnitude of $H \approx 20.5$, corresponding to an absolute magnitude

[1] `http://www2.keck.hawaii.edu/inst/mosfire/etc.html`

$M_H \approx -9.4$. If the continuum emission in this source is mainly due to the donor star, this absolute magnitude would mean it is still most likely an RSG. A deeper observation might then reveal stellar absorption lines.

Acknowledgements

MH would like to thank Nick Konidaris for his help with the MOSFIRE DRP. We thank Tom Marsh for developing MOLLY. The data presented herein were obtained at the W.M. Keck Observatory, which is operated as a scientific partnership among the California Institute of Technology, the University of California and the National Aeronautics and Space Administration. The Observatory was made possible by the generous financial support of the W.M. Keck Foundation. The authors wish to recognize and acknowledge the very significant cultural role and reverence that the summit of Mauna Kea has always had within the indigenous Hawaiian community. We are most fortunate to have the opportunity to conduct observations from this mountain.

SUMMARY

Ultraluminous X-ray sources (ULXs) derive their name from the fact that their luminosity is above the Eddington luminosity of a 10 $M_{\odot}$ black hole (BH). This sets them apart from normal (Galactic) X-ray binaries (XRBs), as those do not generally reach such high luminosities. There are two possible scenarios to explain the high luminosities of ULXs. One possibility is that they contain neutron star or stellar mass BH accretors, like normal XRBs, but are exceeding their Eddington limit. The other option is that they contain BHs that are (much) more massive than the stellar mass BHs found in Galactic XRBs, either massive stellar BHs (20 – 100 $M_{\odot}$) or intermediate mass BHs (IMBHs; 100 – 10^5 $M_{\odot}$).

A new hyperluminous X-ray source

The most extreme ULXs, with luminosities above 10^{41} erg s^{-1}, are considered too luminous to be explained as stellar mass BHs in a super-Eddington state. These sources are sometimes called hyperluminous X-ray sources, or HLXs. Only a handful of these are known, and they are strong candidates to contain IMBHs. Because of this, and because a group of two objects is not yet much of a group, finding more of them is important. In **Chapter 2** we describe our X-ray (*Chandra*) and optical (*HST*) observations of CXO J1225, a source that was reported first by Jonker et al. (2010) as a candidate HLX, recoiling SMBH or X-ray bright supernova. That first classification was based on one archival *Chandra* observation, one *HST* detection (in the g'-band) and *HST* upper limits in the *U*- and z'-bands. We obtained six new *Chandra* observations and one *HST* observation, and found that the X-ray count rate of the source varies by at least a factor 60. This implies that this source, like the most famous HLX source HLX-1 in ESO 243-49, goes through outburst-quiescence cycles. Its optical counterpart is also variable, which is a strong indication that the optical and X-ray sources are indeed related. In our X-ray observations, we discovered one new outburst of the source, although in that observation it was not as bright as when it was first detected. Quick Directors Discretionary Time follow-up observations, two and three weeks after the detection of the new outburst, show that it declines swiftly.

Based on its observed properties, the most probable scenario is that CXO J1225 is an outbursting HLX. Spectroscopic observations of its optical counterpart will be difficult to obtain, but are necessary to confirm the distance to this source (and thus its classification as an HLX). This is only the second HLX to be discovered that shows outbursts, after HLX-1, which is a very strong candidate to host an IMBH. This makes CXO J1225 an interesting IMBH candidate as well. Studying this source will teach us more about this class of objects.

Optical spectra of ULXs

To gain more insight into the physical nature of ULXs, reliable measurements of their accretor masses are indispensable. The most reliable way to measure the mass of a compact object in a binary system is through dynamical mass measurements. This method has the great advantage that it does not depend on (often uncertain) modelling of the broadband X-ray spectrum of the ULX. However, it does depend on spectroscopic observations of the donor star, and in the case of ULXs these are difficult to come by. One of the reasons is that there are no ULXs in the Milky Way; the nearest are found at a few Mpc, which means that their donor stars are faint optical or NIR sources. For some ULXs, obscuration by dust lanes is also a problem.

Those ULXs that do have bright optical counterparts were the obvious first candidates for optical spectroscopic studies. In **Chapter 3** we present optical spectra, obtained with the VLT/FORS2, of four ULXs with bright optical counterparts. Three of these proved to be background AGN. The fourth source, ESO 306-003, shows a spectrum consistent with that of a HII region, with indications that part of the ionizing flux could be due to the ULX. We do not detect a stellar companion to this ULX, and the emission lines from the HII region can not be used for dynamical mass measurements. These results confirm earlier findings from several authors, that ULX candidates with bright optical counterparts (and thus low X-ray-to-optical flux ratios) are predominantly background AGN. However, even though the risk of finding background AGN is quite high, so is the potential gain of finding an accreting IMBH in a globular cluster, which would have optical photometric properties similar to the optical sources we obtained spectra of. An optical spectrum is necessary to distinguish between those two possibilities.

Another reason why dynamical mass measurements are difficult to obtain is that in ULXs where we do observe an optical counterpart, the optical light is often dominated by emission from the accretion disc. There are only two ULXs for which it has been possible to obtain optical spectra of the donor star. One of these, M101 ULX-1, has a Wolf-Rayet donor star. Liu et al. (2013) used the emission lines in its spectrum to measure a radial velocity curve, but the emission lines may originate in the (variable) wind of the star and thus the measured radial velocities may not represent the actual radial velocity of the star. The other ULX with donor star features visible in its optical spectrum has a blue supergiant donor. Although there are photospheric absorption lines present in its spectrum, the star is affected by X-ray heating and it is not possible to measure its radial velocity curve (Motch et al. 2014). Nevertheless, from the optical spectroscopic observations these authors could determine that both these ULXs probably contain stellar mass BHs.

ULX donor stars are generally expected to be massive stars, both because of the high mass transfer rates that are necessary to maintain the high X-ray luminosities of these sources and because of their association with star forming regions. Therefore, it is not unexpected that the donor stars found to date are a blue supergiant and a Wolf-Rayet star. However, from stellar evolution scenarios it is clear that some ULXs may also have red supergiant (RSG) donor stars. The realisation that such counterparts would be excellent targets for a dynamical mass measurement campaign formed the basis for this thesis. The reason is that they are very bright in the NIR, where emission from the disc is not as important as it is in the optical part of the

spectrum. In addition, because these stars are much larger and therefore in much wider orbits than blue supergiant donors, X-ray heating is expected to be unimportant.

NIR photometry and spectroscopy of ULX counterparts

To search for ULXs with candidate RSG donor stars we started an observing campaign to obtain NIR (*H*- and/or *K*-band) images of ULXs within 10 Mpc. In **Chapter 4** we report the results of the first part of this campaign. We observed 62 ULXs, using the Very Large Telescope (VLT) for sources in the Southern hemisphere and the William Herschel Telescope (WHT) and the MMT for sources in the Northern hemisphere. Of those 62 ULXs, 17 have a counterpart in our images. Six of those are either star clusters or background AGN, but 11 have photometric properties consistent with those of RSGs. The fact that we detect only a fraction of the ULXs in our NIR images, while they are at similar distances, points towards intrinsic differences between ULX systems: for instance, the systems that show relatively strong NIR emission might have larger accretion discs than the ones that do not, or there may be strong nebular lines present that are absent in other sources. Alternatively, these systems may contain red supergiant donor stars that are intrinsically bright in the NIR. If the NIR emission indeed originates from a late-type donor star, these systems are excellent candidates for future spectroscopic studies to find dynamical masses for their black holes.

In Chapters 5 and 6 we describe the first spectroscopic follow-up observations of six of the RSG candidates described in Chapter 4. For the imaging campaign we could make use of 4 meter class telescopes, but for the spectroscopy we need the largest telescopes and best instruments that are currently available. In the Southern hemisphere this is the VLT with the X-shooter spectrograph; in the North, the Keck telescopes on Hawaii with MOSFIRE. **Chapter 5** describes our VLT/X-shooter observations of the counterpart of a ULX (J0047) in NGC 253. From the NIR spectra it is clear that this is an M-type star, its radial velocity confirms its association with NGC 253, and its brightness is such that it can only be an RSG. X-shooter has a very large spectral range, from the near UV to the NIR. In the optical and NUV parts of the spectrum we do not detect the counterpart (as expected for an RSG), but we do detect emission lines from a nearby star forming region. The ratios of these lines change as a function of distance to the ULX. At larger distances, the line ratios are consistent with a normal HII region, ionized by UV-radiation from young, hot stars. Closer to the ULX, the line ratios indicate that part of the ionizing radiation comes from an X-ray source. This shows that the ULX and the nebula are likely related. Interestingly, the radial velocity of the RSG differs from that of the nebula by 66 ± 6 km s^{-1}, which may be the result either of a SN kick, requiring a system containing a $\gtrsim 50\ M_{\odot}$ black hole, and/or of orbital radial velocity variations in the ULX binary system, requiring a $\gtrsim 100\ M_{\odot}$ black hole. Depending on the radius of the RSG, the orbital period expected for such a binary system is $\sim 4.5 - 15$ years. More observations are needed to search for the radial velocity shifts that would confirm this.

In **Chapter 6** we report on our Keck/MOSFIRE *H*-band spectroscopic observations of five ULX counterparts (two in NGC 925, two in NGC 4136, and Holmberg II X-1). The spectra show a great diversity. The candidate counterparts of two ULXs (J022721+333500 in NGC 925 and J120922+295559 in NGC 4136) have spectra consistent with those of (M-type) RSGs.

We obtained two epochs of spectroscopy of the candidate counterpart to J022721+333500, separated by 10 months, but discovered no radial velocity variations with a 2-σ upper limit of 40 km s^{-1}. If the RSG is the donor star of the ULX, the most likely options are that either the system is seen at low inclination ($i < 40°$), or the BH mass is less than 100 $M_{\odot}$, unless the orbital period is longer than 6 years. The spectrum of the counterpart to J120922+295559 shows emission lines on top of its stellar spectrum. The remaining three counterparts do not show absorption lines that can be associated with the atmosphere of a star; their spectra are instead dominated by emission lines. These emission lines may originate in a nebula, or in the accretion disc — although the latter is ruled out for the [Fe II] line in J120922+295559, as it is spatially offset from the spectrum of the counterpart. If the emission lines are indicative of nebulae, it is as yet unclear if these are powered by the ULX.

Outlook

Out of 11 candidate RSG counterparts that we identified based on photometry, six have been observed spectroscopically and three of those were identified as RSGs. Based on these numbers, we expect five or six RSG counterparts in our sample of 62 ULXs, $\sim 10\%$ (although the uncertainty on this fraction is large due to the low number statistics involved). The total number or ULX candidates currently known within 10 Mpc is around 150, although ~ 20 of those are located in heavily absorbed or very crowded regions such as galactic nuclei. For those sources it is not feasible to detect the counterpart. By observing all other ULXs within 10 Mpc we may expand the number of RSG counterparts to ~ 10 – 15.

The next step is to obtain multiple epochs of spectroscopy for those ULXs with RSG counterparts, to search for radial velocity variations. The orbital periods we expect for these systems range from almost a year (for an RSG with $R_{\star}$ = 200 $R_{\odot}$) to over ten years (for $R_{\star}$ > 1000 $R_{\odot}$), so there have to be at least a few months in between the spectra to maximize the chance of detecting a radial velocity shift. We did this already for one candidate counterpart to J022721+333500 in NGC 925, with 10 months in between the spectra, and found an upper limit on the radial velocity shift of 40 km s^{-1}. If an RSG shows radial velocity shifts, this will be the ultimate proof that it is indeed the donor star of the ULX, and we can proceed to measure the radial velocity curve and determine a lower limit on the mass of the BH. If, even with a sample of $10 - 15$ RSGs, none of them exhibit radial velocity shifts, this would be an indication that these sources are predominantly seen at low inclination. This would mean that beaming of the X-ray radiation probably plays a role in causing the high luminosities of ULXs, although studies of optical nebulae powered by ULXs constrain the beaming factors — in those sources — to a few at most.

The counterparts for which we already obtained spectroscopic identifications are those that are the brightest in our sample. Even for these, we need at least 3 hours on a 10 meter telescope to obtain a signal to noise ratio of ~ 10 (with the exception of the counterpart to J0047 in NGC 253, which is almost 2 magnitudes brighter than the other counterparts in our sample because its host galaxy is located at only 3.4 Mpc, whereas most other host galaxies are at 8 – 10 Mpc). The next generation of ground-based 30 meter class telescopes, expected to come online in the 2020's, and the *James Webb Space Telescope*, scheduled for launch in 2018, will make

these observations much easier. Until then, we will need long observations with 10 meter class telescopes to reach our goal of obtaining dynamical mass measurements of the accretors in ULXs.

SAMENVATTING

Röntgenlicht uit de ruimte

Als je naar de hemel kijkt zijn het de sterren en sterrenstelsels die het meest in het oog springen. Dat zijn de objecten die voornamelijk straling uitzenden in zichtbaar licht, het kleine deel van het electromagnetisch spectrum waarvoor onze ogen gevoelig zijn. Op andere golflengtes ziet de hemel er heel anders uit. Met een infraroodcamera zouden we bijvoorbeeld vooral de koele sterren en stofwolken zien. In het ultraviolet zijn het juist de jonge, hete sterren die opvallen. En in röntgenlicht zien we compacte objecten, zoals neutronensterren en zwarte gaten, die materie opslokken uit hun omgeving (zie Figuur 1).

Röntgenlicht wordt tegengehouden door de aardse atmosfeer. Dit is heel nuttig voor het leven op Aarde, aangezien röntgenstraling grote schade kan aanbrengen aan bijvoorbeeld ons DNA. Het maakt het echter een stuk lastiger om röntgenstraling uit de ruimte te bestuderen: dat kan alleen met instrumenten die zich boven de atmosfeer bevinden. De eerste waarnemingen van röntgenlicht uit de ruimte werden gedaan in de jaren '60, met geigertellers op raketten die korte ruimtevluchten maakten. Destijds was de verwachting dat deze raketvluchten weinig interessants zouden opleveren, aangezien normale sterren maar weinig röntgenlicht uitzenden. De zon was, zo was het idee, waarschijnlijk de enige röntgenbron die zichtbaar zou zijn. Tijdens de eerste raketvlucht werd echter een röntgenbron ontdekt in het sterrenbeeld Scorpius die maar liefst een miljoen keer zo helder was als de zon. Meer raketvluchten en uiteindelijk, vanaf de jaren '80, satellieten met röntgendetectoren, leidden tot de ontdekking van nog veel meer heldere röntgenbronnen.

Inmiddels is duidelijk dat de meeste van deze röntgenbronnen compacte objecten zijn waar materie naartoe stroomt (dit proces heet accretie). De bronnen die we in onze eigen Melkweg zien zijn zogeheten röntgendubbelsterren (zie Figuur 2). Zulke systemen bestaan uit een compact object en een normale ster. Het compacte object kan zowel een neutronenster als een zwart gat zijn, maar omdat de focus in dit proefschrift ligt op zwarte gaten zal ik het vanaf nu alleen daar over hebben. Als de normale ster dicht genoeg bij het zwarte gat staat, worden de buitenste lagen van de ster sterker aangetrokken door het zwarte gat dan door de ster zelf en gaat er gas stromen van de ster naar het zwarte gat. Op weg naar het zwarte gat verliest het gas potentiële energie en vormt het een (accretie)schijf. Deze schijf wordt bijzonder heet, zodat hij een groot deel van zijn straling uitzendt als röntgenlicht (het is dus niet het zwarte gat zelf dat licht uitzendt). De zwarte gaten in röntgendubbelsterren zijn *stellaire massa zwarte gaten*. Ze hebben een massa van 5 – 20 zonsmassa's en ontstaan uit de implosie van de kern van een zeer zware ster.

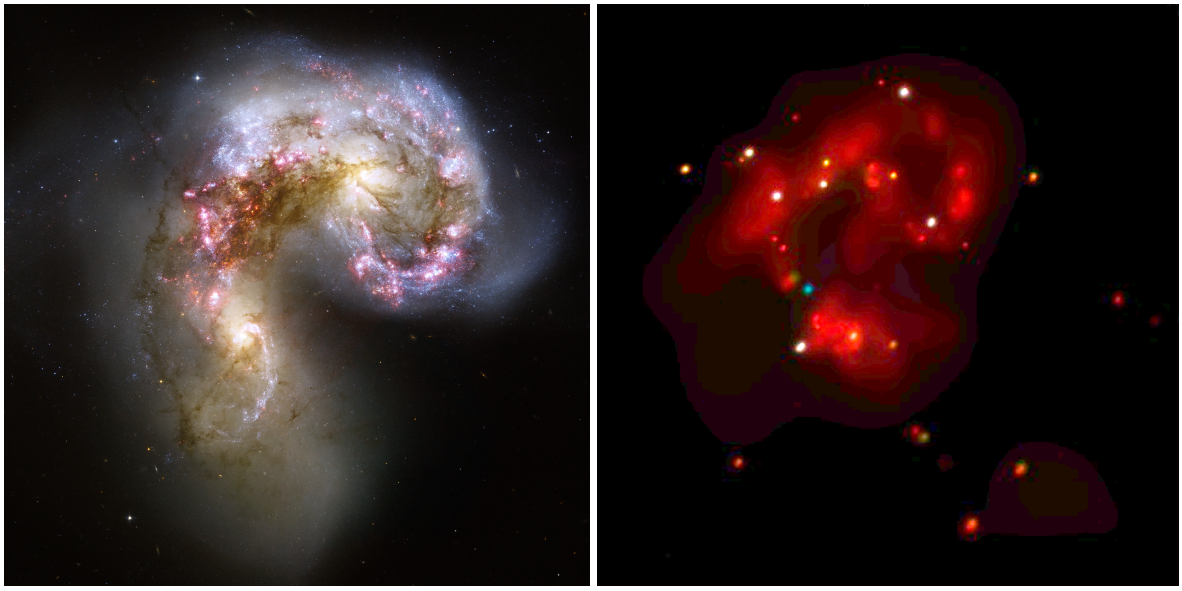

Figuur 1: *Links:* Een afbeelding van de Antennae sterrenstelsels, twee sterrenstelsels die met elkaar aan het samensmelten zijn, gemaakt met de *Hubble Space Telescope*. Op deze afbeelding, in zichtbaar licht, zijn de sterren te zien: blauwe sterren zijn jong en heet, rode sterren zijn ouder en koeler. Roze duidt op licht met een specifieke golflengte dat wordt uitgezonden door waterstof, en wijst op gebieden waar nieuwe sterren worden gevormd. Er is ook veel stof te zien dat geen zichtbaar licht doorlaat. (Afbeelding gemaakt door: Hubble/European Space Agency) *Rechts:* Dezelfde sterrenstelsels, nu zoals gezien door de *Chandra*-satelliet in röntgenlicht. De vage gloed komt van heet gas, de puntbronnen zijn allemaal zwarte gaten. (Afbeelding gemaakt door: NASA/SAO/CXC/Fabbiano et al. 2001)

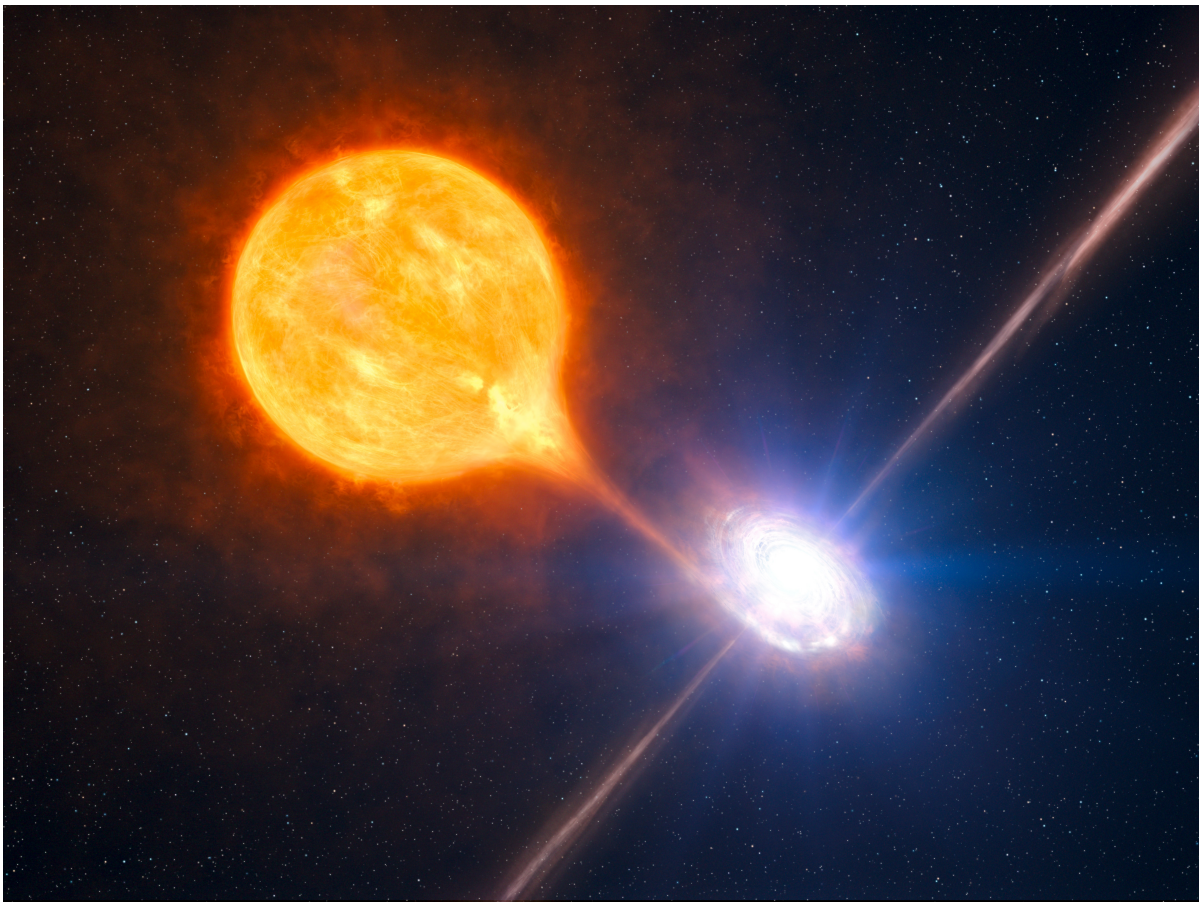

Figuur 2: Een artistieke weergave van een röntgendubbelster. Het zwarte gat bevindt zich in het midden van de accretieschijf (wit). De donorster (oranje) voedt de accretieschijf. Ook de straalstromen, die onder bepaalde omstandigheden worden gelanceerd vanaf een punt vlakbij het zwarte gat, zijn te zien (roodachtig). Afbeelding gemaakt door: ESO/L. Calçada/M. Kornmesser

We zien ook veel sterke röntgenbronnen die zich niet in de Melkweg bevinden, maar veel verder weg staan. Dit zijn *superzware zwarte gaten* die materie uit hun omgeving accreteren. Deze superzware zwarte gaten zijn meer dan 100.000 keer zo zwaar als de zon — het zwaarste zwarte gat dat we kennen is zelfs 10 miljard keer zo zwaar als de zon. Vrijwel elk sterrenstelsel, inclusief de Melkweg, bevat zo'n superzwaar zwart gat in het centrum. Ze worden echter pas zichtbaar als sterke röntgenbronnen als ze veel materie accreteren ('actief' worden). Zulke röntgenbronnen noemen we actieve sterrenstelsels (*Active Galactic Nuclei* of AGN).

Ultraheldere röntgenbronnen

Dankzij röntgensatellieten zoals XMM-*Newton* en *Chandra*, allebei gelanceerd in 1999, kunnen we nu ook röntgendubbelsterren bestuderen in andere sterrenstelsels dan de Melkweg. Een interessante ontdekking die daarbij gedaan werd is dat sommige sterrenstelsels röntgenbronnen bevatten die veel helderder zijn dan normale röntgendubbelsterren. Voor accreterende systemen zoals röntgendubbelsterren bestaat er een theoretische limiet op hoe helder ze kunnen schijnen. Op een deeltje in de accretieschijf rond een zwart gat werken tegengestelde krachten:

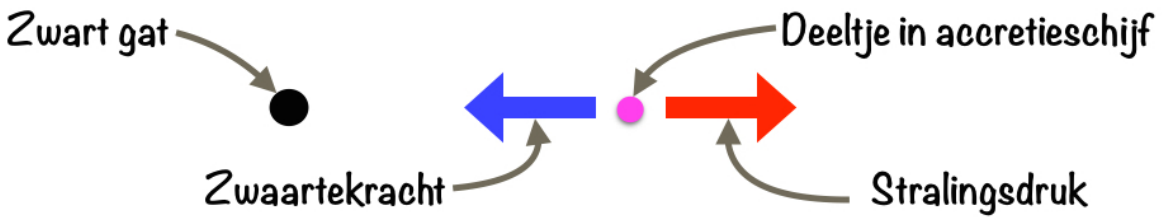

Figuur 3: Schematische weergave van de Eddingtonlimiet. De zwaartekracht (blauw) trekt de deeltjes naar het zwarte gat toe, terwijl de stralingsdruk (rood) de deeltjes juist wegduwt.

de zwaartekracht, die het deeltje aantrekt, en de stralingsdruk vanuit het centrum, die het deeltje juist wegduwt (zie Figuur 3). Als de stralingsdruk sterker is dan de zwaartekracht wordt de materie rond het zwarte gat dus weggeblazen in plaats van naar het zwarte gat toe te vallen. Met andere woorden: als de röntgendubbelster te helder schijnt, zal hij zijn eigen massa- en daarmee energietoevoer afsnijden. De limiet waar zwaartekracht en stralingsdruk precies in evenwicht zijn is dus de theoretisch maximaal haalbare lichtkracht voor een stabiel accreterend systeem. Deze limiet heet de Eddingtonlimiet, of ook wel de Eddingtonlichtkracht. De Eddingtonlimiet is afhankelijk van de massa van het zwarte gat: een zwaarder zwart gat heeft een sterkere zwaartekracht en kan dus meer licht uitzenden. De Eddingtonlichtkracht van een zwart gat van 10 zonsmassa's is 1.3×10^{39} erg s^{-1} (de *erg* is een eenheid van energie: 1 joule is 10^7 erg, dus een lichtkracht van 10^{39} erg s^{-1} staat gelijk aan 10^{32} joule per seconde, ongeveer een miljoen keer de lichtkracht van de zon).

De röntgendubbelsterren in de Melkweg, met zwarte gaten met massa's van 5 – 20 keer die van de zon, houden zich over het algemeen keurig aan de Eddingtonlimiet en zijn niet helderder dan 10×10^{39} erg s^{-1}. Sommige sterrenstelsels bevatten echter röntgenbronnen die vele malen helderder zijn. Ze bevinden zich echter niet in het centrum van hun sterrenstelsel, dus het zijn geen superzware zwarte gaten. Omdat deze bronnen helderder zijn dan de Eddingtonlichtkracht van een zwart gat van 10 zonsmassa's noemen we ze ultraheldere röntgenbronnen (*Ultraluminous X-ray sources* of ULX-en). Er zijn twee mogelijke verklaringen voor de hoge röntgenlichtkracht van ULX-en. Eén mogelijkheid is dat ze zwarte gaten bevatten die (veel) zwaarder zijn dan de stellaire massa zwarte gaten, maar minder zwaar dan de superzware zwarte gaten. De tweede optie is dat deze bronnen 'normale' stellaire massa zwarte gaten bevatten, maar in een ander accretieregime dan de röntgendubbelsterren in de Melkweg, waardoor ze over hun Eddingtonlimiet heen gaan.

Optie 1 is interessant omdat zwarte gaten met massa's tussen 20 en 100.000 zonsmassa's nog niet ontdekt zijn, hoewel er goede redenen zijn om aan te nemen dat ze wel bestaan. Zwarte gaten met massa's van 20 – 100 zonsmassa's noemen we *massieve stellaire zwarte gaten*, omdat ze — net als de stellaire massa zwarte gaten — waarschijnlijk kunnen ontstaan door het instorten van een enkele ster. Omdat de sterren waaruit massieve stellaire zwarte gaten zouden kunnen ontstaan extreem zwaar zijn (en daarom zeer zeldzaam) is de verwachting dat dit soort zwarte gaten minder vaak voorkomt dan de lichtere stellaire massa zwarte gaten. Zwarte gaten met een massa groter dan ongeveer 100 zonsmassa's kunnen niet meer ontstaan

door de instorting van een enkele ster (al is het helemaal niet zeker waar deze grens precies ligt — de bovengrens zou ook best een paar honderd zonsmassa's kunnen zijn). Zwarte gaten met een massa 100 – 100.000 zonsmassa's noemen we daarom *middelzware zwarte gaten*. Deze zouden in het vroege heelal gevormd kunnen worden door de instorting van gaswolken, of door het samensmelten van zware sterren in sterclusters met extreem hoge sterdichtheden. Deze middelzware zwarte gaten zouden vervolgens kunnen dienen als startpunt voor het ontstaan van de superzware zwarte gaten die we zien in vrijwel elk sterrenstelsel, maar waarvan we nog niet precies begrijpen hoe ze gevormd zijn.

Optie 2 — dat ULX-en stellaire massa zwarte gaten bevatten die helderder zijn dan de Eddingtonlichtkracht — is ook interessant, omdat dit ons meer kan leren over deze extreme fase van het accretieproces. Uit simulaties is gebleken dat super-Eddington accretie wel degelijk mogelijk is: onder de juiste omstandigheden kan de totale lichtkracht van een röntgendubbelster een paar keer de Eddington lichtkracht zijn. Daarnaast speelt *beaming* een belangrijke rol. De Eddingtonlimiet is een limiet op de lichtkracht — de totale hoeveelheid energie per seconde die de ULX uitzendt in alle richtingen. Wat we op aarde meten is de flux — de energie per seconde per vierkante centimeter die op de telescoop valt. Daaruit berekenen we de lichtkracht door aan te nemen dat de flux isotroop is, in alle richtingen hetzelfde. Als dat niet het geval is, doordat de straling voornamelijk in één richting wordt uitgezonden, is de lichtkracht die we berekenen veel groter dan de werkelijke lichtkracht. Zo kan een röntgendubbelster die in werkelijkheid een lichtkracht heeft van zo'n twee keer de Eddingtonlichtkracht, eruit zien als een bron van wel 20 keer de Eddingtonlichtkracht.

Op dit moment kennen we enkele honderden ULX kandidaten, waarvan de meerderheid slechts één keer is waargenomen en niet in detail is bestudeerd. Uit hoge kwaliteit röntgenspectra[2] van een aantal ULX-en is gebleken dat niet alleen hun lichtkracht, maar ook de vorm van hun spectra verschilt van normale röntgendubbelsterren. Dit is een aanwijzing dat in elk geval sommige ULX-en waarschijnlijk stellaire massa zwarte gaten bevatten die helderder zijn dan de Eddingtonlimiet. Van één ULX is inmiddels bekend dat hij geen zwart gat, maar een neutronenster bevat. Neutronensterren zijn minder zwaar dan zwarte gaten: maximaal zo'n drie zonsmassa's. De Eddingtonlimiet van een neutronenster is dus ook lager, en deze ULX is zo'n 100 keer helderder dan zijn Eddingtonlimiet. Hoewel er wel naar gezocht is, zijn er nog geen andere ULX-en waarvan we zeker weten dat het compacte object een neutronenster is. De allerhelderste ULX-en — met een lichtkracht van meer dan 10^{41} erg s^{-1}, dus meer dan 100 keer de Eddingtonlichtkracht van een zwart gat van tien zonsmassa's — noemen we ook wel hyperheldere röntgenbronnen (*Hyperluminous X-ray sources* of HLX-en). Deze zijn zo helder dat het erg onwaarschijnlijk is dat ze stellaire massa zwarte gaten bevatten. Dit maakt deze bronnen tot goede kandidaten om middelzware zwarte gaten te vinden. Er zijn echter maar twee van dit soort bronnen bekend.

[2]Een spectrum is een opname waarin het licht van een ster, sterrenstelsel of ander object uiteen is gerafeld naar golflengte. Zo kunnen we niet alleen de totale hoeveelheid licht meten, maar precies zien hoeveel licht wordt uitgezonden op welke golflengte.

Een nieuwe HLX

In Jonker et al. (2010) hadden wij al eerder een derde kandidaat-HLX beschreven. Op basis van de op dat moment beschikbare data (één korte röntgenwaarneming, gedaan in 2008, uit het archief van de *Chandra* satelliet, waarin een röntgenbron te zien was met een lichtkracht van 2×10^{41} erg s^{-1}, en een detectie van een bron op diezelfde plaats in een ouder plaatje van de *Hubble Space Telescope* (HST) in zichtbaar licht) konden we niet vaststellen wat deze bron precies was. Dankzij nieuwe data, zowel in röntgen (met de *Chandra* satelliet) als zichtbaar licht (met HST), hebben we nu meer duidelijkheid. In **Hoofdstuk 2**: *Discovery of a second outbursting hyperluminous X-ray source* beschrijven we deze waarnemingen. Na de waarneming waarin de bron gedetecteerd was als een potentiële HLX was er een langere *Chandra* waarneming in 2012 waarin de röntgenbron niet meer zichtbaar was. Vervolgens is er een waarneming uit april 2014, waarin de bron nét gedetecteerd wordt, om weer te verdwijnen in juni van datzelfde jaar. In een derde waarneming, in november 2014, is de kandidaat-HLX vervolgens weer zichtbaar als een heldere röntgenbron, een factor vier zwakker dan in de eerste waarneming. De twee laatste waarnemingen, twee en drie weken later, laten zien dat de bron snel minder helder wordt: in de laatste waarneming is hij helemaal niet meer te zien. In de nieuwe HST waarneming, in zichtbaar licht, is de bron nog steeds zichtbaar, hoewel minder helder dan eerst. De combinatie van al deze waarnemingen stelt ons in staat om de meeste andere opties uit te sluiten en te concluderen dat deze bron hoogstwaarschijnlijk een echte HLX is. Zonder een meting van de roodverschuiving (en daarmee afstand) van de bron kunnen we hier niet helemaal zeker van zijn, maar het gedrag van deze bron vertoont overeenkomsten met dat van een andere HLX. Dit maakt hem tot een heel interessante kandidaat om een middelzwaar zwart gat te bevatten.

De meeste kandidaat-HLX-en blijken echter op veel grotere afstand te staan dan het sterrenstelsel waar ze bij lijken te horen, waardoor hun lichtkracht zwaar onderschat wordt. Dit zijn AGN die zo ver weg staan dat het sterrenstelsel waar ze in staan niet meer zichtbaar is. Enkele voorbeelden hiervan zijn te vinden in **Hoofdstuk 3**: *VLT/FORS2 observations of four high-luminosity ULX candidates*. In dit hoofdstuk bespreken we vier kandidaat-ULX-en die ook relatief helder zijn in zichtbaar licht, waardoor het mogelijk is om hun roodverschuiving te meten. Drie van de vier bleken AGN in de achtergrond te zijn. Dit is in overeenstemming met eerdere resultaten van andere auteurs: ULX kandidaten die ook helder zijn in zichtbaar licht, zijn meestal geen echte ULX-en. Dit soort bronnen zouden echter ook middelzware zwarte gaten kunnen zijn met een groep sterren (een bolhoop) om zich heen. Daarom is het nog steeds interessant om hun roodverschuiving te meten: zo'n middelzwaar zwart gat in een bolhoop zou een belangrijke ontdekking zijn.

Massabepaling van zwarte gaten

De enige manier om uit te vinden of ULX-en middelzware zwarte gaten bevatten of stellaire massa zwarte gaten die over hun Eddingtonlimiet heen gaan, is door de massa van de zwarte gaten op een betrouwbare manier te meten. De meest betrouwbare manier om massa's van zwarte gaten te meten is door een zogeheten dynamische massabepaling. Hierbij maken we

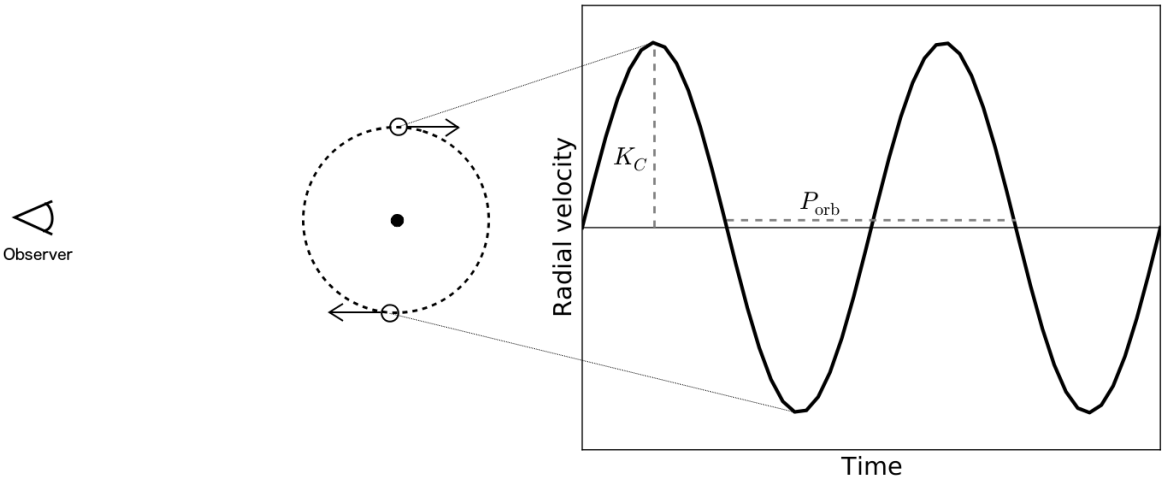

Figuur 4: Een theoretische radiële snelheidscurve van een ster die om een zwart gat draait. De baanperiode ($P_{\rm orb}$) en de radiële snelheidsamplitude van de donorster (K_C) kunnen worden bepaald uit de curve.

gebruik van het feit dat alle bekende zwarte gaten zich in een dubbelstersysteem bevinden. In zo'n dubbelstersysteem draaien beide objecten om het gemeenschappelijk zwaartepunt. De manier waarop dat gebeurt wordt beschreven door de wetten van Kepler, die we bijvoorbeeld ook gebruiken om de bewegingen van planeten in ons zonnestelsel te beschrijven. De beweging van het zwarte gat kunnen we niet meten, maar door de snelheid en omlooptijd van de donorster te bepalen, kunnen we een ondergrens berekenen voor de massa van het zwarte gat. Als we die massa precies willen berekenen, moeten we ook weten hoe zwaar de donorster is en onder welke hoek we het dubbelstersysteem zien. De snelheid en omlooptijd van de donorster kunnen we meten met behulp van spectra van het zichtbare of nabij-infrarode licht van de ster. In zo'n spectrum zijn, afhankelijk van het type donorster, absorptielijnen te zien van waterstof of andere elementen die zich in de atmosfeer van de ster bevinden. Door de golflengte van deze absorptielijnen te vergelijken met de rustgolflengtes, die bekend zijn uit laboratoriummetingen, kunnen we de rood- of blauwverschuiving van de ster meten. De verhouding tussen deze verschuiving in golflengte en de rustgolflengte is gelijk aan de verhouding tussen de snelheid van de ster en de lichtsnelheid. We meten op deze manier alleen de snelheid waarmee de ster van ons af of naar ons toe beweegt (dit noemen we de radiële snelheid); we kunnen niet zien hoe snel de ster vanuit ons oogpunt gezien opzij beweegt, daarvoor staan deze bronnen te ver van ons vandaan. Door de snelheid van de ster op verschillende momenten te meten, kunnen we een *radiële snelheidscurve* opbouwen (zie Figuur 4). Uit deze curve kunnen we de baanperiode van het dubbelstersysteem ($P_{\rm orb}$) en de radiële snelheidsamplitude van de donorster (K_C) bepalen. Deze kunnen we invullen in de massafunctie (zie Vergelijking 1.2) om een ondergrens te bepalen voor de massa van het zwarte gat.

Deze methode om massa's van zwarte gaten te meten is met succes toegepast op zo'n 20 röntgendubbelsterren in de Melkweg. Elke poging om dezelfde methode voor ULX-en te gebruiken is tot nu toe echter mislukt. Hiervoor zijn een aantal redenen, waaronder het feit dat we alleen ULX-en vinden in andere sterrenstelsels; ze staan dus ver weg, waardoor de

donorsterren erg lichtzwak zijn. Een andere reden is dat de accretieschijf van ULX-en ook veel zichtbaar licht uitstraalt, waardoor het spectrum van de donorster meestal niet te zien is. En als het spectrum van de donorster wel te zien is, is er nog het probleem dat de kant van de donorster die naar het zwarte gat is gericht, verhit wordt door de sterke röntgenstraling. Dit zorgt ervoor dat de absorptielijnen in het spectrum niet meer bruikbaar zijn om radiële snelheden te meten. Een mogelijke oplossing voor al deze problemen is te vinden in ULX-en met een rode superreus als donorster. Een rode superreus is een zware, koele, grote en zeer heldere ster (met een massa van 10 – 40 zonsmassa's, oppervlaktetemperatuur van minder dan $\sim 4000^{\circ}$ C, een straal van ongeveer 100 – 1500 keer die van de zon, en een lichtkracht van ongeveer 10.000 – 500.000 keer die van de zon). Hun grote helderheid betekent dat we ze tot op grote afstand kunnen zien. Daarnaast zenden rode superreuzen het grootste deel van hun straling uit als nabij-infrarood licht. De accretieschijf is daar juist minder helder, waardoor een nabij-infrarood spectrum wel gedomineerd wordt door de donorster. En omdat rode superreuzen zo groot zijn, staan ze op een grotere afstand van het zwarte gat dan kleinere donorsterren (als ze dichterbij hadden gestaan, zouden ze al eerder in hun ontwikkeling massa gaan overdragen en nooit tot een rode superreus evolueren). Hierdoor speelt verhitting van de ster door röntgenstraling geen belangrijke rol.

Nabij-infrarode waarnemingen van ULX-en

De realisatie dat ULX-en met een rode superreus als donorster uitstekende kandidaten zijn voor dynamische massabepaling, vormde de basis voor dit proefschrift. Aangezien nog niemand anders onderzoek had gedaan naar nabij-infrarode straling van ULX-en, was de eerste stap om afbeeldingen te maken van de meest nabije ULX-en in het nabij-infrarood. Dit is beschreven in **Hoofdstuk 4**: *Near-infrared counterparts of ultraluminous X-ray sources*. We hebben nabij-infrarode afbeeldingen gemaakt van 62 ULX-en die zich op maximaal 30 miljoen lichtjaar van ons vandaan bevinden, omdat dat de maximale afstand is waarop we nog een nabij-infrarood spectrum kunnen nemen van een rode superreus met de grootste telescopen die op dit moment bestaan. Voor dit onderzoek hebben we gebruik gemaakt van drie telescopen: de Very Large Telescope (VLT) in Chili, voor ULX-en die vanaf het zuidelijk halfrond te zien zijn, en de William Herschel Telescope (WHT) op La Palma en de MMT in Arizona voor de ULX-en op het noordelijk halfrond. Van de 62 ULX-en die we hebben bekeken zijn er 17 die ook zichtbaar zijn in het nabij-infrarood. Van zes van deze weten we dat het zeker geen rode superreuzen zijn, omdat ze ofwel veel te helder zijn (dit zijn waarschijnlijk AGN in de achtergrond), ofwel omdat het geen puntbronnen zijn (dit zijn waarschijnlijk groepjes sterren die te dicht bij elkaar staan om individuele sterren te onderscheiden). De overige elf zijn mogelijk ULX-en met een rode superreus als donorster. Om er achter te komen of dit inderdaad het geval is, moeten we nabij-infrarode spectra van deze bronnen bestuderen.

In **Hoofdstuk 5**: *Discovery of a red supergiant counterpart to RX J004722.4-252051, a ULX in NGC 253*, en **Hoofdstuk 6**: *Keck/MOSFIRE spectroscopy of five ULX counterparts*, beschrijven we de spectra van zes van de elf mogelijke rode superreuzen. Hoofdstuk 5 gaat over een ULX in NGC 253. Van alle ULX-en met een mogelijke rode superreus als donorster in ons onderzoek staat deze het dichtst bij ons. We hebben deze bron waargenomen met X-

shooter, een spectrograaf op de VLT die niet alleen het nabij-infrarode spectrum geeft, maar ook het zichtbare en nabij-ultraviolette licht opvangt. Door het nabij-infrarode spectrum te vergelijken met dat van sterren van verschillende types, kunnen we aantonen dat deze bron inderdaad een rode superreus is die in NGC 253 staat. Daarnaast zien we in het zichtbare en nabij-ultraviolette licht een nevel die gedeeltelijk verlicht wordt door de ULX. Tussen de nevel en de rode superreus is wel een snelheidsverschil van 66 km s^{-1}. Dit zou erop kunnen wijzen dat de rode superreus om een zwart gat heen draait.

In Hoofdstuk 6 beschrijven we de nabij-infrarode spectra van vijf ULX-en op het noordelijk halfrond. Deze spectra hebben we gemaakt met het MOSFIRE instrument op de Keck telescoop op Hawaii. Twee van deze spectra komen overeen met die van rode superreuzen; de andere drie zien er heel anders uit, met sterke emissielijnen die zouden kunnen wijzen op de aanwezigheid van een nevel. Van één van de rode superreuzen hebben we twee spectra, tien maanden van elkaar genomen. De snelheid van de rode superreus is echter hetzelfde in deze twee spectra, waardoor we nog niet zeker weten of dit inderdaad de donorster is van de ULX.

Vooruitzichten

Van onze huidige set van 62 ULX-en die zijn waargenomen in het nabij-infrarood zijn er elf met mogelijk een rode superreus als begeleider. Van zes van deze elf hebben we nabij-infrarode spectra, en drie daarvan bleken inderdaad rode superreuzen te zijn. Gebaseerd op deze (kleine) steekproef verwachten we nog twee of drie rode superreuzen in de overige vijf kandidaten. Door onze zoektocht uit te breiden naar alle ULX-en binnen 30 miljoen lichtjaar kunnen we het aantal rode superreuzen nog verdubbelen. De volgende stap is nu om meerdere spectra van deze rode superreuzen te nemen en te zoeken naar sterren die snelheidsvariaties laten zien. Dit is het ultieme bewijs dat we een rode superreus hebben ontdekt die om een zwart gat heen draait. Omdat de verwachte baanperiodes voor dit soort systemen erg lang zijn (ongeveer 1 – 15 jaar, afhankelijk van de afmeting van de rode superreus) moeten we hier lang voor wachten. De spectroscopische waarnemingen van deze rode superreuzen is op het randje van wat we kunnen doen met de huidige technologie. Om een bruikbaar spectrum te verkrijgen, moeten we deze bronnen minstens drie uur lang waarnemen met de grootste telescopen die we op dit moment hebben (de VLT van 8 meter en de Keck telescoop van 10 meter). De volgende generatie telescopen op de grond, met diameters tussen de 25 en 39 meter, en in de ruimte, zoals de *James Webb Space Telescope*, zullen dit soort onderzoek eenvoudiger maken. Totdat die instrumenten operationeel zijn hebben we lange waarnemingen nodig om ons uiteindelijke doel te bereiken: het meten van de massa's van zwarte gaten in ULX-en.

BIBLIOGRAPHY

Abazajian, K. N., Adelman-McCarthy, J. K., Agüeros, M. A., et al. 2009, *The Seventh Data Release of the Sloan Digital Sky Survey*, ApJS, 182, 543

Abolmasov, P., Fabrika, S., Sholukhova, O., & Afanasiev, V. 2007, *Spectroscopy of optical counterparts of ultraluminous X-ray sources*, Astrophysical Bulletin, 62, 36

Abramowicz, M. A., Czerny, B., Lasota, J. P., & Szuszkiewicz, E. 1988, *Slim accretion disks*, ApJ, 332, 646

Adelman-McCarthy, J. K., Agüeros, M. A., Allam, S. S., et al. 2007, *The Fifth Data Release of the Sloan Digital Sky Survey*, ApJS, 172, 634

Appenzeller, I., Fricke, K., Fürtig, W., et al. 1998, *Successful commissioning of FORS1 - the first optical instrument on the VLT.*, The Messenger, 94, 1

Bachetti, M., Harrison, F. A., Walton, D. J., et al. 2014, *An ultraluminous X-ray source powered by an accreting neutron star*, Nature, 514, 202

Bachetti, M., Rana, V., Walton, D. J., et al. 2013, *The Ultraluminous X-Ray Sources NGC 1313 X-1 and X-2: A Broadband Study with NuSTAR and XMM-Newton*, ApJ, 778, 163

Bailin, J., Bell, E. F., Chappell, S. N., Radburn-Smith, D. J., & de Jong, R. S. 2011, *The Resolved Stellar Halo of NGC 253*, ApJ, 736, 24

Balser, D. S., Rood, R. T., Bania, T. M., & Anderson, L. D. 2011, *H II Region Metallicity Distribution in the Milky Way Disk*, ApJ, 738, 27

Barger, A. J., Cowie, L. L., Capak, P., et al. 2003, *Optical and Infrared Properties of the 2 Ms Chandra Deep Field North X-Ray Sources*, AJ, 126, 632

Barnard, R. 2010, *In-depth studies of the NGC253 ULXs with XMM-Newton: remarkable variability in ULX1, and evidence for extended coronae*, MNRAS, 404, 42

Begelman, M. C. 2002, *Super-Eddington Fluxes from Thin Accretion Disks?*, ApJ, 568, L97

Begelman, M. C., Volonteri, M., & Rees, M. J. 2006, *Formation of supermassive black holes by direct collapse in pre-galactic haloes*, MNRAS, 370, 289

Belczynski, K., Bulik, T., Fryer, C. L., et al. 2010, *On the Maximum Mass of Stellar Black Holes*, ApJ, 714, 1217

Bertin, E. 2006, *Automatic Astrometric and Photometric Calibration with SCAMP*, in Astronomical Society of the Pacific Conference Series, Vol. 351, Astronomical Data Analysis Software and Systems XV, ed. C. Gabriel, C. Arviset, D. Ponz, & S. Enrique, 112

Bertin, E. & Arnouts, S. 1996, *SExtractor: Software for source extraction.*, A&AS, 117, 393

Bertin, E., Mellier, Y., Radovich, M., et al. 2002, *The TERAPIX Pipeline*, in Astronomical Society of the Pacific Conference Series, Vol. 281, Astronomical Data Analysis Software and Systems XI, ed. D. A. Bohlender, D. Durand, & T. H. Handley, 228

Blaauw, A. 1961, *On the origin of the O- and B-type stars with high velocities (the "run-away" stars), and some related problems*, Bull. Astron. Inst. Netherlands, 15, 265

Blandford, R. D. & McKee, C. F. 1982, *Reverberation mapping of the emission line regions of Seyfert galaxies and quasars*, ApJ, 255, 419

Bradt, H. V., Rothschild, R. E., & Swank, J. H. 1993, *X-ray timing explorer mission*, A&AS, 97, 355

Caballero-García, M. D. & Fabian, A. C. 2010, *X-ray reflection in a sample of X-ray bright ultraluminous X-ray sources*, MNRAS, 402, 2559

Cardelli, J. A., Clayton, G. C., & Mathis, J. S. 1989, *The relationship between infrared, optical, and ultraviolet extinction*, ApJ, 345, 245

Casares, J. & Jonker, P. G. 2014, *Mass Measurements of Stellar and Intermediate-Mass Black Holes*, Space Sci. Rev., 183, 223

Cash, W. 1979, *Parameter estimation in astronomy through application of the likelihood ratio*, ApJ, 228, 939

Chattopadhyay, A. K., Chattopadhyay, T., Davoust, E., Mondal, S., & Sharina, M. 2009, *Study of NGC 5128 Globular Clusters Under Multivariate Statistical Paradigm*, ApJ, 705, 1533

Chen, Y.-P., Trager, S. C., Peletier, R. F., et al. 2014, *The X-shooter Spectral Library (XSL). I. DR1: Near-ultraviolet through optical spectra from the first year of the survey*, A&A, 565, A117

Chilingarian, I., Brown, W., Fabricant, D., et al. 2013, *Data Reduction Pipeline for the MMT Magellan Infrared Spectrograph*, in Astronomical Society of the Pacific Conference Series, Vol. 475, Astronomical Data Analysis Software and Systems XXII, ed. D. N. Friedel, 189

Colbert, E. J. M. & Mushotzky, R. F. 1999, *The Nature of Accreting Black Holes in Nearby Galaxy Nuclei*, ApJ, 519, 89

Colbert, E. J. M. & Ptak, A. F. 2002, *A Catalog of Candidate Intermediate-Luminosity X-Ray Objects*, ApJS, 143, 25

Copperwheat, C., Cropper, M., Soria, R., & Wu, K. 2005, *Optical and infrared signatures of ultra-luminous X-ray sources*, MNRAS, 362, 79

Copperwheat, C., Cropper, M., Soria, R., & Wu, K. 2007, *Irradiation models for ULXs and fits to optical data*, MNRAS, 376, 1407

Corral-Santana, J. M., Casares, J., Shahbaz, T., et al. 2011, *Evidence for a black hole in the X-ray transient XTE J1859+226*, MNRAS, 413, L15

Couto da Silva, T. C. & de Souza, R. E. 2006, *Optical spectroscopy for a sample of southern binary galaxies*, A&A, 457, 425

Cox, A. N. 2000, Allen's astrophysical quantities, ed. Cox, A. N.

Cseh, D., Grisé, F., Corbel, S., & Kaaret, P. 2011, *Broad Components in Optical Emission Lines from the Ultra-luminous X-ray Source NGC 5408 X-1*, ApJ, 728, L5

Cseh, D., Grisé, F., Kaaret, P., et al. 2013a, *Towards a dynamical mass of the ultraluminous X-ray source NGC 5408 X-1*, MNRAS, 435, 2896

Cseh, D., Kaaret, P., Corbel, S., et al. 2013b, *Unveiling recurrent jets of the ULX Holmberg II X-1: evidence for a massive stellar-mass black hole?*, ArXiv e-prints

Cseh, D., Kaaret, P., Corbel, S., et al. 2014, *Unveiling recurrent jets of the ULX Holmberg II X-1: evidence for a massive stellar-mass black hole?*, MNRAS, 439, L1

Cseh, D., Webb, N. A., Godet, O., et al. 2015, *On the radio properties of the intermediate-mass black hole candidate ESO 243-49 HLX-1*, MNRAS, 446, 3268

D'Abrusco, R., Massaro, F., Ajello, M., et al. 2012, *Infrared Colors of the Gamma-Ray-detected Blazars*, ApJ, 748, 68

Dalcanton, J. J., Williams, B. F., Seth, A. C., et al. 2009, *The ACS Nearby Galaxy Survey Treasury*, ApJS, 183, 67

Dall'Osso, S., Perna, R., & Stella, L. 2015, *NuSTAR J095551+6940.8: a highly magnetized neutron star with super-Eddington mass accretion*, MNRAS, 449, 2144

Davies, B., Kudritzki, R.-P., & Figer, D. F. 2010, *The potential of red supergiants as extra-galactic abundance probes at low spectral resolution*, MNRAS, 407, 1203

Davies, B., Kudritzki, R.-P., Plez, B., et al. 2013, *The Temperatures of Red Supergiants*, ApJ, 767, 3

Davis, D. S. & Mushotzky, R. F. 2004, *XMM-Newton Observations of an Intermediate X-Ray Object in NGC 2276*, ApJ, 604, 653

de Blok, W. J. G., Walter, F., Brinks, E., et al. 2008, *High-Resolution Rotation Curves and Galaxy Mass Models from THINGS*, AJ, 136, 2648

de Vaucouleurs, G., de Vaucouleurs, A., Corwin, Jr., H. G., et al. 1991, Third Reference Catalogue of Bright Galaxies. Volume I: Explanations and references. Volume II: Data for galaxies between 0^h and 12^h. Volume III: Data for galaxies between 12^h and 24^h.

Dickey, J. M. & Lockman, F. J. 1990, *H I in the Galaxy*, ARA&A, 28, 215

Dolphin, A. E. 2000, *WFPC2 Stellar Photometry with HSTPHOT*, PASP, 112, 1383

Done, C., Gierliński, M., & Kubota, A. 2007, *Modelling the behaviour of accretion flows in X-ray binaries. Everything you always wanted to know about accretion but were afraid to ask*, A&A Rev., 15, 1

Doroshenko, V., Santangelo, A., & Ducci, L. 2015, *Searching for coherent pulsations in ultra-luminous X-ray sources*, A&A, 579, A22

Drilling, J. S. & Landolt, A. U. 2000, Normal Stars, ed. A. N. Cox, 381

Drozdovsky, I. O. & Karachentsev, I. D. 2000, *Photometric distances to six bright resolved galaxies*, A&AS, 142, 425

Durrell, P. R., Sarajedini, A., & Chandar, R. 2010, *Deep HST/ACS Photometry of the M81 Halo*, ApJ, 718, 1118

Ebisawa, K., Życki, P., Kubota, A., Mizuno, T., & Watarai, K.-y. 2003, *Accretion Disk Spectra of Ultraluminous X-Ray Sources in Nearby Spiral Galaxies and Galactic Superluminal Jet Sources*, ApJ, 597, 780

Ebisuzaki, T., Makino, J., Tsuru, T. G., et al. 2001, *Missing Link Found? The "Runaway" Path to Supermassive Black Holes*, ApJ, 562, L19

Eddington, A. S. 1916, *On the radiative equilibrium of the stars*, MNRAS, 77, 16

Ekşi, K. Y., Andaç, İ. C., Çıkıntoğlu, S., et al. 2015, *The ultraluminous X-ray source NuSTAR J095551+6940.8: a magnetar in a high-mass X-ray binary*, MNRAS, 448, L40

Eldridge, J. J., Langer, N., & Tout, C. A. 2011, *Runaway stars as progenitors of supernovae and gamma-ray bursts*, MNRAS, 414, 3501

Elias, J. H., Frogel, J. A., & Humphreys, R. M. 1985, *M supergiants in the Milky Way and the Magellanic Clouds Colors, spectral types, and luminosities*, ApJS, 57, 91

Elvis, M., Maccacaro, T., Wilson, A. S., et al. 1978, *Seyfert galaxies as X-ray sources*, MNRAS, 183, 129

Fabbiano, G. 1989, *X rays from normal galaxies*, ARA&A, 27, 87

Fabbiano, G., Zezas, A., & Murray, S. S. 2001, *Chandra Observations of "The Antennae" Galaxies (NGC 4038/9)*, ApJ, 554, 1035

Falcke, H., Körding, E., & Markoff, S. 2004, *A scheme to unify low-power accreting black holes. Jet-dominated accretion flows and the radio/X-ray correlation*, A&A, 414, 895

Farrell, S. A., Servillat, M., Pforr, J., et al. 2012, *A Young Massive Stellar Population around the Intermediate-mass Black Hole ESO 243-49 HLX-1*, ApJ, 747, L13

Farrell, S. A., Webb, N. A., Barret, D., Godet, O., & Rodrigues, J. M. 2009, *An intermediate-mass black hole of over 500 solar masses in the galaxy ESO243-49*, Nature, 460, 73

Fender, R. P., Homan, J., & Belloni, T. M. 2009, *Jets from black hole X-ray binaries: testing, refining and extending empirical models for the coupling to X-rays*, MNRAS, 396, 1370

Feng, H. & Kaaret, P. 2008, *Optical Counterpart of the Ultraluminous X-Ray Source IC 342 X-1*, ApJ, 675, 1067

Feng, H. & Soria, R. 2011, *Ultraluminous X-ray sources in the Chandra and XMM-Newton era*, New A Rev., 55, 166

Ferrara, A., Salvadori, S., Yue, B., & Schleicher, D. 2014, *Initial mass function of intermediate-mass black hole seeds*, MNRAS, 443, 2410

Ferrarese, L. & Ford, H. 2005, *Supermassive Black Holes in Galactic Nuclei: Past, Present and Future Research*, Space Sci. Rev., 116, 523

Few, J. M. A., Arp, H. C., & Madore, B. F. 1982, *Ring galaxies. I - Kinematics of the southern ring galaxy AM 064-741*, MNRAS, 199, 633

Filippenko, A. V. & Chornock, R. 2001, *XTE J1859+226*, IAU Circ., 7644, 2

Förster Schreiber, N. M. 2000, *Moderate-Resolution Near-Infrared Spectroscopy of Cool Stars: A New K-Band Library*, AJ, 120, 2089

Frank, J., King, A., & Raine, D. J. 2002, Accretion Power in Astrophysics: Third Edition

Freudling, W., Romaniello, M., Bramich, D. M., et al. 2013, *Automated data reduction workflows for astronomy. The ESO Reflex environment*, A&A, 559, A96

Fridman, A. M., Afanasiev, V. L., Dodonov, S. N., et al. 2005, *The orientation parameters and rotation curves of 15 spiral galaxies*, A&A, 430, 67

Fruscione, A., McDowell, J. C., Allen, G. E., et al. 2006, *CIAO: Chandra's data analysis system*, in Society of Photo-Optical Instrumentation Engineers (SPIE) Conference Series, Vol. 6270, Society of Photo-Optical Instrumentation Engineers (SPIE) Conference Series

Gao, Y., Wang, Q. D., Appleton, P. N., & Lucas, R. A. 2003, *Nonnuclear Hyper/Ultraluminous X-Ray Sources in the Starbursting Cartwheel Ring Galaxy*, ApJ, 596, L171

Garmire, G. P., Bautz, M. W., Ford, P. G., Nousek, J. A., & Ricker, Jr., G. R. 2003, *Advanced CCD imaging spectrometer (ACIS) instrument on the Chandra X-ray Observatory*, in Society of Photo-Optical Instrumentation Engineers (SPIE) Conference Series, Vol. 4851, X-Ray and Gamma-Ray Telescopes and Instruments for Astronomy., ed. J. E. Truemper & H. D. Tananbaum, 28–44

Gehrels, N. 1986, *Confidence limits for small numbers of events in astrophysical data*, ApJ, 303, 336

Ghez, A. M., Salim, S., Weinberg, N. N., et al. 2008, *Measuring Distance and Properties of the Milky Way's Central Supermassive Black Hole with Stellar Orbits*, ApJ, 689, 1044

Ghisellini, G., Della Ceca, R., Volonteri, M., et al. 2010, *Chasing the heaviest black holes of jetted active galactic nuclei*, MNRAS, 405, 387

Giacconi, R., Branduardi, G., Briel, U., et al. 1979, *The Einstein /HEAO 2/ X-ray Observatory*, ApJ, 230, 540

Giacconi, R., Gursky, H., Paolini, F. R., & Rossi, B. B. 1962, *Evidence for x Rays From Sources Outside the Solar System*, Physical Review Letters, 9, 439

Gil de Paz, A., Boissier, S., Madore, B. F., et al. 2007, *The GALEX Ultraviolet Atlas of Nearby Galaxies*, ApJS, 173, 185

Gilfanov, M. & Merloni, A. 2014, *Observational Appearance of Black Holes in X-Ray Binaries and AGN*, Space Sci. Rev., 183, 121

Gillessen, S., Eisenhauer, F., Trippe, S., et al. 2009, *Monitoring Stellar Orbits Around the Massive Black Hole in the Galactic Center*, ApJ, 692, 1075

Gladstone, J. C., Copperwheat, C., Heinke, C. O., et al. 2013, *Optical Counterparts of the Nearest Ultraluminous X-Ray Sources*, ApJS, 206, 14

Gladstone, J. C., Roberts, T. P., & Done, C. 2009, *The ultraluminous state*, MNRAS, 397, 1836

Gliozzi, M., Satyapal, S., Eracleous, M., Titarchuk, L., & Cheung, C. C. 2009, *A Chandra View of NGC 3621: A Bulgeless Galaxy Hosting an AGN in Its Early Phase?*, ApJ, 700, 1759

Godet, O., Barret, D., Webb, N. A., Farrell, S. A., & Gehrels, N. 2009, *First Evidence for Spectral State Transitions in the ESO 243-49 Hyperluminous X-Ray Source HLX-1*, ApJ, 705, L109

Godet, O., Lombardi, J. C., Antonini, F., et al. 2014, *Implications of the Delayed 2013 Outburst of ESO 243-49 HLX-1*, ApJ, 793, 105

Greene, J. E. & Ho, L. C. 2007, *A New Sample of Low-Mass Black Holes in Active Galaxies*, ApJ, 670, 92

Grisé, F., Kaaret, P., Corbel, S., et al. 2012, *Optical Emission of the Ultraluminous X-Ray Source NGC 5408 X-1: Donor Star or Irradiated Accretion Disk?*, ApJ, 745, 123

Grisé, F., Pakull, M. W., & Motch, C. 2006, *The Ultraluminous X-ray Source in Holmberg IX and its Environment*, in IAU Symposium, Vol. 230, Populations of High Energy Sources in Galaxies, ed. E. J. A. Meurs & G. Fabbiano, 302–303

Gutiérrez, C. M. 2006, *Optical Counterparts of Ultraluminous X-Ray Sources*, ApJ, 640, L17

Gutiérrez, C. M. 2013, *Five fake ultra-luminous X-ray sources*, A&A, 549, A81

Gutiérrez, C. M. & López-Corredoira, M. 2005, *The Nature of Ultraluminous X-Ray Sources*, ApJ, 622, L89

Gutiérrez, C. M. & López-Corredoira, M. 2007, *Eight more ultra luminous X-ray candidates unmasked*, A&A, 472, 87

Gutiérrez, C. M. & Moon, D.-S. 2014, *Optical Study of the Hyper-luminous X-Ray Source 2XMM J011942.7+032421*, ApJ, 797, L7

Güver, T. & Özel, F. 2009, *The relation between optical extinction and hydrogen column density in the Galaxy*, MNRAS, 400, 2050

Haggard, D., Cool, A. M., Heinke, C. O., et al. 2013, *A Deep Chandra X-Ray Limit on the Putative IMBH in Omega Centauri*, ApJ, 773, L31

Haiman, Z. & Loeb, A. 2001, *What Is the Highest Plausible Redshift of Luminous Quasars?*, ApJ, 552, 459

Harrison, F. A., Craig, W. W., Christensen, F. E., et al. 2013, *The Nuclear Spectroscopic Telescope Array (NuSTAR) High-energy X-Ray Mission*, ApJ, 770, 103

Heinke, C. O., Bahramian, A., Degenaar, N., & Wijnands, R. 2015, *The nature of very faint X-ray binaries: hints from light curves*, MNRAS, 447, 3034

Heinke, C. O., Cohn, H. N., & Lugger, P. M. 2009, *The Discovery of a Very Faint X-Ray Transient in the Globular Cluster M15*, ApJ, 692, 584

Heinzeller, D. & Duschl, W. J. 2007, *On the Eddington limit in accretion discs*, MNRAS, 374, 1146

Herrmann, K. A., Ciardullo, R., Feldmeier, J. J., & Vinciguerra, M. 2008, *Planetary Nebulae in Face-On Spiral Galaxies. I. Planetary Nebula Photometry and Distances*, ApJ, 683, 630

Hlavacek-Larrondo, J., Carignan, C., Daigle, O., et al. 2011, *Deep Hα observations of NGC 253: a very extended and possibly declining rotation curve?*, MNRAS, 411, 71

Ho, L. C. 2008, *Nuclear Activity in Nearby Galaxies*, ARA&A, 46, 475

Hobbs, G., Lorimer, D. R., Lyne, A. G., & Kramer, M. 2005, *A statistical study of 233 pulsar proper motions*, MNRAS, 360, 974

Hong, J., van den Berg, M., Schlegel, E. M., et al. 2005, *X-Ray Processing of ChaMPlane Fields: Methods and Initial Results for Selected Anti-Galactic Center Fields*, ApJ, 635, 907

Horne, K. 1986, *An optimal extraction algorithm for CCD spectroscopy*, PASP, 98, 609

Humphreys, E. M. L., Reid, M. J., Greenhill, L. J., Moran, J. M., & Argon, A. L. 2008, *Toward a New Geometric Distance to the Active Galaxy NGC 4258. II. Centripetal Accelerations and Investigation of Spiral Structure*, ApJ, 672, 800

Immler, S. & Lewin, W. H. G. 2003, *X-Ray Supernovae*, in Lecture Notes in Physics, Berlin Springer Verlag, Vol. 598, Supernovae and Gamma-Ray Bursters, ed. K. Weiler, 91–111

Immler, S., Wang, Q. D., Leonard, D. C., & Schlegel, E. M. 2003, *A Deep Chandra X-Ray Observation of NGC 1637*, ApJ, 595, 727

Jacobs, B. A., Rizzi, L., Tully, R. B., et al. 2009, *The Extragalactic Distance Database: Color-Magnitude Diagrams*, AJ, 138, 332

Jonker, P. G., Heida, M., Torres, M. A. P., et al. 2012, *The Nature of the Bright ULX X-2 in NGC 3921: A Chandra Position and HST Candidate Counterpart*, ApJ, 758, 28

Jonker, P. G., Torres, M. A. P., Fabian, A. C., et al. 2010, *A bright off-nuclear X-ray source: a type IIn supernova, a bright ULX or a recoiling supermassive black hole in CXOJ122518.6+144545*, MNRAS, 407, 645

Kaaret, P. & Corbel, S. 2009, *A Photoionized Nebula Surrounding and Variable Optical Continuum Emission from the Ultraluminous X-Ray Source in NGC 5408*, ApJ, 697, 950

Kaaret, P., Corbel, S., Prestwich, A. H., & Zezas, A. 2003, *Radio Emission from an Ultraluminous X-ray Source*, Science, 299, 365

Kaaret, P., Feng, H., & Gorski, M. 2009, *A Major X-Ray Outburst From an Ultraluminous X-Ray Source in M82*, ApJ, 692, 653

Kaaret, P., Simet, M. G., & Lang, C. C. 2006, *A 62 Day X-Ray Periodicity and an X-Ray Flare from the Ultraluminous X-Ray Source in M82*, ApJ, 646, 174

Kaaret, P., Ward, M. J., & Zezas, A. 2004, *High-resolution imaging of the HeII λ4686 emission line nebula associated with the ultraluminous X-ray source in Holmberg II*, MNRAS, 351, L83

Karachentsev, I. D., Sharina, M. E., Dolphin, A. E., et al. 2002, *New distances to galaxies in the Centaurus A group*, A&A, 385, 21

Karachentsev, I. D., Sharina, M. E., Dolphin, A. E., et al. 2003, *Galaxy flow in the Canes Venatici I cloud*, A&A, 398, 467

King, A. & Lasota, J.-P. 2014, *HLX-1 may be an SS433 system*, MNRAS, 444, L30

King, A. R. 2004, *Ultraluminous X-ray sources and star formation*, MNRAS, 347, L18

King, A. R. 2009, *Masses, beaming and Eddington ratios in ultraluminous X-ray sources*, MNRAS, 393, L41

King, A. R., Davies, M. B., Ward, M. J., Fabbiano, G., & Elvis, M. 2001, *Ultraluminous X-Ray Sources in External Galaxies*, ApJ, 552, L109

Kluźniak, W. & Lasota, J.-P. 2015, *An ultraluminous nascent millisecond pulsar*, MNRAS, 448, L43

Knapp, G. R., Pourbaix, D., Platais, I., & Jorissen, A. 2003, *Reprocessing the Hipparcos data of evolved stars. III. Revised Hipparcos period-luminosity relationship for galactic long-period variable stars*, A&A, 403, 993

Kong, A. K. H., Soria, R., & Farrell, S. 2015, *New X-ray Outburst of ESO 243-49 HLX-1*, The Astronomer's Telegram, 6916, 1

Körding, E., Falcke, H., & Markoff, S. 2002, *Population X: Are the super-Eddington X-ray sources beamed jets in microblazars or intermediate mass black holes?*, A&A, 382, L13

Kraft, R. P., Burrows, D. N., & Nousek, J. A. 1991, *Determination of confidence limits for experiments with low numbers of counts*, ApJ, 374, 344

Kraft, R. P., Kregenow, J. M., Forman, W. R., Jones, C., & Murray, S. S. 2001, *Chandra Observations of the X-Ray Point Source Population in Centaurus A*, ApJ, 560, 675

Lançon, A., Hauschildt, P. H., Ladjal, D., & Mouhcine, M. 2007, *Near-IR spectra of red supergiants and giants. I. Models with solar and with mixing-induced surface abundance ratios*, A&A, 468, 205

Lang, C. C., Kaaret, P., Corbel, S., & Mercer, A. 2007, *A Radio Nebula Surrounding the Ultraluminous X-Ray Source in NGC 5408*, ApJ, 666, 79

Langer, N. & Maeder, A. 1995, *The problem of the blue-to-red supergiant ratio in galaxies.*, A&A, 295, 685

Lanzoni, B., Mucciarelli, A., Origlia, L., et al. 2013, *The Velocity Dispersion Profile of NGC 6388 from Resolved-star Spectroscopy: No Evidence of a Central Cusp and New Constraints on the Black Hole Mass*, ApJ, 769, 107

Lasota, J.-P., Alexander, T., Dubus, G., et al. 2011, *The Origin of Variability of the Intermediate-mass Black-hole ULX System HLX-1 in ESO 243-49*, ApJ, 735, 89

Lasota, J.-P., King, A. R., & Dubus, G. 2015, *X-ray Transients: Hyper- or Hypo-Luminous?*, ApJ, 801, L4

Lattimer, J. M. 2012, *Astrophysical and laboratory constraints for the dense matter equation of state*, in American Institute of Physics Conference Series, Vol. 1484, American Institute of Physics Conference Series, ed. S. Kubono, T. Hayakawa, T. Kajino, H. Miyatake, T. Motobayashi, & K. Nomoto, 319–326

Lauberts, A. & Valentijn, E. A. 1989, The surface photometry catalogue of the ESO-Uppsala galaxies (Garching, European Southern Observatory)

Laycock, S. G. T., Maccarone, T. J., & Christodoulou, D. M. 2015, *Revisiting the dynamical case for a massive black hole in IC10 X-1*, MNRAS, 452, L31

Lehmann, I., Becker, T., Fabrika, S., et al. 2005, *Integral field spectroscopy of the ultraluminous X-ray source Holmberg II X-1*, A&A, 431, 847

Levesque, E. M., Massey, P., Olsen, K. A. G., et al. 2005, *The Effective Temperature Scale of Galactic Red Supergiants: Cool, but Not As Cool As We Thought*, ApJ, 628, 973

Lin, D., Webb, N. A., & Barret, D. 2012, *Classification of X-Ray Sources in the XMM-Newton Serendipitous Source Catalog*, ApJ, 756, 27

Lira, P., Lawrence, A., & Johnson, R. A. 2000, *Multiwavelength study of the nuclei of a volume-limited sample of galaxies - I. X-ray observations*, MNRAS, 319, 17

Liu, J. 2011, *Chandra ACIS Survey of X-ray Point Sources in 383 Nearby Galaxies. I. The Source Catalog*, ApJS, 192, 10

Liu, J., Orosz, J., & Bregman, J. N. 2012, *Dynamical Mass Constraints on the Ultraluminous X-Ray Source NGC 1313 X-2*, ApJ, 745, 89

Liu, J.-F. & Bregman, J. N. 2005, *Ultraluminous X-Ray Sources in Nearby Galaxies from ROSAT High Resolution Imager Observations I. Data Analysis*, ApJS, 157, 59

Liu, J.-F., Bregman, J. N., Bai, Y., Justham, S., & Crowther, P. 2013, *Puzzling accretion onto a black hole in the ultraluminous X-ray source M 101 ULX-1*, Nature, 503, 500

Liu, J.-F., Bregman, J. N., & Seitzer, P. 2002, *The Optical Counterpart of an Ultraluminous X-Ray Object in M81*, ApJ, 580, L31

Liu, Q. Z. & Mirabel, I. F. 2005, *A catalogue of ultraluminous X-ray sources in external galaxies*, A&A, 429, 1125

López-Corredoira, M. & Gutiérrez, C. M. 2006, *Toward a clean sample of ultra-luminous X-ray sources*, A&A, 454, 77

Lützgendorf, N., Kissler-Patig, M., Noyola, E., et al. 2011, *Kinematic signature of an intermediate-mass black hole in the globular cluster NGC 6388*, A&A, 533, A36

Maccarone, T. J., Kundu, A., Zepf, S. E., & Rhode, K. L. 2007, *A black hole in a globular cluster*, Nature, 445, 183

Madau, P. & Rees, M. J. 2001, *Massive Black Holes as Population III Remnants*, ApJ, 551, L27

Mapelli, M., Annibali, F., Zampieri, L., & Soria, R. 2013, *A minor merger scenario for the ultraluminous X-ray source ESO 243-49 HLX-1 - II. Constraints from photometry*, MNRAS, 433, 849

Marsh, T. R., Robinson, E. L., & Wood, J. H. 1994, *Spectroscopy of A0620-00 - the Mass of the Black-Hole and an Image of its Accretion Disc*, MNRAS, 266, 137

McClintock, J. E. & Remillard, R. A. 1986, *The black hole binary A0620-00*, ApJ, 308, 110

McClintock, J. E. & Remillard, R. A. 2006, Black hole binaries, ed. W. H. G. Lewin & M. van der Klis, 157–213

McLean, I. S., Steidel, C. C., Epps, H., et al. 2010, *Design and development of MOSFIRE: the multi-object spectrometer for infrared exploration at the Keck Observatory*, in Society of Photo-Optical Instrumentation Engineers (SPIE) Conference Series, Vol. 7735, Society of Photo-Optical Instrumentation Engineers (SPIE) Conference Series, 1

McLean, I. S., Steidel, C. C., Epps, H. W., et al. 2012, *MOSFIRE, the multi-object spectrometer for infra-red exploration at the Keck Observatory*, in Society of Photo-Optical Instrumentation Engineers (SPIE) Conference Series, Vol. 8446, Society of Photo-Optical Instrumentation Engineers (SPIE) Conference Series, 0

McLeod, B., Fabricant, D., Nystrom, G., et al. 2012, *MMT and Magellan Infrared Spectrograph*, PASP, 124, 1318

McQuinn, K. B. W., Skillman, E. D., Cannon, J. M., et al. 2010, *The Nature of Starbursts. I. The Star Formation Histories of Eighteen Nearby Starburst Dwarf Galaxies*, ApJ, 721, 297

Merloni, A., Heinz, S., & di Matteo, T. 2003, *A Fundamental Plane of black hole activity*, MNRAS, 345, 1057

Mermilliod, J. C., Mayor, M., & Udry, S. 2008, *Red giants in open clusters. XIV. Mean radial velocities for 1309 stars and 166 open clusters*, A&A, 485, 303

Mezcua, M., Farrell, S. A., Gladstone, J. C., & Lobanov, A. P. 2013, *Milliarcsec-scale radio emission of ultraluminous X-ray sources: steady jet emission from an intermediate-mass black hole?*, MNRAS, 436, 1546

Mezcua, M., Roberts, T. P., Lobanov, A. P., & Sutton, A. D. 2015, *The powerful jet of an off-nuclear intermediate-mass black hole in the spiral galaxy NGC 2276*, MNRAS, 448, 1893

Middleton, M. J., Heil, L., Pintore, F., Walton, D. J., & Roberts, T. P. 2015, *A spectral-timing model for ULXs in the supercritical regime*, MNRAS, 447, 3243

Middleton, M. J., Miller-Jones, J. C. A., Markoff, S., et al. 2013, *Bright radio emission from an ultraluminous stellar-mass microquasar in M 31*, Nature, 493, 187

Miller, M. C. & Hamilton, D. P. 2002, *Production of intermediate-mass black holes in globular clusters*, MNRAS, 330, 232

Miller, N. A., Mushotzky, R. F., & Neff, S. G. 2005, *Radio Emission Associated with the Ultraluminous X-Ray Source in Holmberg II*, ApJ, 623, L109

Miller-Jones, J. C. A. 2014, *Astrometric Observations of X-ray Binaries Using Very Long Baseline Interferometry*, PASA, 31, 16

Miller-Jones, J. C. A., Wrobel, J. M., Sivakoff, G. R., et al. 2012, *The Absence of Radio Emission from the Globular Cluster G1*, ApJ, 755, L1

Mineo, S., Gilfanov, M., & Sunyaev, R. 2012, *X-ray emission from star-forming galaxies - I. High-mass X-ray binaries*, MNRAS, 419, 2095

Mineshige, S. & Ohsuga, K. 2011, *Supercritical accretion and ULXs - what can we achieve?*, Astronomische Nachrichten, 332, 402

Monet, D. G., Levine, S. E., Canzian, B., et al. 2003, *The USNO-B Catalog*, AJ, 125, 984

Moon, D.-S., Eikenberry, S. S., & Wasserman, I. M. 2003, *The Evolution of LMC X-4 Flares: Evidence for Super-Eddington Radiation Oozing through Inhomogeneous Polar Cap Accretion Flows?*, ApJ, 586, 1280

Moon, D.-S., Harrison, F. A., Cenko, S. B., & Shariff, J. A. 2011, *Large Highly Ionized Nebulae Around Ultra-luminous X-ray Sources*, ApJ, 731, L32

Moorwood, A., Cuby, J.-G., Biereichel, P., et al. 1998, *ISAAC sees first light at the VLT.*, The Messenger, 94, 7

Mortlock, D. J., Warren, S. J., Venemans, B. P., et al. 2011, *A luminous quasar at a redshift of $z = 7.085$*, Nature, 474, 616

Motch, C., Pakull, M. W., Soria, R., Grisé, F., & Pietrzyński, G. 2014, *A mass of less than 15 solar masses for the black hole in an ultraluminous X-ray source*, Nature, 514, 198

Mukai, K. 1993, *PIMMS and Viewing: proposal preparation tools*, Legacy, vol. 3, p.21-31, 3, 21

Nilson, P. 1973, *Uppsala General Catalogue of Galaxies, 1973, Acta Universitatis Upsalienis, Nova Regiae Societatis Upsaliensis, Series v: a Vol.*, Nova Acta Regiae Soc. Sci. Upsaliensis Ser. V, 0

Ohsuga, K. & Mineshige, S. 2011, *Global Structure of Three Distinct Accretion Flows and Outflows around Black Holes from Two-dimensional Radiation-magnetohydrodynamic Simulations*, ApJ, 736, 2

Ohsuga, K., Mineshige, S., Mori, M., & Kato, Y. 2009, *Global Radiation-Magnetohydrodynamic Simulations of Black-Hole Accretion Flow and Outflow: Unified Model of Three States*, PASJ, 61, L7

Olivares E., F., Hamuy, M., Pignata, G., et al. 2010, *The Standardized Candle Method for Type II Plateau Supernovae*, ApJ, 715, 833

Origlia, L., Moorwood, A. F. M., & Oliva, E. 1993, *The 1.5-1.7 micrometer spectrum of cool stars: Line identifications, indices for spectral classification and the stellar content of the Seyfert galaxy NGC 1068*, A&A, 280, 536

Orosz, J. A., Bailyn, C. D., Remillard, R. A., McClintock, J. E., & Foltz, C. B. 1994, *Quiescent accretion disks in black hole X-ray novae*, ApJ, 436, 848

Pagel, B. E. J., Edmunds, M. G., Fosbury, R. A. E., & Webster, B. L. 1978, *A survey of chemical compositions of H II regions in the Magellanic Clouds*, MNRAS, 184, 569

Pakull, M. W. & Angebault, L. P. 1986, *Detection of an X-ray-ionized nebula around the black hole candidate binary LMC X-1*, Nature, 322, 511

Pakull, M. W. & Mirioni, L. 2002, *Optical Counterparts of Ultraluminous X-Ray Sources*, ArXiv: 0202488

Pasham, D. R., Strohmayer, T. E., & Mushotzky, R. F. 2014, *A 400-solar-mass black hole in the galaxy M82*, Nature, 513, 74

Patruno, A. & Zampieri, L. 2008, *Optical emission from massive donors in ultraluminous X-ray source binary systems*, MNRAS, 386, 543

Peterson, B. M. 2014, *Measuring the Masses of Supermassive Black Holes*, Space Sci. Rev., 183, 253

Peterson, B. M., Bentz, M. C., Desroches, L.-B., et al. 2005, *Multiwavelength Monitoring of the Dwarf Seyfert 1 Galaxy NGC 4395. I. A Reverberation-based Measurement of the Black Hole Mass*, ApJ, 632, 799

Pineau, F.-X., Motch, C., Carrera, F., et al. 2011, *Cross-correlation of the 2XMMi catalogue with Data Release 7 of the Sloan Digital Sky Survey*, A&A, 527, A126

Pintore, F., Zampieri, L., Wolter, A., & Belloni, T. 2014, *Ultraluminous X-ray sources: a deeper insight into their spectral evolution*, MNRAS, 439, 3461

Portegies Zwart, S. F. & McMillan, S. L. W. 2002, *The Runaway Growth of Intermediate-Mass Black Holes in Dense Star Clusters*, ApJ, 576, 899

Poutanen, J., Fabrika, S., Valeev, A. F., Sholukhova, O., & Greiner, J. 2013, *On the association of the ultraluminous X-ray sources in the Antennae galaxies with young stellar clusters*, MNRAS, 432, 506

Poutanen, J., Lipunova, G., Fabrika, S., Butkevich, A. G., & Abolmasov, P. 2007, *Supercritically accreting stellar mass black holes as ultraluminous X-ray sources*, MNRAS, 377, 1187

Poznanski, D., Butler, N., Filippenko, A. V., et al. 2009, *Improved Standardization of Type II-P Supernovae: Application to an Expanded Sample*, ApJ, 694, 1067

Prestwich, A. H., Kilgard, R., Crowther, P. A., et al. 2007, *The Orbital Period of the Wolf-Rayet Binary IC 10 X-1: Dynamic Evidence that the Compact Object Is a Black Hole*, ApJ, 669, L21

Ptak, A., Colbert, E., van der Marel, R. P., et al. 2006, *Optical Counterparts of Ultraluminous X-Ray Sources Identified from Archival HST WFPC2 Images*, ApJS, 166, 154

Raimundo, S. I., Fabian, A. C., Bauer, F. E., et al. 2010, *Radiation pressure, absorption and AGN feedback in the Chandra Deep Fields*, MNRAS, 408, 1714

Reines, A. E., Greene, J. E., & Geha, M. 2013, *Dwarf Galaxies with Optical Signatures of Active Massive Black Holes*, ApJ, 775, 116

Repetto, S., Davies, M. B., & Sigurdsson, S. 2012, *Investigating stellar-mass black hole kicks*, MNRAS, 425, 2799

Roberts, T. P., Gladstone, J. C., Goulding, A. D., et al. 2011, *(No) dynamical constraints on the mass of the black hole in two ULXs*, Astronomische Nachrichten, 332, 398

Roberts, T. P., Goad, M. R., Ward, M. J., et al. 2001, *The identification of an optical counterpart to the super-Eddington X-ray source NGC 5204 X-1*, MNRAS, 325, L7

Roberts, T. P., Warwick, R. S., Ward, M. J., & Goad, M. R. 2004, *Chandra observations of five ultraluminous X-ray sources in nearby galaxies*, MNRAS, 349, 1193

Roberts, T. P., Warwick, R. S., Ward, M. J., & Murray, S. S. 2002, *A Chandra observation of the interacting pair of galaxies NGC 4485/4490*, MNRAS, 337, 677

Roeser, S., Demleitner, M., & Schilbach, E. 2010, *The PPMXL Catalog of Positions and Proper Motions on the ICRS. Combining USNO-B1.0 and the Two Micron All Sky Survey (2MASS)*, AJ, 139, 2440

Rosen, S. R., Webb, N. A., Watson, M. G., et al. 2015, *The XMM-Newton serendipitous survey. VII. The third XMM-Newton serendipitous source catalogue*, ArXiv e-prints

Rousselot, P., Lidman, C., Cuby, J.-G., Moreels, G., & Monnet, G. 2000, *Night-sky spectral atlas of OH emission lines in the near-infrared*, A&A, 354, 1134

Schirmer, M. 2013, *THELI: Convenient Reduction of Optical, Near-infrared, and Mid-infrared Imaging Data*, ApJS, 209, 21

Servillat, M., Farrell, S. A., Lin, D., et al. 2011, *X-Ray Variability and Hardness of ESO 243-49 HLX-1: Clear Evidence for Spectral State Transitions*, ApJ, 743, 6

Shakura, N. I. & Sunyaev, R. A. 1973, *Black holes in binary systems. Observational appearance.*, A&A, 24, 337

Shao, Y. & Li, X.-D. 2015, *A Population of Ultraluminous X-Ray Sources with an Accreting Neutron Star*, ApJ, 802, 131

Shappee, B. J. & Stanek, K. Z. 2011, *A New Cepheid Distance to the Giant Spiral M101 Based on Image Subtraction of Hubble Space Telescope/Advanced Camera for Surveys Observations*, ApJ, 733, 124

Silverman, J. M. & Filippenko, A. V. 2008, *On IC 10 X-1, the Most Massive Known Stellar-Mass Black Hole*, ApJ, 678, L17

Sivakoff, G. R., Jordán, A., Sarazin, C. L., et al. 2007, *The Low-Mass X-Ray Binary and Globular Cluster Connection in Virgo Cluster Early-Type Galaxies: Optical Properties*, ApJ, 660, 1246

Sivakoff, G. R., Kraft, R. P., Jordán, A., et al. 2008, *A Transient Black Hole Low-Mass X-Ray Binary Candidate in Centaurus A*, ApJ, 677, L27

Skrutskie, M. F., Cutri, R. M., Stiening, R., et al. 2006, *The Two Micron All Sky Survey (2MASS)*, AJ, 131, 1163

Smith, R. J., Lucey, J. R., Hudson, M. J., Schlegel, D. J., & Davies, R. L. 2000, *Streaming motions of galaxy clusters within 12000kms^{-1} - I. New spectroscopic data*, MNRAS, 313, 469

Soria, R., Kuntz, K. D., Winkler, P. F., et al. 2012, *The Birth of an Ultraluminous X-Ray Source in M83*, ApJ, 750, 152

Springob, C. M., Masters, K. L., Haynes, M. P., Giovanelli, R., & Marinoni, C. 2009, *Erratum: "SFI++ II: A New I-Band Tully-Fisher Catalog, Derivation of Peculiar Velocities and Data Set Properties" <A href="bib_query?2007ApJS..172..599S"> (2007, ApJS, 172, 599)</A>*, ApJS, 182, 474

Steeghs, D., McClintock, J. E., Parsons, S. G., et al. 2013, *The Not-so-massive Black Hole in the Microquasar GRS1915+105*, ApJ, 768, 185

Steidel, C. C., Rudie, G. C., Strom, A. L., et al. 2014, *Strong Nebular Line Ratios in the Spectra of z ˜ 2-3 Star Forming Galaxies: First Results from KBSS-MOSFIRE*, ApJ, 795, 165

Steinhardt, C. L. & Elvis, M. 2010, *The quasar mass-luminosity plane - I. A sub-Eddington limit for quasars*, MNRAS, 402, 2637

Stern, D., Eisenhardt, P., Gorjian, V., et al. 2005, *Mid-Infrared Selection of Active Galaxies*, ApJ, 631, 163

Strader, J., Chomiuk, L., Maccarone, T. J., et al. 2012, *No Evidence for Intermediate-mass Black Holes in Globular Clusters: Strong Constraints from the JVLA*, ApJ, 750, L27

Strohmayer, T. E. & Mushotzky, R. F. 2003, *Discovery of X-Ray Quasi-periodic Oscillations from an Ultraluminous X-Ray Source in M82: Evidence against Beaming*, ApJ, 586, L61

Sutton, A. D., Done, C., & Roberts, T. P. 2014, *Irradiated, colour-temperature-corrected accretion discs in ultraluminous X-ray sources*, MNRAS, 444, 2415

Sutton, A. D., Roberts, T. P., Gladstone, J. C., & Walton, D. J. 2015, *The hyperluminous X-ray source candidate in IC 4320: another HLX bites the dust*, MNRAS, 450, 787

Sutton, A. D., Roberts, T. P., & Middleton, M. J. 2013, *The ultraluminous state revisited: fractional variability and spectral shape as diagnostics of super-Eddington accretion*, MNRAS, 435, 1758

Sutton, A. D., Roberts, T. P., Walton, D. J., Gladstone, J. C., & Scott, A. E. 2012, *The most extreme ultraluminous X-ray sources: evidence for intermediate-mass black holes?*, MNRAS, 423, 1154

Swartz, D. A., Ghosh, K. K., Tennant, A. F., & Wu, K. 2004, *The Ultraluminous X-Ray Source Population from the Chandra Archive of Galaxies*, ApJS, 154, 519

Swartz, D. A., Soria, R., Tennant, A. F., & Yukita, M. 2011, *A Complete Sample of Ultraluminous X-ray Source Host Galaxies*, ApJ, 741, 49

Swartz, D. A., Tennant, A. F., & Soria, R. 2009, *Ultraluminous X-Ray Source Correlations with Star-Forming Regions*, ApJ, 703, 159

Tananbaum, H., Peters, G., Forman, W., et al. 1978, *UHURU observations of X-ray emission from Seyfert galaxies*, ApJ, 223, 74

Tao, L., Feng, H., Grisé, F., & Kaaret, P. 2011, *Compact Optical Counterparts of Ultraluminous X-Ray Sources*, ApJ, 737, 81

Tao, L., Feng, H., Kaaret, P., Grisé, F., & Jin, J. 2012a, *Chandra and Hubble Space Telescope Observations of the Supersoft ULX in NGC 247: Candidate for Standard Disk Emission*, ApJ, 758, 85

Tao, L., Kaaret, P., Feng, H., & Grisé, F. 2012b, *The Nature of the UV/Optical Emission of the Ultraluminous X-Ray Source in Holmberg II*, ApJ, 750, 110

Terashima, Y., Inoue, H., & Wilson, A. S. 2006, *Hubble Space Telescope Identification of the Optical Counterparts of Ultraluminous X-Ray Sources in M51*, ApJ, 645, 264

Terashima, Y. & Wilson, A. S. 2004, *The Luminous X-Ray Source Population in M51 Observed with Chandra*, ApJ, 601, 735

Theureau, G., Hanski, M. O., Coudreau, N., Hallet, N., & Martin, J.-M. 2007, *Kinematics of the Local Universe. XIII. 21-cm line measurements of 452 galaxies with the Nançay radiotelescope, JHK Tully-Fisher relation, and preliminary maps of the peculiar velocity field*, A&A, 465, 71

Tokunaga, A. T. 2000, Infrared Astronomy, ed. A. N. Cox, 143

Tong, H. 2015, *An accreting low magnetic field magnetar for the ultraluminous X-ray source in M82*, Research in Astronomy and Astrophysics, 15, 517

Tonry, J. L., Dressler, A., Blakeslee, J. P., et al. 2001, *The SBF Survey of Galaxy Distances. IV. SBF Magnitudes, Colors, and Distances*, ApJ, 546, 681

Tully, R. B. 1988, Nearby galaxies catalog

Tully, R. B., Rizzi, L., Shaya, E. J., et al. 2009, *The Extragalactic Distance Database*, AJ, 138, 323

Vacca, W. D., Cushing, M. C., & Rayner, J. T. 2003, *A Method of Correcting Near-Infrared Spectra for Telluric Absorption*, PASP, 115, 389

van der Marel, R. P. 2004, *Intermediate-mass Black Holes in the Universe: A Review of Formation Theories and Observational Constraints*, in "Coevolution of Black Holes and Galaxies", Carnegie Observatories Astrophysics Series; Cambridge University Press; L.C. Ho, Ed., 37

van Paradijs, J. & McClintock, J. E. 1994, *Absolute visual magnitudes of low-mass X-ray binaries.*, A&A, 290, 133

Vernet, J., Dekker, H., D'Odorico, S., et al. 2011, *X-shooter, the new wide band intermediate resolution spectrograph at the ESO Very Large Telescope*, A&A, 536, A105

Villegas, D., Jordán, A., Peng, E. W., et al. 2010, *The ACS Fornax Cluster Survey. VIII. The Luminosity Function of Globular Clusters in Virgo and Fornax Early-type Galaxies and Its Use as a Distance Indicator*, ApJ, 717, 603

Volonteri, M. 2012, *The Formation and Evolution of Massive Black Holes*, Science, 337, 544

Volonteri, M. & Rees, M. J. 2006, *Quasars at z=6: The Survival of the Fittest*, ApJ, 650, 669

Voss, R., Nielsen, M. T. B., Nelemans, G., Fraser, M., & Smartt, S. J. 2011, *On the association of ULXs with young superclusters: M82 X-1 and a new candidate in NGC 7479*, MNRAS, 418, L124

Walton, D. J., Fuerst, F., Harrison, F., et al. 2013, *An Extremely Luminous and Variable Ultraluminous X-Ray Source in the Outskirts of Circinus Observed with NuSTAR*, ApJ, 779, 148

Walton, D. J., Gladstone, J. C., Roberts, T. P., & Fabian , A. C. 2011a, *A large catalogue of ultraluminous X-ray source candidates in nearby galaxies*, Astronomische Nachrichten, 332, 354

Walton, D. J., Harrison, F. A., Bachetti, M., et al. 2015a, *NuSTAR and XMM-Newton Observations of the Extreme Ultraluminous X-Ray Source NGC 5907 ULX1: A Vanishing Act*, ApJ, 799, 122

Walton, D. J., Harrison, F. A., Grefenstette, B. W., et al. 2014, *Broadband X-Ray Spectra of the Ultraluminous X-Ray Source Holmberg IX X-1 Observed with NuSTAR, XMM-Newton, and Suzaku*, ApJ, 793, 21

Walton, D. J., Middleton, M. J., Rana, V., et al. 2015b, *NuSTAR, XMM-Newton, and Suzaku Observations of the Ultraluminous X-Ray Source Holmberg II X-1*, ApJ, 806, 65

Walton, D. J., Roberts, T. P., Mateos, S., & Heard, V. 2011b, *2XMM ultraluminous X-ray source candidates in nearby galaxies*, MNRAS, 416, 1844

Watarai, K.-y., Mizuno, T., & Mineshige, S. 2001, *Slim-Disk Model for Ultraluminous X-Ray Sources*, ApJ, 549, L77

Webb, N., Cseh, D., Lenc, E., et al. 2012, *Radio Detections During Two State Transitions of the Intermediate-Mass Black Hole HLX-1*, Science, 337, 554

Webb, N. A., Barret, D., Godet, O., et al. 2010, *Chandra and Swift Follow-up Observations of the Intermediate-mass Black Hole in ESO 243-49*, ApJ, 712, L107

Webb, N. A., Godet, O., Wiersema, K., et al. 2014, *Optical Variability of the Accretion Disk around the Intermediate-mass Black Hole ESO 243-49 HLX-1 during the 2012 Outburst*, ApJ, 780, L9

Webster, B. L. & Smith, M. G. 1983, *Abundance gradients in galaxies in the Sculptor and Centaurus groups*, MNRAS, 204, 743

Wiersema, K., Farrell, S. A., Webb, N. A., et al. 2010, *A Redshift for the Intermediate-mass Black Hole Candidate HLX-1: Confirmation of its Association with the Galaxy ESO 243-49*, ApJ, 721, L102

Wik, D. R., Lehmer, B. D., Hornschemeier, A. E., et al. 2014, *Spatially Resolving a Starburst Galaxy at Hard X-Ray Energies: NuSTAR, Chandra, and VLBA Observations of NGC 253*, ApJ, 797, 79

Willick, J. A., Courteau, S., Faber, S. M., et al. 1997, *Homogeneous Velocity-Distance Data for Peculiar Velocity Analysis. III. The Mark III Catalog of Galaxy Peculiar Velocities*, ApJS, 109, 333

Winter, L. M., Mushotzky, R. F., & Reynolds, C. S. 2006, *XMM-Newton Archival Study of the Ultraluminous X-Ray Population in Nearby Galaxies*, ApJ, 649, 730

Witte, M. G. & Savonije, G. J. 1999, *Tidal evolution of eccentric orbits in massive binary systems. A study of resonance locking*, A&A, 350, 129

Witte, M. G. & Savonije, G. J. 2001, *Tidal evolution of eccentric orbits in massive binary systems. II. Coupled resonance locking for two rotating main sequence stars*, A&A, 366, 840

Wong, D. S., Chornock, R., & Filippenko, A. V. 2008, *Keck Spectroscopy of ROSAT Ultraluminous X-Ray Source Candidates*, PASP, 120, 266

Wu, X.-B., Wang, F., Fan, X., et al. 2015, *An ultraluminous quasar with a twelve-billion-solar-mass black hole at redshift 6.30*, Nature, 518, 512

Yan, Z., Zhang, W., Soria, R., Altamirano, D., & Yu, W. 2015, *X-ray outbursts of ESO 243-49 HLX-1: comparison with Galactic low-mass X-ray binary transients*, ArXiv e-prints

Zacharias, N., Finch, C., Girard, T., et al. 2009, *Third U.S. Naval Observatory CCD Astrograph Catalog (UCAC3)*, Third U.S. Naval Observatory CCD Astrograph Catalog (UCAC3), VizieR Online Data Catalog I/315, 0

Zampieri, L. & Roberts, T. P. 2009, *Low-metallicity natal environments and black hole masses in ultraluminous X-ray sources*, MNRAS, 400, 677

Zdziarski, A. A. & Gierliński, M. 2004, *Radiative Processes, Spectral States and Variability of Black-Hole Binaries*, Progress of Theoretical Physics Supplement, 155, 99

ACKNOWLEDGEMENTS

During the last four years I have met many great people who have in some way contributed to this thesis. I can't mention every one of you personally, but thank you!

First of all I would like to thank my supervisor, Peter Jonker, for his encouragement and support during the past years. Thank you for giving me the opportunity to present our work at conferences, visit lots of places, and do observations with many different telescopes. Also for always returning my drafts within one or two days, even though sometimes I felt it would have been nice to not have to look at it for a week or so. Manuel, thank you for teaching me to properly prepare my observations (21 flats per filter, right?), and for all your help. I would also like to thank Gijs Nelemans, my promotor, who was not directly involved in the project but always ready to give good advice or help me with practical issues. Tullio, thanks for all the nice conversations about everything. Let's see how big our (former) office jungle will grow in the coming years. Johannes, Anna, Thomas and Arjen, and all our regular visitors: thank you for making the German office a nice place to work. Serena, Laura and Thomas, I really enjoyed our conference trips together. All my other colleagues at SRON and Nijmegen: thank you for making these four years an amazing memory!

Fiona Harrison, Tom Maccarone, Maureen van den Berg and Jeroen Homan, thank you for hosting me at Caltech, Texas Tech, Harvard and MIT.

Ella, Pepijn, Eric, Sander, Christel en alle Explo's: bedankt voor jaren Scoutingplezier en het vullen van vele zaterdagen.

Luke, Jacob, Mirjam, Mauricio, Laurens, Jaap, Jory en aanhang, de (ski)vakanties en etentjes waren altijd supergezellig. Tot volgend jaar in Californië?

Papa, mama, Jan, Hanneke en Annechien, fijn dat jullie al mijn verhalen wilden aanhoren de afgelopen paar jaar. Hanneke, ons briljante ik-betaal-jij-kookt-arrangement was geweldig :). Wiba, bedankt voor Jan ;).

Jan, alles komt goed.

CURRICULUM VITAE

I was born on January 2, 1989, in Voorburg. I grew up in Rijswijk where I attended the catholic primary school 'De Piramide'. When I was seven years old I joined the Scouting Gordongroep in Rijswijk. I remained active there, first as a Scout and later as a leader, until the end of my PhD. In 2001, I went to the Haags Montessori Lyceum in The Hague, where I received my gymnasium diploma (cum laude) in 2006. In secondary school I was mainly interested in (and found that I was good at) math, physics and chemistry, although I also really liked Latin and history. I started my Bachelor in Physics and Astronomy at the Universiteit Utrecht with the intention of studying theoretical physics, but soon found out that I liked astronomy much better. I did my bachelor research project at SRON under the supervision of Peter Jonker. For this project I searched for candidate recoiling supermassive black holes by combining the XMM-*Newton* source catalogue with positions of interacting galaxies from the Sloan Digital Sky Survey. For a smaller, extra research project I extended this search to X-ray sources from the *Chandra* catalogue. This yielded a very interesting candidate, which resulted in a paper (Jonker et al. 2010) and a press release that got quite a lot of attention. Chapter 2 of this thesis describes our follow-up observations of this source. I received my Bachelor degree in 2009 (cum laude) and continued with a Master in Astrophysics and Space Research, still at the Universiteit Utrecht. My master research project, about optical counterparts of ultraluminous X-ray sources, was done at SRON, again under supervision of Peter Jonker who also hired me as a PhD student after I obtained my Master degree (cum laude) in 2011. From 2011 to 2015 I worked as a PhD student both at SRON and at the Radboud Universiteit Nijmegen. During this time I presented my research at several conferences, in Cambridge (USA), Snowbird (USA), Potsdam (Germany), Chicago (USA), Brindisi (Italy), Aspen (USA) and Nunspeet. I also attended the NOVA fall school in Dwingeloo and the SIGRAV graduate school in Como, and I got the opportunity to visit the Lindau meeting with Nobel Laureates in 2012.